



CHORUS

This is the accepted manuscript made available via CHORUS. The article has been published as:

Plasma and trap-based techniques for science with positrons

J. R. Danielson, D. H. E. Dubin, R. G. Greaves, and C. M. Surko

Rev. Mod. Phys. **87**, 247 — Published 17 March 2015

DOI: [10.1103/RevModPhys.87.247](https://doi.org/10.1103/RevModPhys.87.247)

Plasma and trap-based techniques for science with positrons

J. R. Danielson* and D. H. E. Dubin†

*Department of Physics,
University of California, San Diego,
La Jolla CA 92093*

R. G. Greaves‡

*First Point Scientific,
Inc., Agoura Hills,
CA 91301*

C. M. Surko§

*Department of Physics,
University of California,
San Diego, La Jolla,
CA 92093*

Abstract

In recent years, there has been a wealth of new science involving low-energy antimatter (i.e., positrons and antiprotons) at energies ranging from 10^2 to less than 10^{-3} eV. Much of this progress has been driven by the development of new plasma-based techniques to accumulate, manipulate and deliver antiparticles for specific applications. This article focuses on the advances made in this area using positrons. However many of the resulting techniques are relevant to antiprotons as well. An overview is presented of relevant theory of single-component plasmas in electromagnetic traps. Methods are described to produce intense sources of positrons and to efficiently slow the typically energetic particles thus produced. Techniques are described to trap positrons efficiently and to cool and compress the resulting positron gases and plasmas. Finally, the procedures developed to deliver tailored pulses and beams (e.g., in intense, short bursts, or as quasi-monoenergetic continuous beams) for specific applications are reviewed. The status of development in specific application areas is also reviewed. One example is the formation of antihydrogen atoms for fundamental physics [e.g., tests of invariance under charge conjugation, parity inversion and time reversal (the CPT theorem), and studies of the interaction of gravity with antimatter]. Other applications discussed include atomic and materials physics studies and study of the electron-positron many-body system, including both classical electron-positron plasmas and the complementary quantum system in the form of Bose-condensed gases of positronium atoms. Areas of future promise are also discussed. The review concludes with a brief summary and a list of outstanding challenges.

* Contact information: jrdanielson@ucsd.edu

† Contact information: ddubin@ucsd.edu

‡ Contact information: rgreaves@fpsi.edu

§ Contact information: csurko@ucsd.edu

CONTENTS

I. Introduction and Overview	3
II. Single-component Plasma Theory for Antimatter Applications	6
A. Cold fluid theory of confinement	6
B. Finite temperature effects and thermal equilibria	8
C. Constants of the motion	10
D. Linear normal modes	11
1. Cylindrical plasmas	11
2. Spheroidal plasmas	13
E. Confinement and heating	14
F. Radial compression with rotating electric fields	16
III. Positron Sources	17
A. Radioisotope sources	17
1. Nuclide selection	17
2. Encapsulated	17
3. Reactor based	17
4. Ion accelerator based	18
5. Spin polarized positrons	18
B. Pair production sources	18
1. Electron accelerators	18
2. Reactor based pair production	18
3. Laser sources	19
C. Positron moderators	19
D. Remoderation and brightness enhancement	19
IV. Antimatter Trapping and Storage	20
A. Overview of Penning-style traps	20
B. Accumulation techniques	20
1. Buffer gas traps	21
2. Trapping in UHV	21
3. Other trapping techniques	22
C. Positron cooling	22
1. Buffer-gas cooling	22
2. Cyclotron cooling	23
3. Evaporative cooling	23
4. Sympathetic cooling	23
D. Long-term antimatter storage	24
1. Loss processes	24
2. Traps for long-term confinement	24
3. Trap-to-trap transfer	26
4. Portable traps	26
V. Diagnostic Techniques for Positron Gases and Plasmas	27
A. Mode-based nondestructive techniques	27
1. Diocotron modes	27
2. Trivelpiece-Gould modes	28
3. Spheroidal modes	28
B. Destructive techniques	29
1. Gauss' law for plasma length	29
2. Imaging areal density profiles	29
3. Particle energy distributions	30
4. Annihilation gamma-ray imaging	30
VI. Plasma Manipulation Techniques	31
A. Radial compression using rotating electric fields	31
1. Coupling <i>via</i> Trivelpiece-Gould modes	31
2. Strong drive regime	32
3. Single particle regime	33
B. Radial positioning using the $m_\theta = 1$ diocotron mode	33
1. Feedback damping and growth	33
2. Autoresonance for off-axis translation	33
C. Controlled heating	34
VII. Trap-based Beams	35
A. Extraction from a buffer-gas trap	35
B. Centerline extraction	35
C. Autoresonance for parallel energy control	35

D.	Pulsed beam production	36
1.	Harmonic potential bunching	36
2.	Timed potential bunching	36
E.	Electrostatic beams	37
F.	Positronium-atom beams	37
VIII.	Tailored Storage and Delivery for Key Applications	37
A.	Creation and study of antihydrogen ($\bar{\text{H}}$)	37
1.	Overview of the experiments	38
2.	Low-energy antiprotons and cold positrons	38
3.	Mixing, $\bar{\text{H}}$ formation, and detection	39
4.	Trapping	40
5.	Measuring $\bar{\text{H}}$ properties	40
B.	Gravity Studies with Antimatter	40
C.	Electron-positron many-body system	41
1.	Quantum effects and a positronium-atom BEC	41
2.	Classical electron-positron (pair) plasmas	42
D.	Atomic and molecular physics with positrons	45
1.	<i>In situ</i> annihilation studies	45
2.	Scattering studies	46
3.	Annihilation as a function of positron energy	46
4.	Laser spectroscopy of positronium	47
5.	Selective ionization of molecules	47
6.	Laboratory modeling of astrophysical processes	47
7.	Trapping and cooling highly charged ions	48
E.	Materials studies	48
1.	Positron annihilation lifetime spectroscopy	48
2.	Positron microscopy	49
IX.	Summary and Concluding Remarks	49
	Acknowledgments	50
	References	50
	Figures	64
	Tables	85

I. INTRODUCTION AND OVERVIEW

The topic of antimatter in our world of matter, which began with the seminal works of Dirac (1930) and Anderson (1932), is now more than eighty years old. Nevertheless, the fact that we live in a world of ordinary matter has presented a major obstacle to using antiparticles in scientific and technological applications, namely annihilation with ordinary matter. Very generally, the technical aspects of generating and manipulating antiparticles have presented major impediments to their use. The focus here is on positron science, since the positron is the lightest stable antiparticle. Having a rest mass of $511 \text{ keV}/c^2$, the positron is the easiest to produce. Thus, positrons have proven to be convenient antiparticles with which to develop antimatter technology and important aspects of antimatter science.

While considerable progress has been made in this regard in recent years, many of the potential uses of antiparticles have yet to be realized. The goal of this article is to review techniques, either developed or under development, to exploit antimatter in a wide range of scientific and technological applications. Previous reviews of important aspects of the positron science and technology related to the topics discussed here include Charlton (1985); Charlton and Humberston (2001); Coleman (2000); Davidson (1990); Gabrielse (2001, 2010); Greaves *et al.* (1994); Holzscheiter and Charlton (1999); Mills (1982, 2010); Robicheaux (2008); Schultz and Lynn (1988); Surko and Greaves (2004); Surko *et al.* (2005).

There has been a continuing desire to develop more efficient antiparticle production methods. As described in Sec. III, current sources of positrons include radioisotopes produced in nuclear reactors, either *in situ* or as portable sources; and the exploitation of bremsstrahlung generated by electron accelerators to produce electron-positron pairs. Unfortunately, as compared with sources of ordinary particles, such as electrons, these techniques are relatively cumbersome to use and are hindered by comparatively low efficiencies. Further, the positrons from such sources are typically born with energies ranging from tens to hundreds of kilo-electron volts. Since many applications require positrons with energies in below 100 eV, and frequently orders of magnitude smaller, efficient methods must be used to slow them. Typical efficiencies for slowing fast positrons from radioisotope sources rarely exceed 10^{-2} for positrons

and can be much lower for accelerator-based positron sources. In Sec. III, we review the most efficient and convenient positron sources currently available and discuss near term prospects for improvements.

Given a suitable source of slow positrons, one frequently wants to tailor collections of antiparticles for specific applications, to create, for example, cold single-component plasma, bright beams, or intense short bursts of antiparticles. Thus another challenge is developing suitable techniques for antiparticle accumulation and storage. An important theme of this review is that advances in antimatter science have been driven by advances in understanding and exploiting the properties of the single component plasma (SCP). This trend is likely to continue for the foreseeable future. The focus on antimatter SCP's arises from two considerations. One is that electrons are so common in our world that great care must be taken to keep positrons separated from them, be it electrons in an atomic or molecular gas or those in condensed phases. A natural way to accomplish this is to store them in vacuum in an electromagnetic trap in the form of single-component plasmas, the theory of which is reviewed in Sec. II.

The second consideration is that single-component plasmas have special confinement properties, so that a positron SCP can be confined for very long periods (e.g., weeks or months are now possible) using a relatively simple arrangement of electromagnetic fields (Malmberg and Driscoll, 1980; O'Neil, 1980b). The most commonly used confinement device for this purpose is the Penning trap. It consists of a uniform magnetic field to restrict motion across the field and an electrostatic potential well in the field direction to prevent escape along the direction of the magnetic field. When a long confinement region, as compared with the diameter of the charge cloud, is arranged using a set of cylindrical confinement electrodes, this device is commonly referred to as a Penning-Malmberg (PM) trap. The theory of operation of this confinement device is reviewed, and alternative approaches are described. As an example, the PM trap requires confinement voltages in excess of the typical particle energy (temperature); and so, if one wants to confine very hot particles for specific experiments (e.g., particles with relativistic energies for electron-positron plasma studies), then the PM trap is not necessarily the best approach.

Assuming good confinement, the experimenter then seeks methods to tailor collections of antiparticles. For example, one might want cold particles and beams for spectroscopy, "bright" beams for microscopy, or to study and exploit many-body effects that result from high antiparticle densities. The challenges presented by these goals and the methods that have been developed to achieve them are described in Secs. IV to VIII. At each stage of antiparticle processing, methods must be developed to characterize the state of the particles, including their energies and distributions in phase (i.e., position and momentum) space. Thus the state of diagnostic techniques for studying and characterizing antimatter gases and plasmas is also reviewed.

In historical perspective, the antimatter technology described here exploits the seminal work of Dehmelt and collaborators to develop the Penning trap as a simple and efficient confinement device for charged particles (Dehmelt, 1990).¹ Modern ideas of confinement of lepton plasmas rely both on that work and work with electrons to create a variety of intense radiation sources, such as traveling wave tubes and klystrons (Pierce, 1954). From those and many other plasma studies, it became clear that relatively dense and cool collections of trapped charge particles exhibit a range of plasma phenomena—oscillations, waves and instabilities, some of which are useful and can be exploited and others deleterious, needing to be avoided.

Early positron technology began with the use of radioisotope sources that produce positrons with energies from a few to hundreds of kilo-electron volts. A range of materials (so-called positron "moderators") were developed to slow the positrons for low-energy experiments. However it is fair to say that the "ideal" positron moderator (i.e., one with efficiency near unity) has yet to be found. The quest for more efficient moderators continues today, and the current state of the art is reviewed in Sec. III.

The origins of efficient positron trapping come from two rather different directions. As illustrated in Fig. 1, in the early 1960's, positron confinement was studied in a magnetic mirror trap (Sec. IV.B.3). The trap was filled with relativistic positrons (initial density $\sim 10^{10} \text{ m}^{-3}$) from the radioisotope ^{19}Ne (Gibson *et al.*, 1960, 1963). The dwell time of the resulting positrons was monitored by measuring the positron flux of 1.0 MeV energy particles exiting the mirror "loss cone" when a gas of stable neon atoms was used to induce de-confinement.

Magnetic-mirror confinement was later used by Mills and collaborators to provide a method of positron-beam-bunching for atomic and surface physics studies (Chu and Mills, 1982; Mills *et al.*, 1989). Mirror confinement was also used by Boehmer and Rynn in an attempt to begin studies of electron-positron (pair) plasmas (Boehmer *et al.*, 1995). While their potential has not yet been fully exploited, magnetic mirrors may well represent an excellent way to confine very energetic positrons and to study the unusual properties of relativistic pair plasma, the latter a topic of much theoretical work spanning decades.

In a very different area and using different trapping techniques, Dehmelt and collaborators conducted the famous Penning-trap experiments, mentioned above, to measure with exquisite precision the fundamental properties of the

¹ The name Penning trap was coined by H. Dehmelt in recognition of F. M. Penning's use of this trap configuration in developing the cold-cathode ion gauge (Penning, 1936).

electron (Dehmelt, 1990). In a natural extension of that work, they also studied positrons, trapping as many as 500 at a time (Dehmelt *et al.*, 1978; Schwinberg *et al.*, 1981).

Exploiting that approach, Leventhal, Brown and collaborators studied positron annihilation on molecular hydrogen to model annihilation from the galactic center (Brown *et al.*, 1984), and Gabrielse used such a device to trap and study the properties of the antiproton (Gabrielse *et al.*, 1986). Nested PM traps are now used routinely to create antihydrogen atoms (Amoretti *et al.*, 2002; Gabrielse *et al.*, 2002).

Along the way, an extension of the PM trap was developed that used a buffer gas to achieve efficient positron capture (Murphy and Surko, 1992; Surko *et al.*, 1988). While the development of the buffer gas trap (BGT) was originally motivated by the desire to have an efficient source of positrons to study test-particle (positron) transport in tokamak fusion devices (Murphy, 1987; Surko *et al.*, 1986), this device has become the method of choice as an efficient positron accumulator to provide ambient-temperature positrons for a wide variety of experiments.

Given success in accumulating collections of positrons, one could then focus on new goals, such as long-term storage, cooling, and compression in real space or in phase space. The Penning-Malmberg trap provided a platform for such endeavors. In a large (e.g., several tesla) magnetic field, cyclotron radiation provided a convenient and efficient cooling mechanism. The particles cool to the ambient temperature, which is usually at 300 K, but can also be cooled to cryogenic temperatures as low as several kelvin. Such positron cooling is crucial in the formation of antihydrogen atoms, such as those illustrated in Fig. 2. A novel method (the “rotating wall technique”) was developed to compress plasmas radially using the torque from rotating electric fields (Danielson and Surko, 2005; Greaves and Surko, 2000; Hollmann *et al.*, 2000). This technique can also be used to mitigate trap imperfections and permit arbitrarily long (“infinite”) confinement times – an ultimate goal of positron trapping.

Often one would like to create very large positron plasmas. One consideration is the Brillouin density limit for confinement of plasma in a uniform magnetic field B . As discussed in Sec. II.A, due to radial space charge electric fields and the presence of the magnetic field, the plasma rotates at a frequency proportional to the plasma density. The limit arises from the fact that there is a maximum value of the plasma number density n_B for which the resulting inward Lorentz force can continue to provide the required centripetal force to keep the spinning plasma confined (Davidson, 1990). While positron plasmas have been created that have densities within an order of magnitude of n_B at low magnetic fields (0.1 T), it has proven much more difficult to approach this limit at higher fields. For example, as discussed in Sec. VI.A, at 5 tesla, where $n_B \sim 10^{20} \text{ m}^{-3}$, current maximum achievable densities are less than $\sim 10^{-3} n_B$. A more frequently encountered practical impediment to confining large numbers of positrons is simply overcoming the space-charge electric fields associated with positron SCP. Namely, the confinement potential V_c must exceed the plasma potential, which is a maximum at the center of the plasma. As discussed in Sec. II.A, for a long cylindrical plasma, this places a limit on N , the number of particles confined per unit plasma length L . For example, for a long cylindrical plasma in a PM trap with radius one third the radius of the cylindrical confining electrodes, the maximum number of particles per unit length that can be confined using a 1 kV confinement potential is $N/L \sim 2.2 \times 10^{11} \text{ m}^{-1}$ (Malmberg and DeGrassie, 1975). Thus confinement of large particle numbers requires large confinement potentials, and this can lead to plasma heating and/or electrical breakdown. Methods are under development to arrange multiple PM traps in parallel in the same vacuum chamber and magnetic field to overcome this limitation (Danielson *et al.*, 2006; Surko and Greaves, 2003).

Given acceptable positron sources, accumulation and confinement techniques, and methods to cool and compress the resulting collections of antimatter, it remains a major challenge to tailor the delivery of the antiparticles for specific end uses. For example, beams with narrow energy spread are desired for atomic and molecular physics scattering and annihilation studies; short pulses are desired for lifetime-spectroscopy studies of material surfaces; and intense bursts are required for the creation of electron-positron plasmas and the formation and study of the positronium molecule (Ps_2 , di-positronium), and ultimately, the creation of a Ps BEC. In other applications, beams with small transverse extent, (i.e., finely focused beams) are desired for microscopy.

In some cases, magnetically guided beams, such as those extracted directly from PM traps, are useful. In other cases, electrostatically guided beams are advantageous, since for example, they enable the use of electrostatic lenses and additional stages of (re)moderation for brightness enhancement. As a consequence of these considerations, as discussed in Secs. VI and VII, much effort has been devoted to developing tailored positron-delivery techniques.

This review is organized as follows. In Sec. II, the underlying theory of SCP confinement in Penning style traps is reviewed, including space charge effects, thermal equilibrium states, linear modes, and radial compression using rotating electric fields. Positron production techniques, moderators, and re-moderation techniques are described in Sec. III. In Sec. IV, a variety of SCP trapping schemes are considered with emphasis on those used most commonly for antimatter physics. The related topic of positron trapping efficiency is discussed, including techniques tailored for specific applications. This section continues with a discussion of the considerations relevant for the long-term storage of positrons, including the prospects for portable antimatter traps.

The broad range of diagnostic techniques developed to characterize antimatter gases and plasmas are described in Sec. V, including non-perturbative techniques that can be used for continuous SCP monitoring, and destructive tech-

niques in situations where they enable more complete characterization of the charge clouds. The range of manipulation techniques developed for plasma and beam control and antimatter delivery are reviewed in Secs. VI and VII. Then the state of antimatter technology in selected key areas of current interest is reviewed in Sec. VIII. Included in this discussion is the range of tools developed for the study of antihydrogen, electron-positron plasmas, positron atomic and molecular physics, a positronium-atom BEC, and materials science. The final section of the review presents a summary and set of concluding remarks.

II. SINGLE-COMPONENT PLASMA THEORY FOR ANTIMATTER APPLICATIONS

As mentioned above, plasmas for which all species have the same sign of charge can be confined for long periods using only static external electric and magnetic fields arranged in a “Penning trap” configuration (Penning, 1936). This arrangement has cylindrical symmetry [coordinates (r, θ, z)] with a magnetic field $B=B\hat{z}$ that is assumed uniform; more generally, B need only have cylindrical symmetry. When the particles are in the plasma state and the plasma is long compared to its diameter, as illustrated in Fig. 3, the device is termed a Penning-Malmberg trap (Malmberg and Driscoll, 1980).

An external electrostatic potential ϕ_{ext} is applied by the application of voltages to a set of cylindrically symmetric electrodes (and possibly end caps) creating an electrostatic potential well in the axial (z) direction that traps particles of a given sign of charge in this direction. However, since ϕ_{ext} satisfies Laplace’s equation

$$\nabla^2 \phi_{\text{ext}}(r, z) = 0, \quad (1)$$

the axial potential well is a saddle-point in the potential, since solutions to Laplace’s equation cannot exhibit local maxima or minima. Thus, this potential will not confine them radially. In addition, the charges repel one another, creating an extra radial electric field that, in the absence of other forces, will cause the plasma to expand radially. To counterbalance this effect, the plasma rotates about the axis of symmetry, so that the resulting inward-directed Lorentz $\mathbf{v} \times \mathbf{B}$ force balances that due to the outward-directed electric fields and the outward centrifugal force due to the rotation of the charge cloud.

A. Cold fluid theory of confinement

For particles with charge q and mass m , the equilibrium fluid equation for a plasma with density n and fluid velocity $\mathbf{v} = v_\theta \hat{\theta}$ yields necessary conditions for confining the plasma

$$mn\mathbf{v} \cdot \nabla \mathbf{v} = qn(\mathbf{E} + \mathbf{v} \times \mathbf{B}), \quad (2)$$

where, for simplicity, we have assumed pressure forces (due to finite temperature) are negligible. The z -component of Eq. (2) implies $E_z = 0$ inside the plasma. The plasma screens out the axial electric field by creating a space charge potential ϕ_p such that the total electrostatic potential $\phi = \phi_p + \phi_{\text{ext}}$ is independent of z within the plasma. This implies that the radial component of \mathbf{E} , $E_r = -\partial\phi/\partial r$, is independent of z within the plasma.

The radial component of Eq. (2) is

$$q(E_r + v_\theta B) + \frac{mv_\theta^2}{r} = 0. \quad (3)$$

Defining the rotation rate $\omega_r = -v_\theta/r$ (the negative sign anticipates that $v_\theta < 0$ for $qB > 0$) we solve Eq. (3) for ω_r , obtaining two solutions

$$\omega_r^{(\pm)} = \frac{\Omega_c}{2} \pm \sqrt{\frac{\Omega_c^2}{4} - \frac{qE_r}{mr}}, \quad (4)$$

where $\Omega_c = qB/m$ is the cyclotron frequency. For small radial electric fields, the fast solution ω_r^+ is nearly Ω_c while the slow solution ω_r^- is given by the $\mathbf{E} \times \mathbf{B}$ drift rotation rate,

$$\omega_r^- \simeq \frac{E_r}{rB}, \quad \left| \frac{qE_r}{mr} \right| \ll \Omega_c^2. \quad (5)$$

Equation (4) indicates that rotation frequencies are in the range

$$0 \leq \omega_r/\Omega_c \leq 1. \quad (6)$$

Equation (4) also implies that there is a maximum electric field beyond which confinement is not possible, namely

$$E_r \leq \frac{m\Omega_c^2 r}{4q}. \quad (7)$$

This inequality sets a maximum possible density termed the Brillouin limit (Brillouin, 1945), which can be understood using Poisson's equation

$$\frac{1}{r} \frac{\partial}{\partial r}(r E_r) = \frac{qn(r, z)}{\varepsilon_0}, \quad (8)$$

recalling that $E_z = 0$ within the plasma. Integrating this equation implies, for radii inside the plasma,

$$E_r(r) = \frac{q}{r\varepsilon_0} \int_0^r dr' r' n(r', z). \quad (9)$$

Since E_r is a function only of r , this equation implies that the density is also dependent only on r within the plasma. Defining the area-weighted mean density $\bar{n}(r)$ as

$$\bar{n}(r) = \frac{2}{r^2} \int_0^r r' dr' n(r'), \quad (10)$$

the inequality Eq. (7) implies that

$$\bar{n}(r) \leq \varepsilon_0 \frac{m\Omega_c^2}{2q^2} \equiv n_B. \quad (11)$$

The maximum possible mean plasma density is termed the Brillouin density n_B , and this is a fairly stringent limit.² The Brillouin densities for positrons and antiprotons are

$$\begin{aligned} n_B &= 4.8 \times 10^{18} \text{ m}^{-3} \left(\frac{B}{1 \text{ tesla}} \right)^2 \quad (\text{positrons}) \\ &= 2.6 \times 10^{15} \text{ m}^{-3} \left(\frac{B}{1 \text{ tesla}} \right)^2 \quad (\text{antiprotons}). \end{aligned} \quad (12)$$

Rewriting n_B as $n_B = B^2/(2\mu_0 mc^2)$, Eq. (11) implies that the relativistic rest energy density of the plasma at the Brillouin limit, $n_B mc^2$, is equal to the magnetic energy density $B^2/2\mu_0$. Thus, the total stored rest energy of a single-component, antimatter plasma is, at best, a fraction of the stored energy in the magnetic solenoid (i.e., since the volume enclosed by the solenoid is always larger than that occupied by the plasma).

For a uniform density plasma, Eq. (8) implies that the electric field *within the plasma* increases linearly with radius

$$E_r = \frac{qn}{2\varepsilon_0} r. \quad (13)$$

Substituting this result into Eq. (3) yields the following formula for a uniform density non-neutral plasma

$$n = 4n_B \frac{\omega_r(\Omega_c - \omega_r)}{\Omega_c^2}. \quad (14)$$

This equation implies that a uniform density plasma has a uniform rotation frequency. The maximum possible density is the Brillouin density n_B , that is achieved when $\omega_r = \Omega_c/2$, consistent with Eq. (4) and Eq. (11).

Returning to the issue of axial confinement, recall that the total plasma potential $\phi = \phi_{\text{ext}} + \phi_p$ is independent of z within the plasma. Thus, the external potential must be sufficiently large to balance the plasma self potential ϕ_p , and this sets minimum conditions on the electrode voltages necessary to trap the plasma. For example, consider the case of a uniform density plasma column with flat ends, long compared to the electrode radius r_w . The electric field

² While the local plasma density can exceed n_B , for example, in a monotonically increasing radial density profile with mean density less than n_B , such profiles tend to be unstable.

within the plasma is given by Eq. (13), and outside the plasma but far from the ends, the electric field is also purely radial, given by

$$E_r = \frac{qnr_p^2}{2\epsilon_0 r}, \quad r > r_p. \quad (15)$$

Assuming $\phi(r_w) = 0$, integration of the radial electric field yields the following expression for ϕ inside the plasma:

$$\phi(r) = \frac{qnr_p^2}{4\epsilon_0} \left[1 + 2 \ln \left(\frac{r_w}{r_p} \right) \right] - \frac{qnr^2}{4\epsilon_0}, \quad r < r_p. \quad (16)$$

Since this potential must be independent of z within the plasma, it has the same form at the plasma ends. In particular, there is a potential difference $\Delta\phi$ between the wall and $r = 0$ given by

$$\Delta\phi = \frac{qnr_p^2}{4\epsilon_0} \left[1 + 2 \ln \frac{r_w}{r_p} \right]. \quad (17)$$

To confine the plasma axially, the voltage applied to the end confinement electrodes must be at least this large. For a cylindrical end electrode long compared to its radius, a voltage of $\Delta\phi$ will be just sufficient for confinement, while for shorter electrodes, a larger applied voltage will be required.

For a positron plasma that fills the cylinder at the Brillouin density, the minimum required voltage is

$$\Delta\phi = 2.2 \times 10^{10} \text{ Volts} \left(\frac{B}{1 \text{ tesla}} \frac{r_w}{1 \text{ m}} \right)^2. \quad (18)$$

Thus, unless r_w is small, high-density single-component plasmas require substantial voltages to confine them, due to the large voltages developed by their unneutralized space charge.

B. Finite temperature effects and thermal equilibria

For a plasma at temperature T , the equilibrium condition of Eq. (8) is replaced by

$$mn\mathbf{v} \cdot \nabla\mathbf{v} = qn(\mathbf{E} + \mathbf{v} \times \mathbf{B}) - \nabla p, \quad (19)$$

where p is the plasma thermal pressure, and as before, $\mathbf{v} = -\omega_r r \hat{\theta}$ is the fluid velocity due to rotation with rate ω_r . Assuming that the plasma is ideal, this pressure p is given by the ideal gas law $p = nk_B T$. Assuming that the temperature is uniform, which is a necessary condition for thermal equilibrium, the axial component of Eq. (19) can be written

$$0 = -qn \frac{\partial\phi}{\partial z} - k_B T \frac{\partial n}{\partial z}. \quad (20)$$

This equation can be integrated to obtain the relation between density and potential,

$$n(r, z) = f(r) e^{-q\phi(r, z)/k_B T}, \quad (21)$$

where $f(r)$ is any function of radius. This Boltzmann-like equation implies that plasma density collects in z at local minima (in z) of the electrostatic potential energy function $q\phi$. The function $f(r)$ is determined by the radial component of Eq. (19)

$$-mn\omega_r^2 r = qn \left(-\frac{\partial\phi}{\partial r} - \omega_r r B \right) - k_B T \frac{\partial n}{\partial r}. \quad (22)$$

This equation can be rewritten as follows:

$$\omega_r = \frac{E_r}{Br} - \frac{k_B T}{qBrn} \frac{\partial n}{\partial r} + \frac{\omega_r^2}{\Omega_c}. \quad (23)$$

The first term is the $\mathbf{E} \times \mathbf{B}$ drift rotation rate; the second term can be recognized as the expression for rotation due to the diamagnetic drift, and the third term is a correction (often small) due to the $\mathbf{F} \times \mathbf{B}$ drift from centrifugal forces. Substituting for n from Eq. (21) and rearranging terms yields, after some cancellations,

$$\frac{k_B T}{f} \frac{\partial f}{\partial r} = -m\omega_r (\Omega_c - \omega_r) r. \quad (24)$$

Thus, the density is determined by the rotation frequency (or vice-versa). For example, if the rotation frequency is uniform in r (rigid rotation), Eq. (24) can be integrated to yield $f = C \exp[-m\omega_r(\Omega_c - \omega_r)r^2/2k_B T]$, and when the result is combined with Eq. (21), one obtains

$$n(r, z) = C e^{-q\phi_{\text{eff}}(r, z)/k_B T}, \quad (25)$$

where C is a constant of integration and the effective potential $q\phi_{\text{eff}}$ is

$$q\phi_{\text{eff}}(r, z) = \frac{1}{2}m\omega_r(\Omega_c - \omega_r)r^2 + q\phi(r, z). \quad (26)$$

Equation (25) describes a confined plasma in a thermal equilibrium state (Dubin and O'Neil, 1999; Malmberg and O'Neil, 1977). Such plasmas have uniform temperature, since nonuniformities in T would eventually dissipate due to thermal conduction. Likewise, such plasmas have a uniform rotation rate, since viscosity will act to remove shears in ω_r . This thermal equilibrium plasma is confined by the effective potential, which becomes large and positive for both large r and large z , making the density exponentially small in these regions.

As discussed in the previous section, the second term in the effective potential produces the required confining potential well in the z direction due to voltages applied to the confinement electrodes. The first term in the effective potential is due to rigid rotation through the uniform magnetic field. It produces a confining potential that is partially offset by the centrifugal potential, which is proportional to ω_r^2 .

This radial confining potential is proportional to r^2 . It has the same form as the potential one would obtain if one replaced rotation through the magnetic field with a rigid uniform cylinder of charge opposite to that of the plasma, with a uniform density n_0 given by

$$n_0 = \frac{2\varepsilon_0 m}{q^2} \omega_r (\Omega_c - \omega_r). \quad (27)$$

This implies that the thermal equilibrium state of a trapped non-neutral plasma is the same as that of a one component plasma (OCP) (Malmberg and O'Neil, 1977), which is a system consisting of a collection of identical charges confined by a neutralizing background charge. This is a useful result since the thermal equilibrium properties of OCP's have received considerable attention, for example, as a model for dense astrophysical matter (Hansen, 1973; Ichimaru, 1982).

At zero temperature, the OCP matches its density to that of the neutralizing background density n_0 , out to a surface of revolution where the supply of charge is exhausted. This is the cold-fluid equilibrium discussed previously, with density given by Eq. (14).

At finite temperatures, the density is given in terms of the potential by Eqs. (25) and (26). In turn, the potential is determined in terms of the density by Poisson's equation

$$\frac{\partial^2 \phi}{\partial r^2} + \frac{1}{r} \frac{\partial \phi}{\partial r} + \frac{\partial^2 \phi}{\partial z^2} = -\frac{n(r, z)}{\varepsilon_0}. \quad (28)$$

Equations (25) and (28) constitute a system of nonlinear equations for the potential ϕ , the Poisson-Boltzmann system, that can be solved uniquely (Prasad and O'Neil, 1979) for given values of the rotation frequency, the temperature, the constant C (determined in terms of the other constants and the total particle number N) and given boundary conditions for ϕ specified by the voltages applied to the confinement electrodes.

The solution has the following qualitative features: the plasma density is uniform and equal to n_0 out to a surface of revolution whose shape is determined by the applied electrode voltages, the total particle number, and the plasma rotation frequency. Beyond this surface of revolution the density falls to zero on the scale of a Debye length $\lambda_D = \sqrt{\varepsilon_0 k_B T / (q^2 n_0)}$ (Davidson and Krall, 1970; Prasad and O'Neil, 1979).

Furthermore, this confined rotating thermal equilibrium plasma has a Maxwellian velocity distribution $f_{eq}(r, z, \mathbf{v})$ that is shifted by the plasma rotation velocity

$$f_{eq}(r, z, \mathbf{v}) = \frac{n(r, z)}{(2\pi k_B T/m)^{3/2}} \times \exp \left[-\frac{1}{2}m \left(\mathbf{v} + \omega_r r \hat{\theta} \right)^2 / k_B T \right]. \quad (29)$$

This result can be recognized as the Boltzmann distribution function. Namely, it may be rewritten as

$$f_{eq}(r, z, \mathbf{v}) = \frac{C}{(2\pi k_B T/m)^{3/2}} \exp[-(h + \omega_r p_\theta)/k_B T], \quad (30)$$

where

$$h = \frac{1}{2}m\mathbf{v}^2 + q\phi \quad (31)$$

is the particle energy, and

$$p_\theta = m\mathbf{v}_\theta r + \frac{qB}{2}r^2 \quad (32)$$

is the θ -component of the canonical angular momentum for a particle in a uniform magnetic field (*i.e.* the momentum variable canonically-conjugate to the angle θ). The combination $h + \omega_r p_\theta$ is the particle energy as seen in a frame rotating with frequency $-\omega_r$ (Landau and Lifshitz, 1976). In this frame, the plasma is stationary, and Eq. (30) has the expected Boltzmann form.

C. Constants of the motion

The functions h and p_θ are related to constants of the motion of the plasma. For example, the total plasma angular momentum P_θ is a constant of the motion, given by

$$P_\theta = \sum_{i=1}^N p_{\theta i}(t) = \int d^3r d^3v f(\mathbf{r}, \mathbf{v}, t) (m\mathbf{v}_\theta r + qBr^2/2), \quad (33)$$

where in the second form, the time-dependent plasma distribution function $f(\mathbf{r}, \mathbf{v}, t)$ is introduced for a system that is not necessarily in equilibrium. The external potential and the applied magnetic field are assumed to be cylindrically symmetric. This, together with the assumed absence of any other forces with a θ component, such as gravity or collisional drag on neutral gas, guarantees that P_θ is a conserved quantity during the plasma evolution. Non- θ -symmetric effects will be considered below.

In addition, the total plasma energy ε is also a constant of the motion,

$$\varepsilon = \int d^3r d^3v f(\mathbf{r}, \mathbf{v}, t) \left(\frac{1}{2}m\mathbf{v}^2 + q\phi_{ext}(r, z) + \frac{1}{2}q\phi_p(r, z, t) \right). \quad (34)$$

The plasma potential ϕ_p evolves in time as the density evolves. This potential is the solution to the Poisson equation (28) with boundary conditions that $\phi_p = 0$ on the surrounding electrodes. The time-independence of the external forces acting on the plasma and the (assumed) absence of non-conservative processes, such as neutral gas drag or radiation, guarantee that the total energy is conserved.

For a thermal equilibrium system, the plasma energy and angular momentum can be written

$$\begin{aligned} P_\theta &= P_\theta(\omega_r, T, N), \\ \varepsilon &= \varepsilon(\omega_r, T, N), \end{aligned} \quad (35)$$

where the particular functional forms can be obtained by substituting Eq. (29) for f into Eq. (33) and Eq. (34). These thermodynamic relations can be inverted in various ways to yield, for example, $\omega_r = \omega_r(P_\theta, T, N)$. Derivatives of these thermodynamic variables with respect to other thermodynamic variables obey a number of useful relations (Dubin and O'Neil, 1999). One such relation that will be used later is

$$\partial\omega_r/\partial P_\theta \leq 0, \quad (36)$$

where the partial derivative is at fixed N and at either fixed T or fixed ε .

Plasma confinement in the radial direction can be understood by considering the total angular momentum. For a sufficiently large magnetic field, the mechanical part of the angular momentum is negligible compared to the vector potential portion, allowing us to approximate Eq. (33) as

$$P_\theta \cong \frac{qB}{2} \int d^3r d^3v f(\mathbf{r}, \mathbf{v}, t) r^2 = \frac{qNB}{2} \langle r^2 \rangle, \quad (37)$$

where $\langle r^2 \rangle$ is the mean-square plasma radius. Since P_θ is a constant of the motion, the mean square plasma radius cannot change during plasma evolution. This is a significant constraint on single-component plasmas. It implies that, in the absence of nonconservative forces, *in order for particles to escape to the wall, other particles must move toward the center of the trap.*

D. Linear normal modes

When the plasma equilibrium is perturbed, the plasma exhibits collective modes of oscillation. Considered here are aspects of the modes that are important for antimatter research. The focus is on electrostatic plasma modes, since electromagnetic corrections are typically negligible in current experiments. Electrostatic plasma oscillations create a perturbed potential $\delta\phi(\mathbf{r}, t)$ that varies in time as $\exp(-i\omega t)$ where the frequency ω may be complex, with the imaginary part caused by damping or growth.

For a plasma in a uniform magnetic field $B\hat{z}$ and undergoing rigid rotation about the z axis, the perturbed potential in cold fluid theory (i.e., neglecting temperature effects) satisfies the differential equation

$$\nabla \cdot \boldsymbol{\varepsilon} \cdot \nabla \delta\phi = 0, \quad (38)$$

where the dielectric tensor $\boldsymbol{\varepsilon}$ in Cartesian coordinates takes the form

$$\boldsymbol{\varepsilon} = \begin{pmatrix} \varepsilon_1 & -i\varepsilon_2 & 0 \\ i\varepsilon_2 & \varepsilon_1 & 0 \\ 0 & 0 & \varepsilon_3 \end{pmatrix}, \quad (39)$$

and where, for a single plasma species, the dielectric constants are

$$\begin{aligned} \varepsilon_1 &= 1 - \omega_p^2/(\bar{\omega}^2 - \Omega_v^2), \\ \varepsilon_2 &= \Omega_v \omega_p^2/[\bar{\omega}(\bar{\omega}^2 - \Omega_v^2)], \\ \varepsilon_3 &= 1 - \omega_p^2/\bar{\omega}^2. \end{aligned} \quad (40)$$

The frequency $\bar{\omega} = \omega + m_\theta \omega_r$ is that seen in the rotating frame (rotating in the θ -direction with frequency $-\omega_r$), $\omega_p = (ne^2/m\epsilon_0)^{1/2}$ is the plasma frequency, and $\Omega_v = \Omega_c - 2\omega_r$ is the vortex frequency. The vortex frequency is the cyclotron frequency as seen in the rotating frame with the shift due to the Coriolis force (Dubin and O'Neil, 1999).

Equation (38) is Maxwell's equation $\nabla \cdot \mathbf{D} = 0$ for a linear medium with a frequency-dependent and anisotropic dielectric tensor $\boldsymbol{\varepsilon}$. Equation (38) can be solved in various geometries, and considered below are two important examples. However, many of the modes of oscillation can also be understood qualitatively from the spatial Fourier transform of Eq. (38), $\varepsilon_1 k_\perp^2 + \varepsilon_3 k_z^2 = 0$. This can be written as a quadratic equation for $\bar{\omega}^2$ with solutions

$$\bar{\omega}^2 = \frac{\Omega_u^2}{2} \pm \frac{\sqrt{k_\perp^2 \Omega_u^4 + k_z^2 (\Omega_v^2 - \omega_p^2)^2}}{2k}, \quad (41)$$

where $\Omega_u = \sqrt{\Omega_v^2 + \omega_p^2}$ is the upper hybrid frequency in a rotating plasma, and $k = \sqrt{k_\perp^2 + k_z^2}$. Equation (41) is the dispersion relation for upper hybrid waves (the upper sign) and magnetized plasma waves (the lower sign) in a uniform plasma. For a large magnetic field, Eq. (41) simplifies to

$$\bar{\omega}^2 = \begin{cases} k_z^2 \omega_p^2 / k^2, & \text{(magnetized plasma waves)} \\ \Omega_v^2 + k_\perp^2 \omega_p^2 / k^2, & \text{(upper hybrid waves)} \end{cases}. \quad (42)$$

The magnetized plasma waves are density compressions and rarefactions with the restoring force due to the perturbed electric field produced by these oscillations. The magnetic field does not enter the dispersion relation, in this large B limit, since plasma motion is only along the direction of the field. The upper hybrid waves are essentially cyclotron oscillations that produce density compressions, which, in turn, induce an extra restoring force, thereby increasing the oscillation frequency.

In Eqs. (41) and (42) k_z and k_\perp can take on any values, but in a bounded plasma, they are quantized. Also, in bounded plasmas, there are additional waves associated with the plasma surface, the diocotron and surface cyclotron waves. Surface plasma waves, which are evanescent plasma waves for which $\varepsilon_1/\varepsilon_3 > 0$, also exist, but only for plasmas near the Brillouin limit with $\Omega_v^2 < \omega_p^2$ (Bollinger *et al.*, 1993). In the next section, normal modes are discussed for two bounded plasma geometries of importance to trapped antimatter research, cylindrical and spheroidal plasmas.

1. Cylindrical plasmas

Considered here are the electrostatic normal modes of a long uniform-density plasma column with radius r_p and length L ($0 < z < L$), trapped along the axis of a much longer hollow conducting cylinder of radius r_w (Trivelpiece and Gould, 1959). Within the plasma, the perturbed potential has the form

$$\delta\phi(\mathbf{r}, t) = J_{m_\theta}(k_\perp r) \exp(im_\theta \theta - i\omega t) \cos(k_z z), \quad (43)$$

where the nonnegative integer m_θ is the azimuthal mode number, $k_z = m_z\pi/L$ is the axial wavenumber, and $J_{m_\theta}(x)$ is a Bessel function of the first kind. The transverse wavenumber parameter k_\perp depends on k_z and $\bar{\omega}$ through the relation

$$k_\perp^2 = -k_z^2 \varepsilon_3 / \varepsilon_1. \quad (44)$$

The dispersion relation is obtained by matching Eq. (43) to the perturbed potential outside the plasma (a solution to Laplace's equation) yielding

$$\varepsilon_1 k_\perp r_p \frac{J'_{m_\theta}(k_\perp r_p)}{J_{m_\theta}(k_\perp r_p)} + m_\theta \varepsilon_2 = k_z r_p \frac{I'_{m_\theta}(k_z r_p) K_{m_\theta}(k_z r_w) - I_{m_\theta}(k_z r_w) K'_{m_\theta}(k_z r_p)}{I_{m_\theta}(k_z r_p) K_{m_\theta}(k_z r_w) - I_{m_\theta}(k_z r_w) K_{m_\theta}(k_z r_p)}. \quad (45)$$

For long axial wavelengths (i.e., $k_z r_w \ll 1$), the right hand side simplifies to

$$\varepsilon_1 k_\perp r_p \frac{J'_{m_\theta}(k_\perp r_p)}{J_{m_\theta}(k_\perp r_p)} + m_\theta \varepsilon_2 = \begin{cases} -m_\theta \frac{1+(r_p/r_w)^{2m_\theta}}{1-(r_p/r_w)^{2m_\theta}}, & m_\theta > 0 \\ -\frac{1}{\log(r_w/r_p)}, & m_\theta = 0 \end{cases} \quad (46)$$

a. Diocotron modes. Diocotron modes have $m_\theta > 0$, and $k_z = 0$. Taking the $k_z \rightarrow 0$ limit of Eq. (46), and noting that $k_\perp \propto k_z$ [cf. Eq. (44)], $m_\theta(\varepsilon_1 + \varepsilon_2) = -m_\theta \frac{1+(r_p/r_w)^{2m_\theta}}{1-(r_p/r_w)^{2m_\theta}}$. This can be solved for ω to yield

$$\omega + m_\theta \omega_r = -\frac{\Omega_v}{2} \pm \sqrt{\frac{\Omega_v^2}{4} + \omega_p^2 \frac{1-(r_p/r_w)^{2m_\theta}}{2}}. \quad (47)$$

There are two solutions: a high-frequency surface cyclotron wave (cf. Sec. II.D.1.c) and the low-frequency diocotron branch. For $|\Omega_c| \gg \omega_p$, and using $\omega_r \simeq \omega_p^2/2\Omega_c$ and Eqs. (5) and (13), the low-frequency solution is

$$\omega_{m_\theta} = -\omega_r \left[m_\theta - 1 + \left(\frac{r_p}{r_w} \right)^{2m_\theta} \right]. \quad (48)$$

The diocotron modes are z -independent, low frequency distortions of the plasma column which propagate azimuthally due the $\mathbf{E} \times \mathbf{B}$ drift created by the perturbed potential (Fig. 4). For this reason the frequency scales as $1/B$. The frequency is negative (for positrons), which means physically that the azimuthal phase velocity of the modes, ω/m_θ , is in the same direction as the plasma rotation (for positrons, the $-\hat{\theta}$ direction). The perturbed potential inside the plasma is found from the $k_z \rightarrow 0$ limit of Eq. (43),

$$\delta\phi(\mathbf{r}, t) = Cr^{m_\theta} \exp(im_\theta\theta - i\omega t). \quad (49)$$

An important feature of the diocotron modes is the fact that they are “negative energy modes.” The distorted plasmas shown in Fig. 4 have lower potential energies than the corresponding cylindrically-symmetric equilibrium plasma with the same density, and they have negligible excess kinetic energy since the $\mathbf{E} \times \mathbf{B}$ drift fluid velocities in the mode are small for large B . Therefore the total plasma energy with the mode present is lower than the original equilibrium. For example, the $m_\theta = 1$ mode is attracted to its image charge in the wall electrode. A key feature of these modes is that they can be driven unstable by processes that remove energy and angular momentum from the plasma, such as resistance in the wall electrodes (White *et al.*, 1982), or collisions with other species (Fajans, 1993; Kabantsev *et al.*, 2003; Levy *et al.*, 1969). The diocotron modes are useful both for diagnostic purposes (Sec. V.A.1) and for plasma manipulation (Sec. VI.B).

b. Trivelpiece-Gould (TG) modes. The TG modes are finite k_z plasma oscillations, with frequencies proportional to the plasma frequency. Since typically $\omega_p \ll \Omega_c$, again one can take $\varepsilon_1 = 1$ and $\varepsilon_2 = -\omega_p^2/(\bar{\omega}\Omega_c) \ll 1$ in Eq. (45) or Eq. (46). Then from Eq. (44), $k_\perp^2 = -k_z^2 \varepsilon_3$ which can be rewritten as $\bar{\omega}^2 = \omega_p^2 k_z^2 / (k_z^2 + k_\perp^2)$, the dispersion relation for magnetized plasma waves [Eq. (42)]. A (typically small) temperature correction to this relation yields the TG dispersion relation (Anderegg *et al.*, 2003)

$$\bar{\omega}^2 = \frac{k_z^2 \omega_p^2}{k_\perp^2 + k_z^2} + \frac{3k_z^2 T}{m}, \quad (50)$$

where this temperature correction assumes the density remains uniform, even at finite T . The perpendicular wavelength k_{\perp} must still be solved for using Eq. (45) [or Eq. (46), if $k_z r_w \ll 1$.]

There are many solutions corresponding to TG modes that have radial oscillations within the plasma column. For example, for $m_{\theta} = 0$ and $k_z r_w \ll 1$, the equation for k_{\perp} , given by Eq. (46), is

$$k_{\perp} r_p \frac{J_1(k_{\perp} r_p)}{J_0(k_{\perp} r_p)} = \frac{1}{\log(r_w/r_p)}, \quad (51)$$

which can be solved numerically. For $r_w \gg r_p$, all but one of the solutions of Eq. (51) satisfy $k_{\perp} r_p \cong j_{1,n}$ for $n = 1, 2, 3, \dots$, where $j_{m,n}$ is the n 'th zero of the Bessel function $J_m(x)$. These modes have n radial nodes in the potential eigenfunction – that is, the axial fluid velocity changes sign as a function of radius. There is an additional solution,

$$k_{\perp} r_p \cong \sqrt{2/\log(r_w/r_p)}. \quad (52)$$

This mode has no radial nodes. It is, therefore, typically the easiest to excite and observe in experiments (Sec. V.A.2).

The $m_{\theta} > 0$ TG modes can also be excited and observed using azimuthally sector electrodes. For these modes, it can be shown, using Eq. (46), that when $k_z r_w \ll 1$, $r_w \gg r_p$ and $|\bar{\omega}| \gg m_{\theta} |\omega_r|$ (which allows us to set $m_{\theta} \varepsilon_2 = 0$), $k_{\perp} r_p \cong j_{m_{\theta}-1,n}$, $n = 1, 2, \dots$. The number of radial nodes in the perturbed potential equals $n - 1$, and so $n = 1$ has no radial nodes. On the other hand, if $|\bar{\omega}| \ll m_{\theta} |\omega_r|$, one can show that $k_{\perp} r_p \cong j_{m_{\theta},n}$ (Prasad and O'Neil, 1983). The $m_{\theta} > 0$ modes play a role in field-error transport (Sec. II.E) and radial compression using rotating electric fields (the rotating wall technique, Sec. VI.A).

c. Upper hybrid, surface cyclotron, and Bernstein modes. These are modes with frequencies near the cyclotron frequency. Assuming $|\Omega_c| \gg \omega_p$, the upper-hybrid branch has frequencies that follow from Eq. (44), taking $\varepsilon_3 = 1$: $\bar{\omega}^2 = \Omega_v^2 + \omega_p^2 k_{\perp}^2 / k^2$ [see Eq. (42)]. The possible values of k_{\perp} are found by solving Eq. (45) or Eq. (46). For example, when $k_z r_w \ll 1$ and $r_p \ll r_w$, one can show that $k_{\perp} r_p \cong j_{1,n}$ for $m_{\theta} = 0$ and $k_{\perp} r_p \cong j_{m_{\theta}-1,n}$ for $m_{\theta} > 0$, the same as for the TG modes.

Another type of high frequency mode, the surface cyclotron mode, exists for $m_{\theta} > 0$ and $k_z \rightarrow 0$. This mode is a z -independent distortion of the plasma column similar to a diocotron mode, but has a mode frequency close to $-\Omega_c$, i.e. the mode has a phase velocity in the direction of rotation (the $-\hat{\theta}$ direction for positrons) which is also the direction of cyclotron rotation. The frequency of the surface cyclotron mode is given by the high frequency branch of Eq. (47) which, for $|\Omega_c| \gg \omega_p$, can be written

$$\omega = -\Omega_c - \omega_r \left[m_{\theta} - 1 - \left(\frac{r_p}{r_w} \right)^{2m_{\theta}} \right]. \quad (53)$$

This mode frequency differs from the $k_z = 0$ lab-frame (negative) upper hybrid mode frequency, $-\Omega_u - m_{\theta} \omega_r \simeq -\Omega_c - \omega_r(m_{\theta} - 1)$, by the image charge factor $\omega_r(r_p/r_w)^{2m_{\theta}}$.

For positrons (or electrons) all such modes are typically high frequency; and consequently, they are difficult to observe or excite. However, for antiprotons, the temporal cyclotron frequency $|f_c| = 96 \text{ MHz } B/[1 \text{ tesla}]$, and so they can be observed using standard techniques.

The $m_{\theta} = 1$ surface cyclotron mode, described by Eq. (53), is a center of mass motion of the plasma column (see Fig. 4) with a frequency shift away from the “bare” cyclotron frequency due only to image charge effects.

In addition to the surface cyclotron and upper-hybrid modes, there can also be modes near all multiples of the cyclotron frequency, the so-called Bernstein modes (Bernstein, 1956). These modes are not described by Eqs. (45) or (46). The frequency shifts for such modes are strongly temperature dependent, and might therefore also be a useful temperature diagnostic if they could be controllably excited and observed. Approximate dispersion relations for the Bernstein modes have been obtained (Dubin, 2005), but have not yet been carefully compared to experiment.

2. Spheroidal plasmas

Another important geometry is that of plasmas that are spheroids with comparable major and minor radii and dimensions small compared to the distance to surrounding electrodes. Such spheroidal plasmas are formed when the external Penning trap potential produced by the electrodes is harmonic in both r and z ,

$$q\phi_{\text{ext}}(\mathbf{r}) = \frac{1}{2} m \omega_z^2 (z^2 - \frac{1}{2} r^2), \quad (54)$$

where ω_z is the harmonic trap frequency. The electrostatic normal modes for such plasmas, neglecting image-charge effects, have been determined analytically in the cold-fluid limit (Dubin, 1991). This assumes the spheroids are small compared to r_w . The dispersion relation depends on the aspect ratio $\alpha = L/(2r_p)$ of the spheroid, where L is the spheroid's axial length and r_p its radius,

$$\varepsilon_3 k_1 \frac{P_l^{m_\theta'}(k_1)}{P_l^{m_\theta}(k_1)} + m_\theta \alpha^2 \varepsilon_2 = k_2 \frac{Q_l^{m_\theta'}(k_2)}{Q_l^{m_\theta}(k_2)}, \quad (55)$$

where $P_l^m(x)$ and $Q_l^m(x)$ are Legendre functions of the first and second kind respectively (the branch chosen for $Q_l^m(x)$ is such that $\lim_{x \rightarrow \infty} Q_l^m(x) = 0$), primes denote derivatives with respect to the argument, $k_1 = \alpha/\sqrt{\alpha^2 - \varepsilon_3/\varepsilon_1}$, $k_2 = \alpha/\sqrt{\alpha^2 - 1}$, and the spheroidal mode number l can take on any integer value greater than or equal to m_θ . The integer $l - m_\theta$ measures the number of nodes in the perturbed potential eigenmode as one travels along a great circle of the spheroid from pole to pole. Within the plasma, these eigenmodes can be represented as order l polynomials in x , y and z .

The $(l, m_\theta) = (1, 0)$ mode is of particular interest, as this mode is an axial oscillation of the entire center of mass of the spheroid, with $\delta\phi = Aze^{-i\omega t}$, and frequency ω_z . This implies a relation between the plasma frequency, ω_z , and the aspect ratio given by Eq. (55) $\varepsilon_3 = k_2 \frac{Q_l^0(k_2)}{Q_l^0(k_2)}$, which can be re-written

$$\omega_p^2 = \omega_z^2(\alpha^2 - 1)/Q_l^0(k_2). \quad (56)$$

This result is plotted as a dashed line in Fig. 5.

Higher-order modes are also routinely excited in the experiments. In Fig. 5, some of the cylindrically-symmetric modes with frequencies of order ω_p are shown along with a schematic diagram of the velocity perturbations associated with the modes (Tinkle *et al.*, 1994). Note that the number of distinct $m_\theta = 0$ plasma modes for a given l is the closest integer lower than, or equal to $(l + 1)/2$; different modes with the same l value have different internal velocities, some with radial nodes similar to the TG modes in cylindrical columns. For very oblate spheroids some of these modes could be thought of as drumhead modes (e.g., the lowest frequency $l = 3$ mode in Fig. 5).

Finite temperature corrections for these modes have also been calculated Dubin (1993), and have been used to measure the plasma temperature (Sec. V.A.3). The thermal corrections for these modes, such as (2,0), (2,1), (3,0) and (4,0), in the large B limit are given in (Dubin, 1993). Corrections for the first two modes take the form $\omega^2 = \omega_0^2 + \Delta\omega^2$; for the first two modes,

$$\Delta\omega^2 = 20 \frac{k_B T}{mL^2} \left(1 + 2 \frac{\omega_0^2}{\omega_p^2}\right), \quad (2, 0) \quad (57)$$

$$= 10 \frac{k_B T}{mr_p^2} \frac{\omega_0^2}{\omega_p^2}, \quad (2, 1) \quad (58)$$

where ω_0 is the cold-fluid frequency given by Eq. (55). They all have a form similar to that given by Eq. (50) for TG modes in cylindrical plasmas. A somewhat larger thermal correction for the (2,0) mode was given in Tinkle *et al.* (1994), due to the fact that the change in the radial density profile with T was neglected.

In addition to modes near the plasma frequency, Eq. (55) also describes modes near the cyclotron frequency as well as $\mathbf{E} \times \mathbf{B}$ drift modes with frequencies of order $1/B$ (Bollinger *et al.*, 1993; Dubin, 1991).

E. Confinement and heating

The rotation frequencies for typical trapped antimatter plasmas in the slow-rotation mode range from tens of kilohertz to megahertz. This follows from Eq. (5) and Eq. (13), for typical densities ranging from 10^{12} to 10^{16} m⁻³ and magnetic fields from 0.01 to several tesla. This relatively rapid rotation is required in order to produce the Lorentz force necessary for radial confinement. Thus any process that reduces the plasma's rotation rate will reduce the radial confining force and cause the plasma to expand until it comes in contact with the wall and annihilates. For example, collisions between the plasma and a neutral background gas produce a drag on the rotating plasma. As discussed in Sec. II.E, this transport mechanism has been studied in some detail. However, when the neutral gas pressure is reduced to sufficiently low levels (e.g., UHV), other processes appear to determine the expansion rate (cf. Sec. II.E).

Any external force with a θ component will produce a torque on the plasma, changing the canonical angular momentum, and thus changing the rotation frequency through Eq. (35). A force that acts opposite to the direction of

rotation, such as the neutral gas drag, will slow the plasma rotation. Similarly, a force caused by a static asymmetry in the external fields will also act as a drag on the plasma. It is currently believed that particle loss rates in UHV, for example, are caused by such asymmetries (Sec. II.E). For example, if the external potential ϕ_{ext} or magnetic field \mathbf{B} is not θ -symmetric (due, say, to slight misalignments of the electrodes or solenoid) there will be a torque on the plasma,

$$\frac{dP_\theta}{dt} = -q \int d^3r d^3v f(\mathbf{r}, \mathbf{v}, t) \left(\frac{\partial \phi_{\text{ext}}}{\partial \theta} - \frac{\mathbf{v}}{c} \cdot \frac{\partial \mathbf{A}}{\partial \theta} \right), \quad (59)$$

where $\mathbf{A}(\mathbf{r})$ is the vector potential. This integral would vanish if the fields were independent of θ , or if the distribution function were θ -symmetric; however, any asymmetry in ϕ_{ext} and/or \mathbf{A} produces a corresponding asymmetry in f that acts to create a nonzero torque.

The asymmetries in f are typically largest near the surface of the plasma, since Debye-shielding tends to reduce their effect in the interior. Hence, the torque and plasma heating are concentrated near the plasma surface. However, an important exception to this occurs when the field error excites a plasma mode or modes. Modes with $m_\theta \neq 0$ can be resonantly excited by a field error when their frequency is zero (as seen in the lab frame), producing large $m_\theta \neq 0$ perturbations throughout the plasma column that increase the torque and heating (Bollinger *et al.*, 1993; Danielson and Surko, 2006a; Heinzen *et al.*, 1991; Keinigs, 1981, 1984).

These modes are waves traveling against the rotational velocity of the equilibrium plasma, so that they are stationary perturbations in the lab frame. Such so-called zero frequency modes (ZFM) are exceptionally deleterious for confinement (Sec. V.A.2). Fortunately they occur only for special combinations of the plasma length, radius and density which can be determined by setting $\omega = 0$ in Eqs. (55) or (56).

If the asymmetry force is small, so that the system remains close to thermal equilibrium during the expansion process, general arguments imply that the rate of change of angular momentum can be written

$$\frac{dP_\theta}{dt} = \int d^3r \omega_r \mu(r, z, t), \quad (60)$$

where μ is a non-negative transport coefficient and ω_r is the plasma rotation rate as determined in terms of the density, temperature, and electric field by Eq. (23) (Dubin, 2008). The functional form of μ depends sensitively on the form of the external fields, and is a subject of current research. However, the fact that μ is nonnegative (which follows from the second law of thermodynamics) and that ω_r/Ω_c is also nonnegative [see Eq. (6)], implies that static field errors act to slow the plasma rotation; from Eq. (60), $\Omega_c dP_\theta/dt \geq 0$. When combined with Eq. (36) this implies $\partial/\partial t (\omega_r/\Omega_c) \leq 0$.

In spite of more than three decades of work, a predictive theory of transport in single component plasmas (beyond that due to gas scattering) in experimentally realizable PM traps has yet to be developed. As discussed in Sec. IV.D.1, experiments on electron plasmas measured the loss rates for plasmas in different Penning traps and established an approximate scaling with the plasma length and magnetic field (Driscoll and Malmberg, 1983; Malmberg *et al.*, 1982). However, more recent experiments, designed specifically to study trapped particle effects, indicate a more complex picture in which several different types of neoclassical radial particle transport compete (Dubin and Tsidulko, 2011; Kabantsev and Driscoll, 2010; Kabantsev *et al.*, 2010).

It is currently thought that small axial variations in the magnetic field and/or external potential act to trap particles axially, producing separate populations of trapped and passing particles. Asymmetry fields have different effects on the separate populations, causing strong gradients in the velocity distribution function f across the separatrices that separate these populations from one another in phase space. These gradients in f drive strong radial transport as collisions act to return f to an equilibrium Maxwellian form. The overall conclusion is that trapped particles, due to extrinsic asymmetries, likely play an important role in determining the level of outward transport in PM style traps.

In addition to plasma expansion, static field errors also cause plasma heating. One way to understand this effect is to note that, because the errors are static, the total plasma energy ε , given by Eq. (34), is still a constant of the motion even though P_θ is not. As the plasma expands radially, its electrostatic potential energy decreases, and since ε is constant, this reduction must be made up for by an increase in the plasma thermal energy; in other words, the field error converts potential energy into kinetic energy, heating the plasma.

A quantitative thermodynamic approach has been developed, again assuming that the system remains close to thermal equilibrium as the plasma evolves. In this case, an entropy function $S(\varepsilon, P_\theta)$ can be defined that satisfies (Dubin and O'Neil, 1999)

$$TdS = d\varepsilon + \omega_r dP_\theta, \quad (61)$$

which is analogous to the well-known TdS equation for a gas, $TdS = dE + pdV$. For processes caused by static

asymmetries of interest here, $d\varepsilon = 0$ so Eq. (61) can be written as

$$T \frac{dS}{dt} = \omega_r \frac{dP_\theta}{dt}. \quad (62)$$

The second law for an isolated system with $d\varepsilon = 0$ requires that $TdS \geq 0$, which implies $\omega_r dP_\theta/dt \geq 0$; in other words, the torque dP_θ/dt from static asymmetries must act to oppose the rotation velocity $v_\theta = -r\omega_r$, as discussed previously in relation to Eq. (60). Substituting for the torque from Eq. (60) yields $\int d^3r \mu(r, z, t) \omega_r^2 \geq 0$, proving that the transport coefficient μ is nonnegative.

More generally, if processes (such as radiation) are also acting so as to cause energy change, the rate of change of entropy given by Eq. (62) can be related to the rate of change of plasma temperature by applying various Maxwell relations, the result is (Dubin and O'Neil, 1999)

$$c_{P_\theta} \frac{dT}{dt} = \left(\omega_r - T \left. \frac{\partial \omega_r}{\partial T} \right|_{P_\theta} \right) \frac{dP_\theta}{dt} + \frac{d\varepsilon}{dt}, \quad (63)$$

where $c_{P_\theta} = d\varepsilon/dT|_{P_\theta}$ is the plasma specific heat at constant angular momentum, a positive-definite quantity. For a cold plasma many Debye lengths in radius, the second term in the parenthesis is small compared to the first, and for a large ideal plasma with $N \gg 1$, it has been shown that $c_{P_\theta} = Nk_B d/2$ where d is the number of degrees of freedom for an individual particle; for point charges $d = 3$. In this case Eq. (63) can be written as

$$\frac{3}{2} Nk_B \frac{dT}{dt} = \omega_r \frac{dP_\theta}{dt} + \frac{d\varepsilon}{dt}, \quad (64)$$

yielding the rate of change of plasma temperature due to external torques and/or processes that cause energy changes. Since $\omega_r \frac{dP_\theta}{dt} \geq 0$ for static field errors, the first term on the right hand side must lead to heating; while the second term can cause either heating or cooling depending on its sign.

F. Radial compression with rotating electric fields

As discussed further in Sec. VI.A, the deleterious effects on plasma confinement due to field asymmetries can be reduced or even reversed using a technique called the ‘‘rotating wall’’ (RW) (Huang *et al.*, 1997). The name refers to the following concept: a trap with an arbitrarily large external field asymmetry can still confine the plasma if the entire trap is made to rotate at the desired plasma rotation rate. While rotating the trap (and solenoid) at tens or hundreds of kilohertz or faster is impractical, it is possible to mimic a rotating trap by creating an asymmetry field that rotates.

If the field rotates faster than the plasma, the resulting torque will act to increase the plasma rotation rate, opposing the effect of static field errors. This can be understood by considering the energy ε' as seen in a frame rotating with the field, at a constant rate ω_{RW} . The energy ε' is related to the laboratory frame energy ε by $\varepsilon' = \varepsilon + \omega_{RW} P_\theta$. When this result is applied to Eq. (61), the TdS equation becomes

$$TdS = (\omega_r - \omega_{RW}) dP_\theta + d\varepsilon'. \quad (65)$$

Since the rotating perturbation is static in this frame, ε' is a constant of the motion (in the absence of other energy loss processes such as radiation), thus $d\varepsilon' = 0$. The second law then implies

$$(\omega_r - \omega_{RW}) dP_\theta/dt \geq 0, \quad (66)$$

so the sign of the torque due to the rotating field depends on whether field rotation frequency ω_{RW} is greater or less than ω_r . When $\omega_{RW} > \omega_r$, $dP_\theta/dt \leq 0$ implying that the torque acts to increase the rotational velocity $v_\theta = -r\omega_r$.

In current rotating wall designs, the rotating field is electrostatic, produced by suitably phased sinusoidally-varying time-dependent potentials applied to one or more azimuthally-sectored electrodes (see Sec. VI.A). At least $2l$ equal sectors are required in order to produce a rotating field with a dominant θ dependence of the form $\sin[l(\theta - \omega_0 t)]$. The more sectors one uses, the closer the field can be to the purely rotating form assumed above.

Because a rotating field is time-dependent, it does work on the plasma, causing heating (since $TdS/dt \geq 0$). Therefore, some mechanism to cool the plasma is necessary. As discussed in Sec. VI.A, various cooling mechanisms have been used: for leptons, cyclotron radiation and inelastic collisions with a molecular buffer gas, and for pure ion plasmas, laser cooling.

III. POSITRON SOURCES

Positrons for laboratory use are produced either by radioactive decay or pair production. Decay by positron emission can occur for nuclei that have a deficiency of neutrons. Pair production occurs when particles having kinetic energy of more than twice the electron rest mass interact with a heavy nucleus. In both cases, the resulting positrons possess a broad range of kinetic energies up to and above the electron rest mass and must be moderated to low energies in order to be utilized in traps.

A. Radioisotope sources

1. Nuclide selection

The selection of nuclides for radioisotope sources is determined by several factors. Most important are the half life, branching ratio for positron emission *vs.* the competing decay mode of electron capture, the end point of the positron energy spectrum, and the energy and intensity of any accompanying high energy gamma rays emitted with the positron. Table I shows a selection of positron emitting nuclides that have either been demonstrated or discussed as positron sources together with the most important parameters.

The nuclides are produced by irradiating suitable targets in nuclear reactors or ion accelerators. Following this, the desired nuclide is separated by chemical means and deposited on a substrate.

For portable positron sources, a longer half-life is a desirable feature since it minimizes the frequency at which the source must be replaced and, hence, the attendant risks in transporting and handling radioactive material. On the other hand, an excessively long half life means a lower specific activity, i.e, that a larger mass of the nuclide is required to produce a given activity. This means that positrons produced below the surface of the source must penetrate a greater thickness of material leading to increased self absorption. The obvious remedy of reducing the source thickness and increasing its diameter is unsatisfactory, since it leads to larger diameter beams. The most widely used nuclide is ^{22}Na since its properties represent the best overall compromise of parameters.

2. Encapsulated

For many applications positron emitting nuclides can be employed as portable encapsulated sources designed to function in an ultrahigh vacuum environment. Isotopes that are available in low vapor pressure metallic form such as ^{58}Co can be plated into a metal substrate. High vapor pressure materials can be sealed in a vacuum tight capsule behind a thin foil window that transmits high energy positrons.

The radioactive material is usually deposited on a high- Z substrate to increase positron emission through reflection. In some cases a low- Z material with poor reflection properties such as beryllium is deliberately chosen in order to improve the polarization of the emitted positrons. Encapsulated ^{22}Na sources have been manufactured commercially with activities up to 150 mCi. However current commercial sources are limited to ≤ 50 mCi (Krause-Rehberg *et al.*, 2004; van der Walt and Vermeulen, 2004). This has motivated efforts, discussed below, to create more intense sources at nuclear reactors or using particle accelerators. Other encapsulated sources that have utilized are ^{58}Co (Vallery *et al.*, 1994) and ^{68}Ge (Skalsey and Vanhouse, 1988)??

3. Reactor based

While encapsulated sources with half lives of months to years are convenient for small-scale devices, they are limited to activities of less than one Ci because of self absorption and safety issues. If higher positron fluxes are required, the sources must be utilized at the facility where they are produced. In this case short half-life isotopes are preferred because of the mitigating effect on self absorption. One approach is to use isotopes produced by neutron capture in a nuclear reactor. This approach was demonstrated by (Lynn *et al.*, 1987) at the Brookhaven high flux reactor who developed a high intensity positron beam using reactor produced ^{64}Cu . Other potential isotopes for reactor-based sources include ^{79}Kr (Mills, 1992) and ^{126}I (Skalsey and Vanhouse, 1988).

4. Ion accelerator based

Another method of producing large activities of short-lived positron emitting nuclides for facility use is to irradiate a suitable target material with high energy particles—usually protons, deuterons or alpha particles—produced by ion accelerators. Required energies range from less than 1 MeV to greater than 60 MeV depending on the reaction involved. The most widely-exploited nuclide is ^{13}N which can be produced by the reaction $^{12}\text{C}(d,n)^{13}\text{N}$ (Hunt *et al.*, 2002; Xie *et al.*, 1994). This is convenient for smaller facilities because of the low threshold energy and large cross section which reduces the cost of the required accelerator. Other ion accelerator based sources have utilized ^{27}Si (Hirose *et al.*, 1995), ^{18}F (Saito *et al.*, 2000), ^{11}C (Stein *et al.*, 1974) and $^{68}\text{Ge}/^{68}\text{Ga}$ (Maekawa *et al.*, 2013).

5. Spin polarized positrons

Due to parity non-conservation in the weak interactions, positrons emitted from a radioisotope with velocity v have a fractional degree of polarization P in the direction of \vec{v} , $P = \pm v/c$, where c is the speed of light (Jackson *et al.*, 1957). While backscattering in the source and other effects can potentially dilute this effect (e.g., to $\leq 50\%$), positrons from ^{22}Na have been shown to have a polarization of $\sim 70\%$ and those from $^{68}\text{Ge} \sim 94\%$ (Coleman and Potter, 2008). Use of moderators (Sec. III.C) does not appreciably dilute the polarization. This technique is expected to play a key role in efforts to create a positronium-atom BEC (Sec. VIII.C.1.c) (Cassidy *et al.*, 2010a).

B. Pair production sources

Positron production using the pair production process offers an alternative to radioisotopes for high flux positron sources. Pair production occurs when a gamma ray photon of suitable energy interacts with a charged particle, usually an atomic nucleus. Since the pair production cross section scales approximately as Z^2 , the most useful target materials are high- Z elements such as Ta, W and Pt.

1. Electron accelerators

One method of generating the high-energy gamma rays required for pair production is to employ bremsstrahlung generated when energetic electrons are decelerated in a beam dump (Howell *et al.*, 1987). The power deposition in the beam dump is substantial (typically tens of kW), and so refractory metals such as Ta, W and Pt are preferred as targets. Since these same materials are also suited for pair production, it is possible to design an integrated beam dump that acts both to produce the gamma rays and convert them into positrons.

Several facilities of this type are currently in operation around the world with electron energies from about 15 MeV to 1.3 GeV (Jungmann *et al.*, 2013; Krause-Rehberg *et al.*, 2008; O'Rourke *et al.*, 2011; Wada *et al.*, 2012; Wang *et al.*, 2008). It is also possible to obtain useful positron output using more modest electron accelerators. For example, Mills *et al.* (1989) demonstrated the production of positron bunches using 18.5 MeV electrons from a microtron accelerator. Finally, a low-energy (4.3 MeV) commercial, table-top electron accelerator has been developed (Liszkay *et al.*, 2013; Rey *et al.*, 2013) that will be used as a positron source for the GBAR experiment at CERN (Debu, 2013) (see Sec. VIII.B).

2. Reactor based pair production

Another source of high energy gamma rays for pair production is a nuclear reactor. One such source utilizes gamma rays from fission products to generate positrons in a converter consisting of thin tungsten tubes (Falub *et al.*, 2002). Another approach is to use high energy gamma-rays produced by thermal neutron capture. This technique was pioneered in the NEPOMUC source now installed in the FRMII reactor in Munich (Hugenschmidt *et al.*, 2012). As shown in Fig. 6, the converter is surrounded by a cadmium shell where high energy gamma rays are generated by the reaction $^{113}\text{Cd}(n,\gamma)^{114}\text{Cd}$. Platinum foils located within the shell act as both the pair production target and the moderator. Moderated positrons are guided out of the reactor to the user area by a magnetic field. A system of similar design has been installed at the PULSTAR reactor in Raleigh, North Carolina (Moxom *et al.*, 2007).

3. Laser sources

A relatively recent development in positron production is the laser positron source. Two generation mechanisms are possible. For thick, high- Z targets, laser-produced hot electrons make high-energy bremsstrahlung photons that produce electron-positron pairs when interacting with the nuclei, while for thinner targets (e.g., $\leq 30 \mu\text{m}$ of gold), the hot electrons produce pairs directly when interacting with the nuclei (Chen *et al.*, 2009). In a recent thick-target experiment, positrons produced in this manner had an energy spread of 2–4 MeV and a mean energy of 4–7 MeV (Chen *et al.*, 2009). While this technique is still in its infancy, ongoing developments in laser technology have the potential to make this a practical alternative for positron production.

C. Positron moderators

Regardless of their source, the positrons possess large kinetic energies and must be slowed down (“moderated”) if they are to be captured in traps. This process is carried out by injecting positrons into a suitable moderator material. Most of the positrons are lost to annihilation during the process, but a small fraction survives having lost all but a few eV of their original energy (Griffith *et al.*, 1978). Typical parameters of various source/moderator combinations are summarized in Table II.

A variety of metals act as positron moderators, the most widely used being tungsten (Lynn *et al.*, 1985), platinum (Hugenschmidt *et al.*, 2012), nickel (Zafar *et al.*, 1989) and copper (Mills, 1980b). Moderation efficiencies are at most $\sim 10^{-3}$ with positron energy spreads of $< 1\text{eV}$. Other materials that have been discussed as positron moderators include diamond (Al-Qaradawi *et al.*, 2002; Brandes *et al.*, 1997; Mills *et al.*, 1992), silicon carbide (Stormer *et al.*, 1996), gallium arsenide (Shan *et al.*, 1994) and gallium nitride (Jørgensen and Schut, 2008).

The metals may be used in the form of foils (Lynn *et al.*, 1985), meshes (Saito *et al.*, 2002) or solid plates (Vehanen *et al.*, 1983). Both single crystals and polycrystalline materials have been employed with single crystals having higher moderation efficiencies (Gramsch *et al.*, 1987). Metallic moderators require careful surface preparation to achieve optimal performance (Zecca *et al.*, 2010). Foils with precisely selected thickness are used in a transmission geometry where positrons are injected on one side of the foils and moderated positrons are emitted from the other side (Lynn *et al.*, 1985). While this geometry is less efficient than reflection geometry, transport of the moderated positrons away from the moderator is simplified because source shadowing by the moderator is eliminated.

The highest efficiency moderator material currently available is solid neon with an efficiency of $\sim 10^{-2}$ and an energy spread of several electron volts (Mills and Gullikson, 1986). The neon film may be deposited directly over the window on the source capsule but higher efficiencies are obtained if the neon is deposited on a conical surface in front of the window (Khatri *et al.*, 1990). Since solid neon requires temperatures of $< 8\text{K}$, the cost and complexity of the equipment is significantly greater than that of metal moderators. Other rare gas solids (Ar, Kr and Xe) also exhibit positron moderation but with reduced efficiency (Mills *et al.*, 1994).

There have been a number of attempts and proposals to improve the efficiency of moderators by promoting diffusion of thermalized positrons to the moderator surface. The concept is to create an internal electric field to increase positron mobility, leading to a “field-assisted” moderator (Beling *et al.*, 1987; Brandes *et al.*, 1997; Jacobsen *et al.*, 1998). If successful, this concept has the potential to dramatically improve positron yields. While some success has been reported in surface-charged rare gas solids (Merrison *et al.*, 1992), no room temperature field-assisted moderator has been demonstrated to date.

D. Remoderation and brightness enhancement

In addition to moderating primary high energy positrons from positron sources, moderators have also been used to remoderate low-energy positron beams (Mills, 1980a). This technique is used to bypass the phase space focusing limitations imposed by Liouville’s theorem. A moderated positron beam is focused to the phase space limit onto a remoderator. The energy of the incident positron beam is optimized for positron reemission (i.e., $\sim 3\text{keV}$, so that the positrons are implanted into the remoderator to depths less than a few hundred nanometers).

The positrons are moderated in the same way as with a primary moderator, but now the efficiency is much higher (up to 30%) because the positrons are closer to the surface and need to lose much less energy in order to thermalize. Because the re-emitted positrons have a much smaller energy spread than the incident ones, they can be refocused to a smaller spot size. The technique can be repeated several times to produce beams suitable for positron microscopy (David *et al.*, 2001) or to create high positron densities. A gas-phase remoderator with an efficiency of 4% has also been developed (Loewe *et al.*, 2008, 2010).

As discussed in Secs. VI.A and VII, rotating electric fields acting on positron plasmas in Penning style traps (i.e., the “rotating wall technique”) can also be used for brightness enhancement, in this case, without particle loss.

IV. ANTIMATTER TRAPPING AND STORAGE

A. Overview of Penning-style traps

The most widely used traps for positrons (and antiprotons) are based on the Penning trap. This cylindrically symmetric trap employs a magnetic field for radial confinement and an electrostatic potential well for confinement along the direction of the magnetic field. The original geometry described by Penning (1936) is shown in Fig. 7(a). It consists of a cylindrical ring electrode and two disk shaped endcap electrodes. For positron confinement the endcaps are biased positively with respect to the ring, thus creating an electrostatic potential well. Penning’s original work used high negative voltages on the confining electrodes and exploited the fact that this geometry confines ionizing electrons for long times in order to create a cold-cathode discharge for use as a vacuum gauge.

A Penning trap with hyperboloidal electrodes was first proposed by Pierce (1954). He noted that the hyperboloidal geometry would lead to a harmonic potential well for confining particles, which would consequently oscillate axially at a well defined frequency. This geometry was used by Paul (1990) and Wuerker *et al.* (1959) for the first rf traps (“Paul traps”) and later by Dehmelt (1990) to confine single charged particles.

Harmonic Penning traps often incorporate compensation electrodes to correct for finite geometry effects and to null out anharmonicities due to non-ideal effects. In a suitably designed trap, it is possible to carry out this tuning without changing the axial, particle-bounce frequency. These are known as “orthogonalized” traps (Gabrielse, 1983). It is also possible to design accurate harmonic potentials using cylindrical electrodes of appropriate sizes, (including orthogonalization) as shown in Fig. 7(c) (Gabrielse and Mackintosh, 1984).

The closed endcap geometries shown in (b) and (c) have been exploited extensively for fundamental studies using single electrons (Van Dyck *et al.*, 1977), protons (DiSciaccia *et al.*, 2013a), positrons (Schwinberg *et al.*, 1981), and antiprotons (DiSciaccia *et al.*, 2013b). They have also been used to confine single ions and small clouds of laser-cooled ions (Bollinger *et al.*, 1994; Wineland *et al.*, 1987).

However, for many applications, open endcap designs are preferred because they provide easier experimental access to the trapped particles. Byrne and Farago (1965) first used a Penning trap with open cylindrical endcaps to produce polarized pulses of electrons. The ring electrode of their trap was relatively short so as to approximate a harmonic potential. Malmberg introduced a similar geometry incorporating an extended ring electrode for the study of pure electron plasmas (Malmberg and DeGrassie, 1975).

In this “Penning-Malmberg” (PM) trap [Fig. 7(d)], for large numbers of particles, the radial electric field in the charge cloud is dominated by the space charge of the particles instead of that due to the potentials on the electrodes. This type of trap has been extensively used for the study of a variety of topics in plasma physics (O’Neil, 1995). The open-endcap geometry can also be designed to produce an orthogonalized harmonic potential as shown in Fig 7(e) (Gabrielse *et al.*, 1989b).

As shown in Fig. 8 Penning traps may also incorporate one or more azimuthally segmented electrode for detection or excitation of plasma waves (DeGrassie and Malmberg, 1980) or the application of rotating electric fields (Sec. VI.A) for plasma compression (Anderegg *et al.*, 1998; Huang *et al.*, 1997).

The most recent development in Penning trap design is the multi-ring trap (MRT) (Higaki and Mohri, 1997; Mohri *et al.*, 1998). As shown in Fig. 7(f), it consists of many short cylindrical electrodes. This architecture permits the potential along the axis of the device to be accurately tailored by applying a suitable bias voltage to each of the electrodes. For example, the trap can be readily converted from a square well potential to a harmonic one (Mohamed *et al.*, 2013). It is also useful for harmonic-potential time bunching as described in Sec. VII.D.1.

B. Accumulation techniques

In order for positrons from sources such as those described in Section III to be trapped in a Penning trap, some energy loss mechanism is required. While numerous techniques have been developed or proposed to do this, the most widely used technique is the buffer gas trap developed by Surko *et al.* (1989), or a variant of it.

1. Buffer gas traps

Positrons can be efficiently accumulated in a Penning trap using inelastic scattering collisions with a suitable buffer gas (Murphy and Surko, 1992), often referred to as a buffer-gas trap (BGT). A typical trap geometry is shown in Fig 9. The trap consists of electrodes of increasing diameter that create three stages of progressively lower gas pressure and electrostatic potential. A high pressure of the buffer gas is maintained in stage I by continuous gas feed with differential pumping so that there is a high probability of incoming positrons making a trapping collision (indicated “A”) on a single pass. The trapped positrons then make further inelastic collisions (“B”) in stage II and finally in stage III (“C”), where the pressure (and hence the annihilation rate) is lowest. The positrons cool to room temperature in stage III.

The trap can be operated using various buffer gases, but it has been found that the most efficient energy loss mechanism is electronic excitation of the $a^1\Pi$ state of nitrogen at 8.8 eV (Marler and Surko, 2005a). As discussed in Sec. VIII.D.2, while the cross section for this process rises rapidly for energies above the threshold, there is a competing loss mechanism, namely positronium formation, which has a similar onset energy. Thus, for optimal trapping efficiency, the positron energy is tuned to ~ 1 V above the threshold, where electronic excitation dominates.

While nitrogen is an efficient gas for positron capture, it is relatively inefficient for cooling the positrons once they have been captured, since its cross sections for vibrational excitations—the principal mechanism for cooling the trapped positrons—are relatively small. It has been found that the addition to the third stage of the trap of gases that have high cross sections for vibrational excitation dramatically decreases the cooling time to room temperature. The most efficient gases used to date for this purpose are CF_4 and SF_6 (Greaves and Surko, 2000; Marler and Surko, 2005b).

As discussed in Sec. VIII, buffer gas traps are now employed in areas such as atomic and molecular physics (Gribakin *et al.*, 2010), dense positronium states (Cassidy *et al.*, 2005), antihydrogen formation (Comeau *et al.*, 2012; Jørgensen *et al.*, 2005) and materials science studies (Sullivan *et al.*, 2010).

Using the three stage design described above, several hundred million positrons can be accumulated with lifetimes of several minutes (Surko *et al.*, 1999). Recently, 4×10^9 positrons were confined in electrodes at 1.2 K in a region where the background pressure was estimated to be $\leq 8 \times 10^{-17}$ mbar, which will be good enough for year-long $\bar{\text{H}}$ confinement (Fitzakerley *et al.*, 2013). In cases where smaller numbers of positrons are required, it is possible to design a simpler and more compact trap with only two stages (Cassidy *et al.*, 2006a; Clarke *et al.*, 2006; Sullivan *et al.*, 2008). In this case, positron lifetimes are reduced to ~ 1 s but with significant reduction in cost and size of the overall system, since the large diameter third stage electrodes are eliminated. This reduces the size of the required solenoid magnet, which is a major cost of the system.

The final stage of the trap can also incorporate a rotating electric field for compressing the positrons radially (Cassidy *et al.*, 2006a; Greaves and Moxom, 2008; Isaac *et al.*, 2011) as described in Sec. VI.A. Positron cloud diameters of less than 1 mm can be easily obtained using this technique.

2. Trapping in UHV

For cases where it is desirable to avoid a buffer gas, a number of positron trapping techniques have been developed. However, the trapping efficiencies of those techniques are typically orders of magnitude less than the buffer gas technique.

a. Electronic damping. Schwinger *et al.* (1981) were the first to trap positrons in a Penning trap from a radioactive source. Trapping was achieved by coupling the axial motion of the positrons to an external resistor incorporated into a network tuned to resonate with the axial bounce frequency. Haarsma *et al.* (1995) further refined this technique.

b. Ps field ionization. Rydberg positronium atoms can also be used for trapping. Electric fields are arranged in the trap sufficiently strong to field-ionize the Rydberg-Ps atoms, and the positrons are then trapped *in situ* (Baker *et al.*, 2008; Estrada *et al.*, 2000; Jelenković *et al.*, 2003).

c. Moderator ramping. Positrons from a moderator can be trapped in Penning trap if the potential on the moderator is steadily increased at a slow rate that is sufficient to prevent reflected positrons from returning to the moderator. The collection time is limited by the total voltage swing that is available although the cycle can be repeated to create a pulsed beam (Conti *et al.*, 1990).

d. Chaotic orbits. Positrons injected into a Penning trap from a vane moderator can be made to undergo chaotic orbits in the trap so that the particle kinetic energy resides in motion perpendicular to the field (Ghaffari and Conti, 1995). Strictly speaking, this process constitutes a quasi-trapping effect rather than true trapping, since the particle motion will eventually re-phase to permit the positrons to leave the trap.

e. Collisions with trapped ions. Positrons injected into a Penning trap containing laser-cooled ions can lose sufficient energy from collisions with the ions to become trapped. In the experiment of Jelenković *et al.* (2003), positrons from a ^{22}Na source were brought through a thin Ti window, then slowed with a Cu moderator, with Coulomb collisions on $^9\text{Be}^+$ ions providing the trapping mechanism. An interesting feature of this technique is that there is centrifugal separation of the ions and positrons with the positrons concentrating in the center of the trap. This effect can be exploited to brightness-enhance positron beams extracted from the trap.

f. Collisions with electrons. Oshima *et al.* (2004) demonstrated that positrons can be trapped by collisions in a dense electron plasma. They found that the presence of H_2^+ ions in the trap significantly increases the trapping rate. They reported trapping efficiencies of up to 1%. This is the highest trapping efficiency from a continuous positron source reported to date using a UHV-compatible technique.

If only small numbers of positrons are required in a UHV environment, the non-buffer-gas techniques described above are useful. However, if large numbers of positrons, or high throughput rates are required, it is generally preferable to use a BGT and isolate it from the experimental region using differential pumping techniques (Comeau *et al.*, 2012; Jørgensen *et al.*, 2005).

3. Other trapping techniques

a. From pulsed sources. For LINAC-based positron sources a simple trapping technique that exploits the pulsed nature of the source can be used. This involves dropping the potential on one of the end caps to permit a positron pulse to enter the trap and then pulling the potential high before the pulse has time to escape. While efficient positron capture requires the incoming pulse to be less than twice the trap length, this condition is usually met for currently available sources. The technique has been employed for “pulse stretching” on LINAC based sources, i.e., for the creation of quasi-steady state beams (Segers *et al.*, 1994).

b. Using a magnetic mirror. The first experiment in which positrons were trapped in a magnetic mirror device was that of Gibson *et al.* (1960) (cf., Sec. IV.D.2.c and Fig. 1). The positrons were released into the mirror field from radioactive neon injected into the device. Positrons outside the loss cone were confined, and confinement times as long as 10 s were measured for relativistic positrons with a broad spectrum of energies up to ≥ 1 MeV. Other experiments with magnetic mirrors are discussed in Sec. VIII.C.2.d.

C. Positron cooling

Similar to positron loss due to annihilation, higher positron temperatures are also typically associated with increased diffusive particle loss. Consequently, an effective cooling mechanism is an absolute necessity for good confinement. Cooling methods available include use of inelastic positron collisions with molecules (i.e., vibrational and/or rotational excitation), cyclotron emission in several tesla magnetic fields, and evaporative cooling. Since evaporative cooling is sacrificial in nature and results in positron loss, it is used only when necessary.

1. Buffer-gas cooling

This technique is simple to implement and relatively efficient. The drawback is that the gas molecules represent sites of annihilation, and so accumulation and storage times are limited. As described above, to avoid Ps formation, positron temperatures are restricted to $T \leq 1$ eV. Since electronic excitation of atoms and molecules requires more energy than this value, cooling must be done using lower energy modes such as molecular vibrational and rotational levels.

Two molecular transitions with particularly large vibrational excitation cross sections are the asymmetric C-F stretch mode in CF_4 and S-F stretch mode in SF_6 (i.e., ν_3 modes at 0.16 and 0.12 eV, respectively) (Greaves and Surko, 2000, 2001; Marler and Surko, 2005b), and so they are routinely used for positron cooling. The cross section for the ν_3 mode of CF_4 is shown in Sec. VIII.D.2, Fig. 51. One caveat is that this energy loss is quantized. Below the mode energy, positrons must cool by exciting other vibrational modes and/or rotational modes. Experimental cooling times for selected molecular gases are summarized in Table III. Petrović and collaborators have simulated positron cooling in BGT's (Banković *et al.*, 2008; Marjanović *et al.*, 2011; Petrović *et al.*, 2013). Presently the accuracy of the simulations is limited by incomplete knowledge of the relevant cross sections (Petrović *et al.*, 2013).

Another facet of gas cooling is that the collisions transfer momentum and, hence, can lead to outward transport. A situation in which this effect can be particularly important is where the plasma density approaches the Brillouin density n_B (Surko *et al.*, 2010). Here, the space-charge electric field E leads to preferred outward excursions upon each collision with the step length $r_E = E(B\omega_c)^{-1}$. Near the Brillouin limit, r_E can be large compared to the positron gyroradius. Estimates indicate that this effect will make it very difficult to approach to within a factor of five or so of n_B (Surko *et al.*, 2010).

2. Cyclotron cooling

An alternative cooling mechanism relies on cyclotron radiation in a large magnetic field (O'Neil, 1980a). The characteristic cooling rate is given by

$$\Gamma_c \equiv \frac{1}{T} \frac{dT}{dt} = \frac{2e^2\Omega_c^2}{9\pi\epsilon_0 mc^3} \simeq 0.26 \left(\frac{B}{1 \text{ tesla}} \right)^2 \text{ s}^{-1}. \quad (67)$$

As illustrated in Fig. 10, for example, the characteristic cooling rate in a 5 T field is approximately 6 s^{-1} . While this is modest compared to what can be done using gas cooling at a cooling gas pressure $\sim 10^{-6}$ torr, cyclotron cooling has the distinct advantage that it can be done in UHV thus avoiding losses due to annihilation and collisional transport. Moreover, by cooling the surrounding electrodes to cryogenic temperatures, one can create a cryogenic positron plasma. There is some evidence that the simple expression in Eq. (67), which is strictly valid only in free space, is not obeyed at low magnetic fields (e.g., $B \leq 2 \text{ T}$) (Beck, 1990; Weber, 2010), but this has not yet been studied carefully.

3. Evaporative cooling

Controlled evaporation of particles from a trap can also be used to produce significant cooling of the remaining cloud since the highest energy particles are preferentially released. If the release is carried out on a timescale that is slow with respect to the thermal equilibration time of the trapped particles, this process can be quite efficient. Andresen *et al.* (2010) demonstrated the evaporative cooling of trapped antiprotons to temperatures as low as 9 K. The technique is likely to be especially useful for the final step in preparing antiprotons and positrons for low-energy antihydrogen production [Sec. VIII.A.2].

4. Sympathetic cooling

It is also possible to cool positrons sympathetically by placing them in thermodynamic contact with a second species. Jelenković *et al.* (2003) placed positrons in the same trap with laser-cooled ${}^9\text{Be}^+$ ions. Positron temperatures $\leq 5 \text{ K}$ (0.4 meV) were achieved in a trap at room temperature. Parallel temperatures as low as the Doppler laser cooling limit (0.5 mK in Be^+) are possible. At such low temperatures the modes of the positron plasma must be treated quantum mechanically. This technique has been proposed to achieve lower positron temperatures for antihydrogen production (Madsen *et al.*, 2013). Another example of sympathetic cooling is the use of electrons to cool antiprotons for antihydrogen production (Sec. VIII.A.2).

D. Long-term antimatter storage

1. Loss processes

For many applications, one would like to accumulate large numbers of positrons, either to deliver them in bursts or store them for later use. This raises the critical issue of positron loss due to transport and annihilation. So-called “direct” annihilation occurs due to overlap of the positron and electron wave functions during a simple collision. In a good quality UHV vacuum, this mechanism is relatively benign. For example, the annihilation time for molecular nitrogen at 10^{-6} torr is 100 s (i.e., typical of the third stage of a BGT), and for molecular hydrogen at a pressure of 3×10^{-10} torr, it is approximately one week (cf. Sec. VIII). Care must be taken, however, to remove even small quantities of large molecules from the system (e.g., grease or oil molecules); since, as discussed in Sec. VIII.D below, positrons can attach to those species in two-body collisions, leading to much higher annihilation rates.

Another important loss process is positronium-atom formation due to positron-molecule collisions. The threshold energy (typically a few electron volts) is the impurity molecule ionization energy minus the positronium binding energy of 6.8 eV. If the positron distribution has a high-energy tail, positrons will continually be lost to Ps formation followed promptly by annihilation. Taking this effect and the molecular species likely to be in a typical vacuum system into consideration, a safe operating condition is positron temperatures $T \leq 1$ eV.

As discussed in Sec. II.E, a separate consideration is positron loss due to transport out of the trap. Any external force with a θ component will exert a torque on the plasma causing it to expand radially. One source of such a torque is the viscous drag on the plasma due to collisions with the neutral background gas. This effect was investigated by Malmberg and Driscoll (1980) who measured electron plasma confinement times as a function of helium pressure for a range of magnetic fields (Fig. 11). However, at sufficiently low pressures, the confinement time is independent of gas pressure and is dominated by other effects. As the pressure is increased, plasma transport induced by gas collisions dominates and the confinement time then scales inversely with gas pressure.

A less obvious source of a drag force arises from the static asymmetries in the trap caused by patch fields on electrodes, machining imperfections, etc. Such asymmetries apply a torque to the plasma leading to plasma expansion. Early experiments on electron plasmas measured the scaling of the expansion rate for plasmas in several different Penning trap designs. Results for the radial expansion rate roughly follow the “Driscoll curve” (Driscoll and Malmberg, 1983; Malmberg *et al.*, 1982)—an $(L/B)^2$ scaling law where L is the length of the plasma.

Asymmetry induced transport is also known to exhibit a density dependence $\Gamma_0 \sim n^2$ (Driscoll *et al.*, 2003). This dependence is unfavorable for the confinement of high density positron plasmas in trap. However, Danielson and Surko (2006b) have identified a new transport regime that occurs at higher density, where the expansion rate becomes independent of density. This is illustrated in Fig. 12. As can be seen in the figure, the data in this regime also exhibit a weaker length dependence (closer to L^1 than L^2). The nature of the transition to this new regime is not clear at present: it appears to be associated with both a rapidly rotating plasma and a plasma in which the inter-particle collision rate ν_c is faster than the bounce frequency f_b . A similar regime has also been observed in laser-cooled ion plasmas at low temperatures (Hollmann *et al.*, 2000).

The theoretical situation regarding such transport is reviewed in Sec. II.E. Model transport experiments and related theory indicate that several different types of neoclassical radial transport (due to trapped particles) are likely operative (Dubin and Tsidulko, 2011; Kabantsev and Driscoll, 2010; Kabantsev *et al.*, 2010). Small axial variations in the magnetic field and/or external potential acting to trap particles, producing separate populations of trapped and passing particles, and strong gradients in the velocity distribution function across these separatrices drive strong radial transport.

Thus practical antimatter trapping schemes must find methods to either live with, or mitigate, significant levels of outward radial particle transport. One possible approach is to create strong (cylindrically symmetric) gradients in B and/or the external potential ϕ_{ext} to eliminate any electrostatic or magnetic wells in the external fields. Another approach, now frequently employed, is to use rotating electric fields for radial compression (the RW technique, Secs. II.F and VI.A) to counter the outward transport.

2. Traps for long-term confinement

a. Penning-Malmberg traps. The focus here is on achieving long-term storage of low-energy positrons (e.g., confined for days or more). Currently, the method to accomplish this is use of a PM trap or some variant of it. To avoid annihilation, a high-quality UHV environment is required (e.g., 10^{-10} – 10^{-11} torr), perhaps using cryogenically cooled electrodes for lower ambient pressures. Currently, this approach has been demonstrated to confine in excess of 10^9 particles for longer than a day (Danielson and Surko, 2006b).

While it is possible to reverse the effects of asymmetry-induced plasma expansion using the rotating wall technique (Sec. VI.A), it is nonetheless desirable to minimize these effects in order to reduce the required amplitude of the RW drive signal which can cause unwanted heating and drive plasma resonances. Significant efforts have been expended to minimize asymmetries in order to reduce plasma losses. These include maintaining high machining tolerances for the electrodes, minimizing patch effects on the electrode surfaces using gold plating and careful alignment of the magnetic field with the geometric axis of the trap.

Mohamed *et al.* (2013) recently demonstrated dramatically improved confinement in a harmonic well. Using an MRT [Fig. 7 (f)], they were able to switch between a harmonic well and a square well configuration while leaving other conditions (including the actual electrodes) unchanged. They observed a lifetime of about 10^4 s for electrons in the harmonic well *vs.* 200 s in the square well. One possible explanation is that the harmonic potential, being monotonic, eliminates the trapped particle effects described above.

On the basis of the current state of knowledge, the preferred trap for accumulating and storing large numbers of positrons would be an MRT configured for a harmonic potential well and operating in the high density regime. The trap would be located in a UHV vacuum chamber and would use a superconducting magnet. Modest application of rotating wall fields could then be used to achieve “infinite” confinement times.

b. Multicell (PM) traps. Both PM and harmonic traps are subject to the space-charge-potential constraint discussed in Sec. II.B. The multicell trap aims to circumvent this using multiple PM traps in close proximity arranged in parallel inside a common solenoid and vacuum system (Danielson and Surko, 2006b; Surko and Greaves, 2003). In such an MCT, one would still need an excellent vacuum, as with the PM trap for long-term confinement. The schematic of a 21 cell trap is shown in Fig. 13, with the parameters listed in Table IV (Danielson *et al.*, 2013). The design goal is to store approximately 10^{12} positrons for days and weeks using kilovolt confining potentials.

Multicell traps based on gold-plated microtrap arrays etched in silicon wafers have also been proposed (Baker *et al.*, 2012). Outstanding issues that must be addressed for this to be a viable approach include enhanced asymmetry-induced transport due to the close proximity of the walls (e.g., electrode diameters ~ 100 μm) and the difficulty in engineering RW compression for very large numbers of cells (e.g., $\geq 10^4$). Cooling is also an outstanding issue, since cyclotron radiation will be evanescent in such small cavities.

c. Magnetic mirrors. The concept of positron confinement in magnetic mirror devices has a long history beginning with the experiment of Gibson, Jordan and Lauer (Gibson *et al.*, 1960). Mills and collaborators used this technique for beam bunching (Chu and Mills, 1982; Mills *et al.*, 1989). Tsytovich and Wharton (1978) proposed its use in conjunction with a relativistic-beam-foil experiment to create, confine, and study pair plasmas. Boehmer *et al.* (1995) employed a mirror device to confine moderated positrons from a ^{22}Na source.

Recently, Higaki *et al.* (2012) began systematic experiments to study single-component electron plasma confinement in the magnetic mirror device illustrated in Fig. 14. Their ultimate goal is simultaneous confinement of electrons and positrons to study pair plasma phenomena. The experiment used a central field of 0.010 T and a mirror ratio $R = 5$. Principal diagnostics include monitoring pick-up on ring and segmented electrodes and dumping plasma onto a phosphor screen. Electron confinement times of 40 ms were achieved for 2×10^7 electrons at a temperature of 1 eV. For such parameters, the charge cloud is just at the threshold of the plasma regime.

While such an arrangement has not yet been used for pair-plasma confinement, magnetic mirrors have considerable promise for studying relativistic pair-plasma phenomena. This is due to the fact that the dominant particle loss mechanism in magnetic mirror devices is the so-called “loss cone”. Namely, particles will be lost in a solid angle in velocity space, oriented along the magnetic axis, of extent $\delta\Omega \sim (\epsilon_{\perp}/\epsilon) = R^{-1}$, where R is the mirror ratio, ϵ_{\perp} is the energy in cyclotron motion, and ϵ is the total particle energy (Chen, 1984). This cone in velocity space will be populated at the Coulomb collision rate ν_c . Thus, losses are expected to decrease rapidly with increasing plasma temperature (i.e., $\nu_c \propto T^{-3/2}$) (Chen, 1984). It is envisioned that one could fill and cyclotron-heat the particles, in which case good confinement could be achieved. Due to the temperature dependence of ν_c , hotter (e.g., relativistic) plasmas will be easier to confine.

d. Stellarators. The stellarator is a plasma confinement device with closed magnetic surfaces. In contrast to the tokamak, which requires an induced current for plasma stability, the stellarator uses external field coils to provide the required twist in the magnetic field. The stellarator has the key advantage that, in principle, it can confine plasmas with arbitrary ratios of positive and negative charge density.

Pedersen and collaborators have developed a simple and compact design for such a device (Pedersen *et al.*, 2006). Illustrated in Fig. 15, the Columbia Nonneutral Torus (CNT) employs four circular coils, two of which are intertwined

and arranged with the normal to the planes of these coils oriented at an angle of 60° to each other (Pedersen *et al.*, 2006). As shown in Fig. 15, the plasma threads around this pair of coils. Operation of the CNT has been demonstrated for both single component electron plasmas (Brenner and Pedersen, 2012), and quasineutral (electron-ion) plasmas (Sarasola and Pedersen, 2012), the former with 90 ms confinement times. As discussed in Sec. VIII.C.2.b, below, plans are being made to study simultaneously confined electron-positron plasmas in a more compact, higher magnetic field version of this device (Pedersen *et al.*, 2012).

e. Levitated Magnetic Dipoles. The levitated magnetic dipole is another closed magnetic geometry. Saitoh and collaborators have been able to hold an electron plasma with density 10^{11} m^{-3} for 300 s (Saitoh *et al.*, 2013; Yoshida *et al.*, 2013). As these authors point out, this device also has considerable promise for the creation and study of pair plasmas.

f. Simple Tori. Stoneking and collaborators have explored single-component electron plasma confinement in a (partial) torus, extending 270° in the toroidal direction (Marler and Stoneking, 2008; Stoneking *et al.*, 2002, 2009). Use of the 270° configuration is motivated by the simplicity with which it can be filled and diagnosed by exploiting access from the ends. A radial electric field in the plane of the torus, imposed by external electrodes, is required to keep the plasma centered vertically. Confinement times of several seconds have been demonstrated for pure electron plasmas at densities of $5 \times 10^{12} \text{ m}^{-3}$. While such a device is unlikely to exhibit confinement superior to a PM trap for a pure positron plasma, a full torus could potentially be useful to study partially neutralized electron-positron plasmas. Recent experiments have begun to explore the dynamics of electron plasmas in the full torus (Stoneking *et al.*, 2013).

3. Trap-to-trap transfer

It is possible to transfer positrons and other particles from one Penning trap to another if they are magnetically connected. The simplest way of accomplishing this is to rapidly drop the potential on the exit gate electrode of the source trap and to capture the pulse of particles in the target trap using the same gate switching techniques used to capture positrons in traps from pulsed sources (Sec. IV.B.3). If the magnetic fields in the two traps are different, then the adiabatic invariant ϵ_{\perp}/B is relevant. In general this is not a problem [e.g., (Jørgensen *et al.*, 2005; Young and Surko, 2006)], but when going from low magnetic fields to high, there is the possibility that the particles will be reflected if the particle transport energy isn't sufficiently large.

Multiple pulses can be captured (“stacked”) as long as the positrons are allowed to cool in the target trap before the next pulse is added. This technique has proven to be a convenient way of extracting positrons from BGT's into UHV environments for antihydrogen production (Comeau *et al.*, 2012; Jørgensen *et al.*, 2005). It is also convenient for producing large positron accumulations from two-stage BGT's, e.g., for dense positronium experiments (Cassidy *et al.*, 2006a). These techniques will be crucial for populating multicell traps (Sec. IV.D.2) and filling portable traps.

4. Portable traps

If it could be made portable, the MCT trap for 10^{12} positrons described above, with confinement and annihilation times exceeding a few weeks, would be at the threshold of a useful portable positron trap. It could be used to transport positrons from an intense source to end users at remote locations. For example, 10^{12} positrons is the equivalent of ~ 80 hours operation of a 20 mCi ^{22}Na source and solid neon moderator. Further, the energy spread of the positrons would be superior by more than an order of magnitude. Such portable traps could avoid issues involved with radioisotope licensing and radiation shielding that can be problematic in many settings and for many end uses.

While one could envision demonstration of a portable positron trap in the near term, it would likely not be very practical.³ However, if there were improvements in magnet technology such that a several-tesla magnetic field could be generated at higher temperatures without the need for expensive cryogenics and/or high-capacity refrigerators, portable traps could be expected to increase the use of positrons in a number of areas, such as the characterization of materials in research laboratories and on chip manufacturing lines.

³ For a heroic early attempt to transport an electron SCP long distances, see Tseng and Gabrielse (1993).

V. DIAGNOSTIC TECHNIQUES FOR POSITRON GASES AND PLASMAS

This Section is devoted to a description of diagnostic techniques that have been developed to measure the parameters of trapped antimatter plasmas such as density and temperature. Most of the techniques are equally useful for trapped positron or electron plasmas, and so many of the techniques that were developed for non-neutral electron plasmas can be directly applied. Here, the focus is on several of the most important and widely used diagnostics including mode-based nondestructive techniques, destructive techniques where either the whole or part of the plasma is ejected, and lastly imaging of the annihilation gammas. Many of these techniques can be, and in some cases have also been, applied to antiproton plasmas.

A. Mode-based nondestructive techniques

As described in Sec. II.D, plasmas exhibit many collective modes of oscillation. The excitation and detection of such oscillations can give important information about parameters of the trapped charge cloud (Bollinger *et al.*, 1993; Dubin, 1991; Heinzen *et al.*, 1991; Tinkle *et al.*, 1994; Weimer *et al.*, 1994). Discussed first are diocotron and Trivelpiece-Gould (TG) modes in cylindrical plasmas. The case of modes in spheroidal plasmas is discussed separately.

1. Diocotron modes

As discussed in Sec. II.D, diocotron modes are z -independent distortions of the plasma column that propagate azimuthally due to the $\mathbf{E} \times \mathbf{B}$ drift created by the perturbed potential (e.g., see Fig. 4 in Sec. II.D). From Eq. (48), for the important case of $m_\theta = 1$, the diocotron frequency can be written to display explicitly the dependence on N/L , the charge per length of the plasma column,

$$\omega_1 = -\frac{N}{L_p} \frac{qc}{4\pi^2\epsilon_0 B r_w^2}. \quad (68)$$

This mode amounts to a rigid displacement of the column off the trap axis rotating about it with frequency ω_1 .

This expression is reasonably accurate for long, cold plasmas (i.e., $r_w/L_p \ll 1$ and $\lambda_D \ll r_p$). However, as shown in Fig. 16, finite-length effects can increase the measured diocotron frequency significantly (Fine and Driscoll, 1998). A more accurate expression for the observed frequency, $\hat{\omega}_1$, is

$$\frac{\hat{\omega}_1}{\omega_1} \approx 1 + \left\{ \frac{j_{01}}{2} \left[\frac{1}{4} + \ln \left(\frac{r_w}{r_p} \right) \right] - 0.671 \right\} \frac{r_w}{L_p}, \quad (69)$$

where j_{01} is the first zero of the Bessel function of the first kind. In Eq. (69), the first term in the curly bracket is due to the confinement field, and the second term is an image charge correction (Fine and Driscoll, 1998). A term that depends on the plasma temperature has been neglected, but is important when $\lambda_D \sim r_p$.

With knowledge of the plasma radius and length, measurement of the linear diocotron frequency, ω_1 , can be used to measure the total charge N nondestructively. By monitoring the diocotron frequency over the course of an experiment, the loss or increase in the number of particles can be measured. Since particle loss is typically associated with changing r_p through plasma expansion, this technique is most useful for only modest changes in the plasma parameters.

These frequencies are accurate for small-amplitude excitation, $d/r_w \ll 1$, where d is the displacement of the plasma column from the axis of symmetry. For larger displacements from the axis the diocotron frequency is nonlinear in d . For $m_\theta = 1$, it is given by

$$\frac{\omega_1^{NL}(d)}{\omega_1} \approx \frac{1}{1 - (d/r_w)^2}, \quad (70)$$

where it is assumed that $(r_p/r_w)^2 \ll 1$ and thus ignores distortions of the cloud (Danielson *et al.*, 2006; Fajans *et al.*, 1999b; Fine and Driscoll, 1998). This nonlinear shift is used in Sec. VI.B to control the plasma position in the plane perpendicular to B .

Higher-order diocotron modes (cf. Fig. 4) can also be excited (Bettega *et al.*, 2007, 2009). For example, the $m_\theta = 2$ diocotron mode can also be a useful density diagnostic. From Eq. (47),

$$\omega_2 \simeq -\omega_r \quad (71)$$

where a term proportional to $(r_p/r_w)^4$ has been dropped. Since $\omega_r \propto n$, measurement of ω_2 gives a nondestructive measure of the plasma density. This technique is routinely used in pure electron plasmas, for example, to monitor plasma transport, using

$$\frac{1}{\langle n \rangle} \frac{d\langle n \rangle}{dt} = \frac{1}{\omega_2} \frac{d\omega_2}{dt}, \quad (72)$$

where $\langle n \rangle$ is the average plasma density (Kabantsev *et al.*, 2010).

2. Trivelpiece-Gould modes

As described in Section II.D, TG modes, are finite k_z , density oscillations of the finite radius plasma column, with a frequency proportional to the plasma frequency (Malmberg and DeGrassie, 1975; Trivelpiece and Gould, 1959). For low temperature plasmas, the dispersion relation for $m_\theta = 0$ modes is [from Eq. (50)]

$$\omega_{\text{TG}} \approx \frac{k_z}{k_\perp} \omega_p \left[1 + \frac{3}{2} \lambda_D^2 k_\perp^2 \right], \quad (73)$$

where, $k_z \approx m_z \pi / L$, k_\perp depends on m_θ and the plasma radius r_p , and it has been assumed that $k_z/k_\perp \ll 1$, as is the case in most experiments. For this case, and assuming $r_p/r_w \ll 1$, k_\perp is given by Eq. (52).

These $m_\theta = 0$ modes can be excited by applying an oscillatory voltage to any cylindrically-symmetric electrode in the proximity of the plasma column. The modes can be detected by observing the oscillating image charge (or image currents) on a separate cylindrically-symmetric electrode. Often, many m_z modes can be detected. Shown in Fig. 17 is a set of $m_\theta = 0$ modes with no radial nodes for m_z up to 10 (Danielson and Driscoll, 1999). Fitting the dispersion relation [Eq. (73)] to these data can give a rough measure of the plasma temperature if the radius and length of the plasma are known.

However, just as for the diocotron modes discussed above, there are finite-length corrections to the TG dispersion relation in Eq. (50). An approximate expression for this correction is $k_z \approx m_z \pi / L_{\text{eff}}$ in Eq. (50) and Eq. (73), where $L_{\text{eff}} \equiv L_p + 0.3r_w + 0.7r_p$ (Jennings *et al.*, 1995). Physically, the wavelength of the axial standing waves on a finite-length column is not quite the plasma length.

The TG modes are strongly Landau-damped in warm plasmas, and thus they are more difficult to detect (Danielson *et al.*, 2004). However, if one of the low m_z modes can be calibrated at low temperatures, then the shift in frequency due to finite T will be proportional to the change in temperature.

The TG modes can also be self-excited by thermal noise and detected with a low-noise amplifier even without applying oscillatory voltages to the electrodes. By measuring the power in the thermal noise spectrum associated with one or more normal modes, the temperature of the plasma can then be obtained fairly accurately (Anderegg *et al.*, 2003; Shiga *et al.*, 2006).

As discussed in Section II.D, the $m_\theta > 0$ TG modes can also be excited and observed using sectorized electrodes. However, these modes are typically not used for diagnostic purposes, but are important in describing field-error transport (e.g., the effect of “zero-frequency modes” in Sec. VI.A.2.a) and the manipulation of plasmas using the rotating wall technique (Sec. VI.A).

3. Spheroidal modes

As discussed in Section II.D, the modes in spheroidal plasmas (e.g., as found in harmonic potential wells), have been analytically calculated by Dubin (1991). From, Eq. (45), the dispersion relation for azimuthally symmetric modes ($m_\theta = 0$) can be written

$$1 - \frac{\omega_p^2}{\omega^2} = \frac{k_2 P_l(k_1) Q_l'(k_2)}{k_1 P_l'(k_1) Q_l(k_2)}, \quad (74)$$

where $k_1 = \alpha(\alpha^2 - 1 + \omega_p^2/\omega^2)^{-1/2}$, $k_2 = \alpha(\alpha^2 - 1)^{-1/2}$, and $\alpha = L/2r_p$ is the aspect ratio of the plasma. P_l , Q_l , P_l' , Q_l' , are Legendre functions of the first and second kinds, and their derivatives, respectively (Tinkle *et al.*, 1994). This dispersion relation for $l = 1$ to 4 was shown in Fig. 5.

The relationship between the harmonic trap frequency, the plasma frequency and the aspect ratio is given by Eq. (56) and is shown as the dashed line in Fig. 5. Combining Eqs. (74) and (56), the mode frequencies (and the plasma

frequency) can be written as solely functions of the plasma aspect ratio (α) and the trap parameters (through the trapping frequency, ω_z) (Bollinger *et al.*, 1993).

Thus, for a cold plasma, measurement of two modes (e.g., the dipole $l = 1$ and quadrupole $l = 2$), can be used to determine α and the plasma density n (from the plasma frequency ω_p). If the total charge is known, the radius, r_p can then be obtained. This effect has been used to measure the plasma parameters of electron and positron plasmas (Amoretti *et al.*, 2003a; Funakoshi *et al.*, 2007; Oxley *et al.*, 2004; Speck *et al.*, 2007; Tinkle *et al.*, 1994). Other experiments have also used the response to a tuned-circuit to independently measure the total charge in the trap (Amoretti *et al.*, 2003b; Feng *et al.*, 1996; Wineland and Dehmelt, 1975).

As discussed in Section II.D, finite temperature corrections have been calculated for these modes in Dubin (1993). Results for the (2,0) and (2,1) modes are given in Eq. (57). Detection of such modes enables non-destructive measurement of the plasma temperature. To do this, most experiments use the (2,0) mode. An example of this temperature dependence for various electron plasmas in a harmonic trap is shown in Fig. 18.

This technique has been successfully used to measure the plasma temperature in a wide range of electron and positron plasmas (Amoretti *et al.*, 2003b; Carraro *et al.*, 2004; Higaki *et al.*, 2002; Tinkle *et al.*, 1994), including the positron plasmas tailored for the creation of low-energy antihydrogen atoms (Funakoshi *et al.*, 2007; Speck *et al.*, 2007). Kuroda *et al.* (2014a) used measurements of the (1,0) and (3,0) modes to study equilibration of antiprotons with an electron plasma following capture.

B. Destructive techniques

Although mode based diagnostics are useful, they may require some form of calibration using a known state of the plasma. Thus it is often desirable to eject all or part of the plasma from the trap to measure plasma properties, such as the number, energy distribution or areal density of the ejected particles, even though this results in antiparticle loss.

1. Gauss' law for plasma length

Most plasma traps consist of stacks of coaxial electrodes. To measure the mean plasma length L_p , a charge sensitive amplifier is attached to a short electrode (labelled here G for Gauss) that covers a portion of the plasma not near the ends (i.e., $L_G < L_p$) (Malmberg and DeGrassie, 1975; Mitchell, 1993). When the plasma is ejected, an image charge signal will remain on electrode G, that will decay with the response time of the amplifier circuit. From Gauss' law, the image charge eN_i on G will be equal to the total charge that was enclosed by the electrode. The total number of trapped particles, N , can be found by ejecting the entire plasma onto a collector plate and measuring the charge with a charge-sensitive amplifier. Knowing N_i and N , the mean plasma length is

$$L_p = L_G \frac{N}{N_i}. \quad (75)$$

This technique is often used to determine the plasma length before measuring the plasma density (described below).

2. Imaging areal density profiles

There are several ways to measure plasma density profiles. All techniques rely on lowering V_c at one end of the plasma rapidly to allow the particles to stream out. Early techniques used arrangements of segmented collector plates or a movable apertured collector and Faraday cup (DeGrassie and Malmberg, 1977, 1980). The technique used now is to accelerate escaping particles with 5–10 keV, then allowing them to impinge on a phosphor screen and imaging the light using a digital camera (Huang *et al.*, 1995; Peurrung and Fajans, 1993). For measurement of small particle numbers, a microchannel plate can be used (Peurrung and Fajans, 1993). Andresen *et al.* (2009) describe detection of electrons, positrons and antiprotons in the same system using this technique.

Examples of such phosphor screen images are shown in Fig. 19. Using this technique, the complete z -integrated plasma profile can be imaged directly, and hence any azimuthal asymmetries of the profile can be studied (Durkin and Fajans, 2000; Fine *et al.*, 1995). Many antimatter plasmas of interest are azimuthally symmetric, in which case the imaged profile can be azimuthally averaged to yield a high resolution radial profile. The main limits to the technique are the amount of light collected and the number of pixels in the camera. Using a cooled, 4 megapixel camera, the typical radial resolution can be 10 μm or less when operating with accelerating voltages ≥ 5 kV and particles per pixel $\geq 10^3$.

If the total of charge is measured using a calibrated charge-sensitive amplifier, the z -integrated density profile can be placed on an absolute scale. Using L_p measured with the Gauss' law technique, the average plasma density can also be determined. Finally, knowing the z -integrated density, the plasma temperature (see below), the trap geometry, and the confining potential, Poisson's equation can be solved to find the absolute, local value of plasma density (Dubin and O'Neil, 1999; Spencer *et al.*, 1993).

3. Particle energy distributions

The other key plasma parameter is the plasma temperature T which, for an equilibrium plasma, sets the distribution of kinetic energies of the plasma particles. In a magnetic field, the energy distribution (and temperature), can be different for motion perpendicular (T_{\perp}) and parallel (T_{\parallel}) to the magnetic field, while in equilibrium, the temperatures are equal, i.e., $T_{\text{eq}} = T_{\perp} = T_{\parallel}$. One of the complications of non-neutral plasmas is that the plasma space charge potential is much larger than the plasma temperature in energy units (i.e., $e\phi_0 \gg T$). Thus, when the plasma is ejected from the trap, the parallel energy spread of the particles is typically dominated by the space charge potential, and direct measurement of the energy of the ejected particles often bears little resemblance to the plasma temperature. However, there are several techniques that have been developed to get around this difficulty. They differ depending on whether the temperature perpendicular or parallel to the magnetic field B is measured.

a. Measurement parallel to B . In general, if the space charge is small (i.e., $\phi_0 \ll T$), then the energy of the ejected plasma particles will be dominated by the applied potential on the trap at ejection. In this case, the spread in energies can be related to T_{\parallel} . As discussed in Sec. VII.B, this principle has been exploited to create high resolution positron beams. In this case, the mean particle energy and the energy spread of the beam can be measured using a retarding-potential-analyzer (RPA) (Gilbert *et al.*, 1997; Hsu and Hirshfield, 1976). However, care must be taken in that the temporal evolution of the plasma during the particle ejection process can alter the energy spread (Natisin *et al.*, 2013). In particular, in the case of rapid particle ejection, the energy spread will still typically be proportional to the plasma temperature, but not exactly equal to T_{\parallel} (Natisin *et al.*, 2013).

When $e\phi_0 \gg T$, the RPA measurement is no longer related simply to T_{\parallel} . In this case, instead of dumping the entire plasma, the confinement potential V_c at one end of the plasma can be lowered slowly while monitoring the number of escaping charges. For a plasma in equilibrium, the escaping particles come from near the radial center of the plasma (Danielson *et al.*, 2007b; Eggleston *et al.*, 1992). Then, when the number of escaping particles is kept small (i.e., $\delta N/N < T/e\phi_0$), the approximate expression for T_{\parallel} in a magnetic field B is

$$T_{\parallel} = -0.95 \left(\frac{\partial \ln N}{\partial V_c} \right)^{-1}, \quad (76)$$

where this expression is typically valid to $\sim 5\%$ (Eggleston *et al.*, 1992). Extensions of this technique have also been used to get information about the radial temperature profile (Aoki *et al.*, 2006; Hart and Peterson, 2006).

b. Measurement perpendicular to B . The standard "magnetic beach" technique can be used to measure the perpendicular temperature (Hsu and Hirshfield, 1976). It relies on the adiabatic invariant of particles in a magnetic field, $E_{\perp}/B = \text{constant}$, and arranging independent control of B in the detector (RPA) region. Using an RPA to measure the mean parallel energy at two magnetic fields, T_{\perp} will be

$$T_{\perp} \approx -B \frac{\Delta E_{\parallel}}{\Delta B}. \quad (77)$$

This has been used to measure T_{\perp} in both non-neutral electron plasmas (DeGrassie and Malmberg, 1980; Hyatt *et al.*, 1987) and positron plasmas (Natisin *et al.*, 2013; Tinkle *et al.*, 1994).

4. Annihilation gamma-ray imaging

A special advantage in the case of antimatter is the ability to use the annihilation products as a diagnostic. For positrons this is the annihilation with either free electrons, those in neutral atoms or molecules, or those in a surrounding material surface. Annihilation with free electrons, for example, can be used to study the properties of classical electron-positron plasmas (cf. Sec. VIII.C.2).

Positron annihilation with electrons, free or bound, is dominated by decay into two 511-keV gamma rays emitted 180° from each other. One characteristic of this technique is that the background is typically small leading to good signal to noise.

The benchmark two-gamma annihilation rate is that due to Dirac. For a positron in a free electron gas of density n_e , the annihilation rate is

$$\Gamma_D = \pi c r_0^2 n_e, \quad (78)$$

where c is the speed of light and r_0 is the classical radius of the electron.

For atoms and small molecules, this expression can be used to estimate the annihilation rate substituting for n_e the density of atoms or molecules $n_e = Z \times n_m$, where n_m is the number density of molecules. Due to the small value of r_0 , the annihilation rate is relatively small. For example, the characteristic annihilation time $\Gamma_D^{-1} \sim 100$ s for an electron density $n_e = 10^{18} \text{ m}^{-3}$.

The intensity of the annihilation radiation can provide a measure of the positron (or surrounding material) density, while the energy spectrum of the radiation provides a measure of the velocity of the annihilating electron-positron pairs (i.e., due to the Doppler effect) (Charlton and Humberston, 2001).

VI. PLASMA MANIPULATION TECHNIQUES

Techniques to measure the plasma temperature and density were discussed in the previous section. In this section, a selection of the most important methods are described by which these parameters can be modified in a controlled manner. This includes density control using rotating electric fields, diocotron-mode manipulation for translation of the plasma column off-axis, and techniques for plasma heating.

A. Radial compression using rotating electric fields

As discussed in Section II.F, an important technique to counteract the effects of inherent trap asymmetries is to apply an external perturbation that rotates faster than the plasma. This “rotating-wall” (RW) technique has the effect of applying a torque on the plasma which compress it. The RW field is created by applying suitably phased sine waves to an azimuthally segmented electrode surrounding the plasma, thus producing an electric field that rotates about the trap axis at a frequency ω_{RW} . The resulting torque will compress the plasma if $\omega_{RW} > \omega_r$, where ω_r is the plasma rotation frequency, and it will cause expansion if $\omega_{RW} < \omega_r$ (Danielson and Surko, 2006a; Dubin and O’Neil, 1999). The effectiveness of this technique depends upon the strength of coupling of the external torque to the plasma. Further, as discussed in Section II.F, since the external torque does work on the plasma and thereby increases the plasma temperature, an efficient plasma cooling mechanism is required (Dubin and O’Neil, 1999).

This technique has been used to compress a variety of single-component plasmas, including large ion clouds (Huang *et al.*, 1997); small ion crystals (Huang *et al.*, 1998); antiprotons (Andresen *et al.*, 2008; Kuroda *et al.*, 2008); and electron (Anderegg *et al.*, 1998; Danielson and Surko, 2005, 2006b; Hollmann *et al.*, 2000; Kiwamoto *et al.*, 2005) and positron plasmas (Cassidy *et al.*, 2005; Deller *et al.*, 2014; Eseev *et al.*, 2013; Greaves and Moxom, 2008; Greaves and Surko, 2000, 2001; Isaac *et al.*, 2011; Jørgensen *et al.*, 2005).

In the absence of other torques, the plasma will compress or expand until it reaches the no-slip condition $\omega_{RW}/m_\theta = \omega_r$, where the slip frequency is $\Delta\omega \equiv \omega_{RW}/m_\theta - \omega_r$ (Dubin and O’Neil, 1999; Huang *et al.*, 1997). As discussed in Section II.E, static trap asymmetries produce a drag on the plasma that results in plasma expansion. In this case, the plasma achieves a *torque-balanced steady state* when the torque from the applied RW fields equals the drag torque, in which case $\Delta\omega > 0$ (Danielson and Surko, 2005; Danielson *et al.*, 2007a).

A number of techniques have been developed to achieve RW plasma compression. The distinguishing feature between those experiments is the mechanism by which the torque is transferred to the plasma and the amount of slip observed when the plasma reaches a steady state.

For ion plasmas, the absorption and re-emission of tangentially directed laser light can be used to inject angular momentum (Bollinger *et al.*, 1994; Heinzen *et al.*, 1991). However, for electron or positron plasmas, the scattering cross section is sufficiently small that this is impractical, and so this technique will not be discussed further.

1. Coupling via Trivelpiece-Gould modes

The first RW experiments on electron plasmas used excitation of $m_\theta > 0$ Trivelpiece-Gould (TG) modes (see Section V.A.2), to provide the required torque (Anderegg *et al.*, 1998; Eggleston *et al.*, 1984; Hollmann *et al.*, 2000; Mitchell,

1993). Such waves can be excited easily; and upon damping, the wave angular momentum is transmitted to the bulk plasma particles (Hollmann *et al.*, 2000; Kiwamoto *et al.*, 2005; Soga *et al.*, 2006). A strong cooling mechanism is necessary for compression, which in this case was cyclotron cooling in a several-tesla magnetic field (cf. Fig. 20). The level of slip in this case, which is related to the TG dispersion relation, is always non-zero (Anderegg *et al.*, 1998).

As shown in Fig. 20 compression is most effective near the $m_\theta = 1$ or $m_\theta = 2$ TG mode frequencies. However, significant heating is associated with the strong compression (Anderegg *et al.*, 1998; Hollmann *et al.*, 2000). From Eq. 50, the TG dispersion relation for $m_\theta > 0$ can be written as $\omega_{TG} \approx m_\theta \omega_r + (k_z/k_\perp) \omega_p$, so the slip can be written as

$$\Delta\omega = \omega_{TG}/m_\theta - \omega_r \approx \frac{k_z}{m_\theta k_\perp} \omega_p, \quad (79)$$

where k_z is the parallel wavenumber and k_\perp is the perpendicular wavenumber, and it is assumed that $k_z \gg k_\perp$ (see Sec. V.A.2). Since this quantity is typically comparable to ω_r , the slip can be quite large, resulting in large heating rates (cf. Fig. 20). As discussed in Sec. V.A.2, the dispersion relation can also have a significant dependence on the plasma temperature. Thus, as the plasma compresses (and heats), the TG mode frequency will change, and this necessitates ramping ω_{RW} for good compression (Anderegg *et al.*, 1998; Hollmann *et al.*, 2000).

Those experiments demonstrated good compression and were able to achieve steady-state confinement (lifetimes of hours to days). However, due to the complicated nonlinear effects and heating, it was difficult to maintain precise steady-state densities.

2. Strong drive regime

Techniques have also been developed to use non-resonant RW excitation for compression of both electron and positron SCP's (Danielson and Surko, 2005, 2006b; Danielson *et al.*, 2007a; Jørgensen *et al.*, 2005). All of the experiments described here used a four-segment, $m_\theta = 1$, RW electrode. The first experiment to apply this technique for positrons was conducted using plasmas with relatively low densities and buffer gas cooling (Greaves and Surko, 2000). Images of the time evolution of the plasma are shown in Fig. 19 above.

Generally, for non-resonant excitation, a large amplitude drive is applied at a fixed frequency ω_{RW} . In this case, the plasma rapidly heats and then compresses on a slower time scale, see Fig. 21. Then, as the compression continues, the slip decreases, and the temperature drops (Danielson and Surko, 2006b). As shown in Fig. 22, if the drive amplitude is sufficiently strong, the compression continues until ω_r almost matches ω_{RW} , achieving a very low-slip steady state (i.e., $\Delta\omega/\omega \ll 1$), in which the plasma has a fairly low temperature (e.g., $T \lesssim 0.1$ eV) (Danielson *et al.*, 2007a).

This technique has been shown to work over a fairly broad range of drive frequencies; and since the slip is small, the plasma density (and thus the plasma radius) can be tuned simply by adjusting ω_{RW} , as shown in Figs. 23 and 24 (Danielson and Surko, 2006b). As long as the drive amplitude exceeds some minimum level, the steady-state density is only weakly dependent on drive amplitude (see Fig. 22). As in the TG-drive experiments, the strong plasma heating during compression necessitates a strong cooling mechanism. All of the experiments described thus far utilized strong cyclotron cooling in a large (e.g., ~ 5 T) magnetic field to keep the plasma temperature low.

a. Zero-frequency modes. Striking aspects of the strong-drive experiments are the relatively sharp transitions between low-density and high-density steady states (cf. Fig. 22) and the absence of this transition for particular values of ω_{RW} (e.g., 1–3 MHz in Fig. 23). The latter has been shown to be due to the presence of so-called “zero-frequency-modes” (ZFM). Due to the plasma rotation, the TG-mode frequency (Sec. V.A.2) can be Doppler-shifted to zero frequency in the lab frame. Consequently, at specific densities (depending on N and L_p), a TG mode can be resonantly driven by either magnetic or electric trap asymmetries (Danielson and Surko, 2006b). Previously, the ZFM's were shown to be important when laser torques were used to compress pure ion plasmas (Heinzen *et al.*, 1991; Mitchell *et al.*, 1999). These modes have also been shown to limit strong-drive compression in experiments with positron plasmas at low magnetic fields and using buffer gas cooling [see Fig. 25 and Cassidy *et al.* (2010b)].

b. Approaching the Brillouin limit. In the case of laser-cooled ion plasmas, the plasma can be compressed all the way to the Brillouin limit (Heinzen *et al.*, 1991), but to date, this has not been achieved for either electron or positron plasmas. The record so far is $1.2 \times 10^{15} \text{ m}^{-3}$ in a field $B \sim 0.04$ T using gas cooling and $f_{RW} \sim 50$ MHz. This corresponds to 17 % of n_B (see Fig. 25). The conditions of this experiment were similar to Cassidy *et al.* (2010b). This limiting density is consistent with the effect described in Sec. IV.C. As the density is increased to approach the

Brillouin limit, the particle orbits exhibit outward radial excursions much larger than the cyclotron radius, in which case gas collisions produce increased radial transport (Surko *et al.*, 2010).

Although the frequency limit for strong-drive compression is presently not known (Danielson and Surko, 2006a), the alignment and uniformity of the magnetic field and the possible excitation of ZFM's are likely impediments to be overcome to achieve higher plasma densities (Cassidy *et al.*, 2010b). While the RW compression experiments at higher magnetic fields (e.g., 5 T) can achieve higher absolute plasma densities, this represents a smaller fraction (e.g., $\sim 10^{-3}$) of the Brillouin limit (Fitzakerley *et al.*, 2013; Jørgensen *et al.*, 2005).

3. Single particle regime

Rotating wall compression in buffer gas-cooled positron plasmas has also been demonstrated in the single particle regime. Those experiments were done both $m_\theta = 1$ and $m_\theta = 2$ RW electrodes. As shown in Fig. 26, compression occurs for ω_{RW} close to the axial bounce frequency, rather than near ω_r (Greaves and Moxom, 2008). Isaac *et al.* (2011) have shown that this effect is analogous to magnetron sideband cooling in which the viscous drag of the buffer gas (used for cooling) plays an intrinsic role.

This is in contrast to the traditional magnetron sideband cooling (Brown and Gabrielse, 1986) technique employed to center small numbers of particles in precision Penning traps, without a buffer gas. In that case, the perturbation was applied, for example, to a compensation electrode, and the frequency tuned to either the lower or upper sideband for compression or expansion, respectively. The required cooling is then achieved by electronic (resistive) damping of the axial motion.

Application of the perturbation as a rotating electric field has the effect of selecting the desired sideband according to the direction of rotation (Isaac, 2013). An important consequence of this is that the technique is applicable even in relatively anharmonic traps where the two sidebands are broad enough to overlap.

B. Radial positioning using the $m_\theta = 1$ diocotron mode

As discussed in Sec. II.D.1.b, the diocotron mode has negative energy, meaning that any dissipation in the system (e.g., resistance in electrical circuits, or gas collisions) can cause it to grow in amplitude. It can, for example, be easily excited by attaching a resistor to one of the azimuthally sectored electrodes (Bettega *et al.*, 2008; White *et al.*, 1982). Depending upon the details of the PM trap and the associated electrical circuits, it can be naturally unstable. A finite-amplitude diocotron mode can also arise when filling a PM trap if the source of particles is even slightly off axis. Finally, it has been shown that positive ions drifting through an electron plasma can excite this (the so-called “ion-resonance instability”) (Bettega *et al.*, 2006; Fajans, 1993; Kabantsev *et al.*, 2003; Levy *et al.*, 1969; Peurrung and Fajans, 1993). Thus, manipulation and control of the diocotron mode is important, and often necessary.

1. Feedback damping and growth

One technique to actively control the amplitude of the diocotron mode is through the use of positive and negative feedback (Fine, 1988). This is done by measuring the image charge of the diocotron mode on one azimuthal sector; then applying the signal on a different azimuthal sector with a modified phase and amplitude. The plasma column can either be driven back to the axis (negative feedback damping), or excited to a large amplitude (positive feedback growth) as desired. In some experiments where the diocotron mode is inherently excited due to electrical resistance in the circuit attached to the electrodes, negative feedback can be used to stably maintain the plasma in the on-axis position (Hollmann *et al.*, 2000).

2. Autoresonance for off-axis translation

For a number of applications, it is important to have the ability to control the position of the plasma in the $r - \theta$ plane. One example is the need to efficiently transfer plasmas into off-axis traps in the “multicell trap” experiment (see Sec. IV.D.2) (Danielson and Surko, 2006b; Danielson *et al.*, 2009). The most effective technique developed to date to accomplish this is to utilize the “autoresonant” excitation of the diocotron mode (Fajans and Friedland, 2001; Fajans *et al.*, 2001). Autoresonance is a generic property of nonlinear oscillators, where a strongly driven oscillator will adjust its amplitude and phase so that its frequency and phase matches the drive frequency and phase. Further it maintains this relationship with the drive even as the drive is varied.

For the $m = 1$ diocotron mode, the nonlinear dispersion relation is given by:

$$\omega_{NL} \approx \omega_1 \frac{1}{1 - (d/r_w)^2} \quad (80)$$

where ω_d is the linear diocotron frequency (see Sec. II.D.1.a), d is the amplitude of the diocotron mode, and r_w is the radius of the confinement electrodes. The plasma is brought into autoresonance by sweeping the drive frequency from below the linear diocotron frequency to a selected, higher frequency. If the drive amplitude is sufficiently large, the excited diocotron mode amplitude (d/r_w) will grow as the mode increases in frequency to match that of the drive [Eq. (80)]. During autoresonant excitation, the diocotron mode remains phase-locked to the applied signal for as long as the drive signal is applied, limited only by plasma expansion. This matching of frequencies and phase occurs for only a limited range of drive amplitudes and sweep rates. If the drive amplitude is too small, the mode is not excited; if the drive amplitude is too large, higher-order nonlinear effects dominate and destroy the autoresonance. Further, if the sweep rate is too fast, then there is insufficient time for the mode to lock to the drive. See the papers by Fajans *et al.* (Fajans *et al.*, 1999a,b, 2000, 2001; Friedland *et al.*, 2000) for details.

Once in autoresonance, the phase-locked plasma can be easily ejected (on a timescale $\ll \omega_D^{-1}$) at any desired displacement or phase in the $r - \theta$ plane. Examples of this procedure with electron plasmas are shown in Fig. 27, where the displacement was set by the drive frequency and the phase chosen to be either 0° , 90° , 180° , or 270° [from Danielson *et al.* (2006)].

C. Controlled heating

There are several techniques to control the plasma temperature. The most common is to oscillate one of the end-confinement electrodes at rf frequencies, either resonantly (through wave excitation) or non-resonantly. In the case of wave excitation, the heating occurs as the wave is damped. In the non-resonant case, the applied voltage couples directly to the bulk plasma.

a. Adiabatic heating. An early study of SCP heating worked in an adiabatic regime, where $\omega_h < \omega_b$, with ω_h the applied (heating) frequency and ω_b the axial particle bounce frequency (Beck *et al.*, 1996; Hyatt *et al.*, 1987). In this case the plasma length and T_{\parallel} oscillate in phase with the voltage, resulting in heating as collisions transfer energy between the parallel and perpendicular degrees of freedom. The adiabatic heating rate is (Cluggish *et al.*, 1998)

$$\frac{1}{T} \frac{dT}{dt} \Big|_{ad} = \frac{4}{3} \nu_{\perp\parallel} \left(\frac{\delta L}{L_p} \right)^2 \left[\frac{\omega_h^2}{\omega_h^2 + (3\nu_{\perp\parallel})^2} \right] \quad (81)$$

where $\delta L/L_p$ is the amplitude of the oscillation (with $\delta L \propto V_h$, the heating voltage), and $\nu_{\perp\parallel}$ is the T_{\perp} to T_{\parallel} collisional equilibration rate. Note, that for large ω_h , this rate is independent of ω_h (Beck *et al.*, 1996; Cluggish *et al.*, 1998).

b. Non-adiabatic heating. Another type of plasma heating works in a non-adiabatic regime, where $\omega_h \gtrsim \omega_b$. In this case, the oscillating potential interacts with particles bouncing at harmonics of the bounce frequency, ω_b . In this case, the heating rate is given by (Cluggish *et al.*, 1998)

$$\frac{1}{T} \frac{dT}{dt} = \frac{(2\pi)^{1/2}}{3} \omega_h \left(\frac{\delta L}{L_p} \right)^2 \sum_{l=1}^{\infty} \left(\frac{\omega_h}{l\omega_b} \right)^5 \exp \left[-\frac{1}{2} \left(\frac{\omega_h}{l\omega_b} \right)^2 \right]. \quad (82)$$

When combined with cyclotron cooling, both of adiabatic and non-adiabatic heating techniques have been able to give stable plasma temperatures in the range of 0.01 – 10 eV (Beck, 1990; Cluggish and Driscoll, 1995).

c. Cyclotron heating. Use has been made of cyclotron resonant heating in several positron- or electron-plasma experiments. In one experiment, the heating of the positron plasma was observed by monitoring the heating of ions that were mixed with the positrons (Jelenković *et al.*, 2002). More recently, cyclotron heating has been used in electron plasmas in order to map out the electromagnetic cavity for one of the trapped antihydrogen experiments (Amole *et al.*, 2012).

VII. TRAP-BASED BEAMS

As discussed above, PM traps are used routinely to accumulate, store and manipulate antimatter plasmas. The focus of this section is description of the efficient methods that have been developed to create cold, bright, pulsed beams of antiparticles. Confining and cooling the particles in a PM trap enables many new capabilities. As discussed in Sec. VIII, applications include cold beams for spectroscopy (e.g., to study positron interactions with atoms, molecules and atomic clusters) (Gribakin *et al.*, 2010; Surko *et al.*, 2005). Other applications include the development of tailored beams for materials studies (Coleman, 2000; Schultz and Lynn, 1988) and for the production of cold antihydrogen atoms (Amoretti *et al.*, 2002; Gabrielse *et al.*, 2002).

A. Extraction from a buffer-gas trap

About a decade after the development of the BGT, it was discovered that thermalized, trapped positrons could be carefully forced over a potential barrier to create a beam with improved energy resolution (e.g., by a factor $\sim 5 - 10$) as compared with positrons from a continuous radioisotope source and moderator (Gilbert *et al.*, 1997). The experimental arrangement is illustrated in Fig. 28. The trap magnetic field is $B \sim 0.1$ T. The beam energy distribution is measured downstream using a retarding potential analyzer. The beam energy is set by the difference between the end gate potential V and the potential V_c on a scattering or annihilation cell. The energy resolution is approximately $\Delta\epsilon = 40$ meV FWHM in total energy spread, comprised of $\Delta\epsilon_{\parallel} = 18$ meV FWHM in energy spread parallel to the magnetic field and $\Delta\epsilon_{\perp} = 25$ meV FWHM (i.e., $k_B T$ at 300 K) in the cyclotron motion perpendicular to the field.

While several modes of operation are possible, a common method is to trap, cool, then release the positrons in bursts. One technique is operation in cycles at a 2–4 Hz rate using 100 to 200 ms fill and cool times, with the bottom of the potential well raised to arrange pulses $\sim 1 \mu\text{s}$ in duration (Gilbert *et al.*, 1997; Sullivan *et al.*, 2002). The slower the well is raised, the narrower the energy distribution, but the longer the pulse duration. However, if the well is raised on a timescale much longer than the bounce time, a poor quality, modulated beam can result, presumably from the excitation of instabilities in the residual nonequilibrium plasma in the trap (Cassidy *et al.*, 2006b). Use of a rapid cooling gas such as CF_4 is essential for short cycle times. For a given total beam energy, the perpendicular energy spread can be decreased by exploiting the adiabatic invariant ϵ_{\perp}/B . As the beam enters a region of lower B , ϵ_{\perp} decreases while ϵ remains constant. This technique is useful for spectroscopic energy-loss measurements (Sullivan *et al.*, 2002).

B. Centerline extraction

While many methods have been developed to create bright beams, including passage through small apertures or, in the case of positrons, remoderation (i.e., focusing and re-thermalization at material surfaces, Sec. III.D), these techniques typically involve unavoidable losses of particles. A nondestructive technique was developed to produce a beam with narrow transverse width and enhanced brightness, without such losses (Danielson *et al.*, 2007b; Greaves *et al.*, 2002; Weber *et al.*, 2008, 2009).

It exploits the fact that, in a PM trap, the plasma space-charge potential, Eq. (17), is largest at the radial plasma center, and so particles from this region escape first when an end confining potential is lowered (Danielson *et al.*, 2007b). A schematic diagram of this technique is shown in Fig. 29. To use all of the particles and for increased brightness, the plasma is compressed radially and maintained at constant density using the RW technique (Danielson and Surko, 2006b). Using this technique, all the trapped plasma can be transformed into a sequence of tailored beam pulses (Weber *et al.*, 2008).

Beams with Gaussian radial profiles and diameters as small as $D = 50 \mu\text{m}$ have been extracted from electron plasmas with $D \approx 2$ mm before compression (Danielson *et al.*, 2007b; Weber *et al.*, 2008). A simple theory predicts that the beam diameter (full width to $1/e$) is $D = 4\lambda_D \propto (T/n)^{1/2}$, where λ_D is the Debye length. This scaling is illustrated in Fig. 30 (Danielson *et al.*, 2007b; Weber *et al.*, 2008, 2009). The favorable scaling of D with T and n indicates that further improvements are possible using colder, higher-density plasmas.

C. Autoresonance for parallel energy control

In Sec. VI.B, a technique was described to use autoresonance to excite a diocotron mode in order to obtain large plasma displacements across a magnetic field [also see Danielson *et al.* (2006) and Canali *et al.* (2011)]. Recently,

autoresonance was used in quasi-harmonic traps to provide control of the parallel energy distribution of an antiproton cloud (Andresen *et al.*, 2011a). In that case, the bounce dynamics in the (slightly) anharmonic parabolic well was nonlinear, with the bounce frequency decreasing as the amplitude of the bounce motion increased (cf. Fig. 31). As discussed in Sec. VIII.A.3, this technique has recently been used to carefully push antiprotons through a positron plasma to create antihydrogen in a precisely controlled manner (Andresen *et al.*, 2011a).

D. Pulsed beam production

Positron traps can be used to produce time-bunched positron beams for a range of applications. The trap itself can be used as the bunching element, or positron pulses from a trap can be injected into a separate bunching stage. If positrons are released from the trap on a timescale of the order of the bounce time, the initial low energy spread of the positrons is largely preserved. The resultant positron pulses are typically of the order of one microsecond. If the trap is dumped on faster timescales, shorter pulses are obtained (at the expense of increased energy spread). For example, Greaves and Moxom (2003) obtained 18-ns positron pulses from a two-stage positron trap using a fast-dump technique. Several techniques have been devised for obtaining shorter pulses, all of which are based on making energy corrections to a positron pulse so that the particles arrive at a designated spatial location at the same time.

Such bunching is subject to the fundamental constraints of Liouville’s theorem, which requires that the phase space volume of the beam be conserved. For time bunching, this turns out to imply that reduced temporal pulse widths can be obtained only at the expense of increased longitudinal energy spreads, and they can never be reduced by more than a factor of $\sim \Delta E_f/\Delta E_i$, where ΔE_f is the final energy spread and ΔE_i is the initial energy spread. Since the energy spread of trapped positrons is much smaller than from other available positron sources, a much greater bunching factor can be obtained for a given increase in parallel energy spread.

1. Harmonic potential bunching

In this technique, the energy correction is applied simultaneously to positrons injected into a trapping region (cavity) of length L . The correction is produced by applying a suitably shaped potential profile to the cavity using one or more fast rise time pulse generators. The positrons exit the cavity with the required energy correction to produce a time focus a distance l from the trap exit.

For the special case of $l = 0$ (i.e., the focus located at the exit of the bunching cavity), and assuming the positron energies are small compared with the energy correction, the required bunching potential varies quadratically with distance upstream from the end of the cavity – so-called “harmonic potential” bunching [see Fig. 32(a)]. If the bunching cavity is short, a good approximation to a quadratic potential can be conveniently provided by a cylindrical cavity with a characteristic aspect ratio. As described in Crane and Mills (1985), this technique was used to bunch positrons from a dc beam producing 470 ps duration pulses (including detector response) at a 50 kHz repetition rate.

This technique has also been implemented using a multi-ring structure in which the pulsed potential on each ring is adjusted separately with either a capacitor chain or separate transistor pulsers (Cassidy *et al.*, 2006a; Hulett *et al.*, 1991; Merrison *et al.*, 2003). This is particularly convenient for positrons accumulated in multi-ring traps, since the trap electrodes can be used to perform the function of the buncher (e.g., to obtain sub-nanosecond pulses). In this case, the trapping potentials are dc-coupled to the trap electrodes for positron accumulation, and the bunching pulses are capacitively-coupled to eject all the positrons from the trap simultaneously with the required energy correction (Cassidy *et al.*, 2006a).

2. Timed potential bunching

Another technique for applying the required energy correction is to pass positrons through an acceleration gap across which a time-varying electric field is applied so positrons entering this region later are given more energy than earlier ones [see Fig 32(b)]. The potential required to produce a time focus at $t = 0$ is

$$V(t) = \frac{ml^2}{2et^2}, \quad (83)$$

where, $t < 0$, and l is the distance from the acceleration gap to the position of the time focus (Mills, 1980c). Using this technique Greaves and Moxom (2003) produced 2-ns positron pulses using an external bunching electrode. Sullivan *et al.* (2010) refined this technique for measurement of positron lifetimes in materials.

E. Electrostatic beams

A limitation on the beams discussed so far is that they reside in a strong magnetic field. This presents a problem for applications that require an electrostatic beam (i.e., a positron beam in a magnetic field-free region) (Charlton and Humberston, 2001; Coleman, 2000; Schultz and Lynn, 1988; Surko *et al.*, 2005). For example, electrostatic beams provide increased sensitivity in studying angular scattering from atomic and molecular targets (Pfluger *et al.*, 2011), and they have long-term potential for use in a positron reaction microscope (Williams *et al.*, 2010). Electrostatic techniques (lenses) can also be used to produce remoderation brightness-enhanced beams (Sec. III.D) for applications such as Ps₂ studies and Ps-BEC formation (Sec. VIII.C.1.c). For these applications, extraction of a PM-trap-based beam from the magnetic field is required, and this can be problematic considering such effects as a potentially dramatic increase in the beam width and/or the mean transverse energy E_{\perp} (Weber *et al.*, 2010).

Nevertheless, a number of experiments that have succeeded in taking positrons (or electrons) from a high magnetic field into a field-free region Akahane (1994); Gerola *et al.* (1995); Greaves and Surko (2002a); Shi *et al.* (1995). Figure 33 shows the experimental arrangement of a recent experiment in which electron plasma was tailored in a PM trap in a 5 T field, then a beam was extracted, transported to a field-free region, and then focused with an electrostatic Einzel lens (Weber *et al.*, 2010).

F. Positronium-atom beams

For both fundamental physics studies and practical applications, it is desirable to develop methods to create monoenergetic beams of Ps atoms. A further goal is to develop a Ps beam tunable in energy. Due to the fact that the Ps atom is neutral and unstable to annihilation, these objectives are considerably more challenging than the creation of high-quality positron beams.

Two approaches are currently being pursued based upon positron trapping techniques. One approach to create a pulsed source of energetic (e.g., kilovolt) Ps atoms involves photodetachment of electrons from a beam of Ps⁻ negative ions (Michishio *et al.*, 2012).

Another approach is being pursued by I. N. Meshkov and collaborators (Meshkov, 2004). In that case, positrons from a BGT feed a storage ring containing electrons, both traveling in the same direction at energies ~ 10 keV. An electron cooler is used to cool both species. The system is expected to produce a bright beam of Ps atoms intended for use in fundamental physics studies.

VIII. TAILORED STORAGE AND DELIVERY FOR KEY APPLICATIONS

The utilization of antimatter for scientific and technical applications has benefited greatly from the antimatter plasma manipulation tools described above. Discussed here are examples of areas in which those tools have made prominent contributions. Topics span the range from tests of fundamental symmetries of the laws of physics to the characterization of materials. In many cases, the interplay between technique development and application has been synergistic; techniques and tools developed for a specific application have found other uses, and the resulting practical experience has, in turn, motivated further developments. Current outstanding challenges and areas for potential improvement are also discussed.

A. Creation and study of antihydrogen ($\bar{\text{H}}$)

The goal is to create, trap and study this simplest, stable neutral form of antimatter, the antihydrogen atom ($\bar{\text{H}}$, i.e., the bound state of the positron and antiproton), and to compare with precision its properties to that of ordinary hydrogen. The experimental challenges that studying $\bar{\text{H}}$ presents have required numerous manipulation techniques, many of which were developed during the past 25 years of antihydrogen research. The experimental approaches and techniques used continue to evolve.

Very energetic $\bar{\text{H}}$ atoms (i.e., with momenta $\sim 2 - 6$ GeV/c) were reported by groups working at CERN and Fermilab in the 1990s (Baur *et al.*, 1996; Blanford *et al.*, 1998). However, there is no known method to slow and trap such fast atoms, and so an entirely different approach was needed. While the quest to create, trap and study $\bar{\text{H}}$ has been going on for more than two decades (Gabrielse *et al.*, 1986), striking progress has been made since the turning

point in 2002 when two collaborations (ATHENA⁴ and ATRAP⁵) reported making low-energy \bar{H} atoms (Amoretti *et al.*, 2002; Gabrielse *et al.*, 2002). Another turning point occurred in 2010 when ALPHA succeeded in trapping antiatoms (Andresen *et al.*, 2010).

1. Overview of the experiments

Experiments are conducted at CERN’s Antiproton Decelerator (AD) facility for low-energy antiprotons (\bar{p}). There are three experiments in operation now and two in the planning stages (Hori and Walz, 2013): ATRAP, ALPHA, ASACUSA, AEGIS and GBAR. The first three have made \bar{H} atoms, and the first two groups have trapped them with the goal of studying them *in situ*. The goal of ASACUSA is to create a beam of \bar{H} and then measure its magnetic moment in a Stern Gerlach experiment (Enomoto *et al.*, 2010; Kuroda *et al.*, 2014b). As discussed in Sec. VIII.B, the AEGIS collaboration plans to measure the effect of earth’s gravity on \bar{H} in a beam experiment (Doser *et al.*, 2012), and the GBAR collaboration plans to measure the free fall of ultracold \bar{H} atoms (Debu, 2013).

The approach used to date to form low-energy \bar{H} is to trap and cool \bar{p} and then allow them, in some fashion, to recombine with cold positrons. This has been accomplished by directly combining positrons and \bar{p} (Amoretti *et al.*, 2002; Gabrielse *et al.*, 2002) and also by charge-exchange collisions between \bar{p} and high-Rydberg-state Ps atoms (Storry *et al.*, 2004). Thus far, the former technique has proven most efficient. The apparatus used by the ATHENA collaboration to create \bar{H} is shown in Fig. 34.

The dominant mechanism for \bar{H} formation appears to be three-body recombination (Glinsky and O’Neil, 1991),



In this reaction the second positron takes away the excess energy. In steady state, the three-body formation rate Γ depends strongly on the inverse of the positron temperature T_p , namely as $\Gamma \sim T_p^{-9/2}$, and so low positron temperatures were expected to be beneficial. However, experiments to date are not done in steady state, and so a weaker dependence upon inverse temperature has been observed (Amoretti *et al.*, 2002), in accord with simulation results (Robicheaux, 2004).

A separate motivation for mixing at low temperatures is the fact that the trap of choice to confine the \bar{H} is a minimum- B trap. Given currently achievable magnetic field strengths and field gradients, the maximum well depth for such traps is <1 K, with energy expressed in kelvin. Thus the \bar{p} temperature, and hence the resulting \bar{H} temperature must be kept as low as possible to create trappable atoms. Creating \bar{H} atoms with such low energies has proven to be the most severe impediment to the efficient trapping of the \bar{H} atoms, and so increasing trapping rates remains an outstanding challenge.

2. Low-energy antiprotons and cold positrons

The AD facility at CERN delivers 100 MeV/c (kinetic energy 5.3 MeV) \bar{p} that have been slowed from 3.6 GeV/c using multiple stages of stochastic and electron cooling (Hori and Walz, 2013). Typically, $\sim 0.2 \mu\text{s}$ long bursts of $\sim 3 \times 10^7$ \bar{p} are delivered every 100 s. Using techniques pioneered by Gabrielse and collaborators, material degraders are used to produce a population of (slow) \bar{p} with kilovolt energies (Gabrielse *et al.*, 1986). The \bar{p} are then captured dynamically in a PM trap in a several-tesla magnetic field by switching an end-gate electrode potential (e.g., by several kilovolts). The trap is pre-loaded with electrons that cool by cyclotron radiation and, in turn, sympathetically cool the \bar{p} (Gabrielse *et al.*, 1989a). Several bursts of \bar{p} can be “stacked” in the PM trap. Successful \bar{H} production has been done with varying numbers of \bar{p} ranging from $\sim 10^4$ to 10^6 .

In some experiments, RW compression of the combined electrons and antiprotons has proven to be useful. Typically, the RW acts on the larger number of electrons, and the \bar{p} are dragged along. If particle temperatures are sufficiently low, there can be centrifugal separation with the \bar{p} on the outside of the column. Experiments have been conducted both with and without RW compression (Andresen *et al.*, 2008; Gabrielse *et al.*, 2012; Kuroda *et al.*, 2008). The paper by Andresen *et al.* (2011b) provides a study of both regimes. Both evaporative (Andresen *et al.*, 2010) and adiabatic (Gabrielse *et al.*, 2011) cooling of the \bar{p} have been used to achieve lower \bar{p} temperatures.

While other positron sources have been used (e.g., ionization of high-Rydberg Ps atoms from a positron remoderator (Haarsma *et al.*, 1995)) or attempted (trapping on an electron target plasma and an ion cloud (Oshima *et al.*, 2004),

⁴ The ATHENA collaboration ended in 2005. Some of its members joined a new collaboration, ALPHA, while other of its members joined another new collaboration AEGIS.

⁵ The TRAP collaboration (≤ 1997) was succeeded by the ATRAP collaboration, with G. Gabrielse the spokesperson for both.

the BGT (Murphy and Surko, 1992) and solid neon moderator is superior in most applications. For example, this technique was first used for \bar{H} formation by ATHENA (Amoretti *et al.*, 2002) and has now become standard for such studies. Concerns about degrading the vacuum (Haarsma *et al.*, 1995) have turned out not to be a problem. Recently, 4×10^9 positrons were confined in electrodes at 1.2 K in a region where the background pressure was estimated to be $\leq 8 \times 10^{-17}$ mbar, which will be good enough for year-long \bar{H} confinement (Fitzakerley *et al.*, 2013). Following trapping and cooling to 300 K in the buffer-gas trap, bursts of positrons are magnetically guided through a pulsed valve into the nested Penning traps in tesla-strength magnetic fields with 50% or greater efficiency (Amoretti *et al.*, 2002; Comeau *et al.*, 2012; Jørgensen *et al.*, 2005).

The positrons are cooled by cyclotron radiation in a cryogenically cooled electrode structure. However, for reasons presently unclear, there is evidence that the positrons do not necessarily reach equilibrium with the surroundings (Amole *et al.*, 2013). Evaporative and/or adiabatic cooling has been used to further reduce the positron temperature (Amole *et al.*, 2012). The \bar{H} formation rate in three-body collisions is proportional to the square of the positron density. The RW technique is used to increase both the positron and antiproton densities (Andresen *et al.*, 2008; Kuroda *et al.*, 2008), and hence Γ . Successful \bar{H} production has been done with varying numbers of positrons from $\sim 3 \times 10^5$ to 8×10^7 . Relatively small clouds of positrons (i.e., as compared with the maximum possible accumulations) are used to keep space-charge electric fields low. Larger space charge electric fields will result in excess \bar{p} energy due to $\mathbf{E} \times \mathbf{B}$ rotation, and this, in turn, results in hotter \bar{H} .

3. Mixing, \bar{H} formation, and detection

As illustrated in Fig. 34, the first low-energy \bar{H} were made using cold positron plasmas and antiprotons in adjacent, nested PM traps. Both ATHENA/ALPHA and ATRAP have formed \bar{H} atoms by forcing the \bar{p} through the cold positrons (Amoretti *et al.*, 2002; Gabrielse *et al.*, 2002). Various methods have been used to accomplish this. The \bar{p} have been heated with rf noise or the bottom of the \bar{p} well raised. Autoresonant excitation of the \bar{p} in their confining well has been used by ALPHA (Andresen *et al.*, 2011a) who find it to be both efficient and stable against fluctuations in the number of trapped positrons and antiprotons (Amole *et al.*, 2014).

The \bar{H} detection apparatus developed by ATHENA provides detailed spatial information about the location of the annihilation events (Amoretti *et al.*, 2002). As illustrated in Fig. 34, silicon strip detectors detect pions from the \bar{p} decays, and an array of CsI crystals detect the two back-to-back 511 keV gamma rays from positron annihilation. The origins of both were reconstructed to an accuracy of ~ 4 mm in space and 5 ms in time. As shown previously in Fig. 2, the \bar{H} annihilations occur at the inner diameter of the surrounding electrodes (Amoretti *et al.*, 2002). They were also able to reconstruct the axial and azimuthal locations of the \bar{p} (and hence \bar{H}) decays in order to better understand the dynamics of the recombination process.

As shown in Fig. 35, the ATRAP collaboration arranged an axially localized region of large electric field. The electric field is used to ionize higher Rydberg state \bar{H} atoms and trap the \bar{p} thus produced, which can later be released and detected. This information was used to gain information about the principal quantum numbers of the antiatoms (Gabrielse *et al.*, 2002). An oscillating electric field was used to measure the velocity of the \bar{H} (Gabrielse *et al.*, 2004b; Pohl *et al.*, 2006).

The \bar{H} atoms made thus far are fragile since they are formed either in, or close to, the so-called guiding-center atom (GCA) regime (Glinsky and O’Neil, 1991). This arises from the fact that, for low-energy \bar{p} in a positron plasma at temperature T_p , the \bar{H} atoms are formed in high Rydberg states with binding energies $\sim T_p$. Since low T_p is favored for higher formation rates, the atoms are fragile. Due to the tesla-strength magnetic fields, the atoms tend to be in states in where the positron cyclotron radius is small compared to the \bar{p} -positron distance. In this case, the atoms obey classical dynamics in which the positrons undergo $\mathbf{E} \times \mathbf{B}$ motion around the \bar{p} (the GCA regime).

Due to their orbital magnetic moments, such atoms are “high-field seekers” and cannot be trapped magnetically. They must undergo further collisions to become more tightly bound for trapping to be possible. The resulting cascade can include a regime of chaotic orbits and a so-called “bottleneck” (Glinsky and O’Neil, 1991; Pohl *et al.*, 2006; Vrinceanu *et al.*, 2004). One approach is to find mixing protocols that either avoid, or quickly take antiatoms out of this regime to the regime of ordinary (tightly bound) atoms. Fortunately, the lower magnetic fields ~ 1 T (Andresen *et al.*, 2008) used to facilitate magnetic trapping narrow the parameter range in which GCA dynamics are important (Robicheaux, 2008).

In the experiments conducted thus far, the transient nature of the \bar{p} -positron recombination process and *in situ* electric fields in the PM mixing traps are important in understanding the \bar{H} formation results (Robicheaux, 2004). Computer simulations indicate that the positron plasmas were sufficiently thin that the \bar{H} formed are very weakly bound and can easily be ripped apart. Shown in Fig. 36 are distributions of positron binding energies in the *circa* 2002 ATHENA and ATRAP experiments. Due to these effects, the interpretation of the field-ionization measurements has evolved over time taking into account the various facets of the mixing and atom-formation processes (Driscoll, 2004;

Gabrielse *et al.*, 2004a; Pohl *et al.*, 2006; Robicheaux, 2008; Vrinceanu *et al.*, 2004). Shown in Fig. 37 is comparison of field ionization data with the results of a simulation that includes arrest of the cascade to tighter binding and re-ionization of weakly bound antiatoms (Pohl *et al.*, 2006).

4. Trapping

The current technique to trap $\bar{\text{H}}$ utilizes a Ioffe-Pritchard type minimum- B trap (Bergeman *et al.*, 1987; Pritchard, 1983; Yang *et al.*, 2008). It provides an attractive potential for $\bar{\text{H}}$ atoms with magnetic moments aligned opposite the local magnetic field direction (so-called “low-field seekers”). The ALPHA apparatus is shown in Fig. 38. It consists of a uniform magnetic field and mirror coils to make a minimum- B well in the axial direction, and axial superconducting rods (Ioffe bars) create a minimum B region in the radial direction. Both octopole and quadrupole configurations (8 or 4 bars) have been used successfully (Andresen *et al.*, 2011b; Gabrielse *et al.*, 2012). Figure 39 shows the data from ALPHA indicating $\bar{\text{H}}$ confinement times in excess of 1000 s. Trapped atoms were detected following fast quenching of the magnetic field. The ability to quench rapidly (i.e., $\simeq 10$ ms) has enabled studies of the dynamics of $\bar{\text{H}}$ release (Amole *et al.*, 2012; Andresen *et al.*, 2011b).

5. Measuring $\bar{\text{H}}$ properties

For trapped $\bar{\text{H}}$, two kinds of measurements of atomic properties have been discussed. One is optical study of the 1S-2S electronic transition by two-photon spectroscopy, where a fractional frequency uncertainty of 5×10^{-15} has now been achieved for hydrogen (Parthey *et al.*, 2011). Experiments of this type are planned by both ATRAP and ALPHA.

A second approach is to measure the spin magnetic moment μ of the $\bar{\text{H}}$ atoms using a microwave resonance technique. The ALPHA collaboration recently conducted a proof of principle experiment of this approach (Amole *et al.*, 2012). The resolution is limited by the nonuniform magnetic field in the minimum- B atom trap. To circumvent this difficulty, ASACUSA plans to make a cold $\bar{\text{H}}$ beam and measure μ using a Stern-Gerlach-type experiment (Enomoto *et al.*, 2010; Kuroda *et al.*, 2014b).

B. Gravity Studies with Antimatter

An outstanding challenge is to test the gravitational interaction between antiparticles and ordinary matter. Due to the weak nature of the gravitational force, this is difficult to accomplish using single charged antiparticles due to so-called patch potentials and other stray electric fields [e.g., see Witteborn and Fairbank (1967)]. To circumvent this problem, several approaches propose to use neutral particles ($\bar{\text{H}}$ or Ps atoms).

The AEGIS collaboration proposes to measure the vertical deflection of a horizontal beam of $\bar{\text{H}}$ in order to determine the earth’s gravitational acceleration g for this antiatom (Doser *et al.*, 2012). The experiment will be done at CERN with antiprotons captured as described above. The scheme for formation of a cold, horizontal $\bar{\text{H}}$ beam is shown in Fig. 40. Bursts of positrons impinge on a nanoporous material to produce a burst of Ps atoms. The Ps atoms exit the material in the direction of a gas of antiprotons in a Penning trap. Using a two-step process, the Ps will be excited optically, first to a quantum number $n = 3$ state, and then to a high-Rydberg state with $n \geq 20$ (Castelli *et al.*, 2008).

The $\bar{\text{p}}$ will be sympathetically cooled by an electron plasma in the $\bar{\text{p}}$ trap that, in turn, will be cooled to 50 mK by cyclotron emission and resistive cooling. The Ps collisions with $\bar{\text{p}}$ will form cold $\bar{\text{H}}$ by charge exchange (Charlton, 1990). The horizontally directed $\bar{\text{H}}$ beam will be formed by Stark acceleration in an inhomogeneous electric field. It is planned to measure the deflection due to gravity using a two-grating Moire deflectometer and a position-sensitive detector. The $\bar{\text{H}}$ velocity will be varied and the vertical deflection measured as a function of time delay from the time of $\bar{\text{H}}$ formation. The initial goal is to measure g to 1%.

In another approach, ALPHA is pursuing measurement of the possible vertical asymmetry of antihydrogen decays when $\bar{\text{H}}$ are released from a minimum- B trap and strike an electrode (Amole *et al.*, 2013).

A new antimatter gravity experiment proposed at CERN is GBAR, which will attempt to measure the free fall of ultracold $\bar{\text{H}}$ atoms produced by sympathetic cooling of $\bar{\text{H}}^+$ ions with laser-cooled atoms in a Penning trap (Debu, 2013). The neutral $\bar{\text{H}}$ atoms will be produced from the $\bar{\text{H}}^+$ ions by laser photodetachment.

There is also a proposal to measure the vertical deflection of a horizontally directed beam of Ps atoms (Mills and Leventhal, 2002). Due to the very weak nature of the gravitational force, all approaches are expected to be exceedingly challenging for any given level of precision and would therefore benefit from colder atoms.

C. Electron-positron many-body system

The advent of efficient positron traps has raised the possibility of studying a wide range of many-positron effects; and in the last decade, this has become an active research area. Discussion of this area is separated into two topics: study of quantum e^+e^- systems and study of classical many body effects.

1. Quantum effects and a positronium-atom BEC

a. Theoretical considerations. In a seminal paper, Wheeler (1946) considered the stability of the many lepton systems Ps^- (i.e., $e^+e^-e^-$), Ps^+ ($e^+e^-e^+$) and Ps_2 . He concluded that the positronium ion (positive or negative) was stable, but due to the accuracy of the calculations at the time, uncertainty remained as to the stability of larger assemblies of leptons.

In a fluid, a relevant measure of the importance of quantum effects is the inter-particle spacing relative to the de Broglie wavelength, $\lambda_{De} = h/p$, where p is the particle momentum and h is Planck's constant. A fluid with number density n will be in the quantum regime when $n \gtrsim \lambda_{De}^{-3}$. For a given temperature, λ_{De} is larger for leptons than for proton-mass particles, and so the quantum fluid regime is easier to access in leptonic systems (i.e., in this case a gas of positronium atoms). Nevertheless, the required densities exceed current capabilities; and so study of the quantum regime will likely be possible only with advanced positron trapping and plasma manipulation techniques.

Shown in Fig. 41 is the predicted phase diagram for the electron-positron system based upon relatively simple considerations (Yabu, 2004). At high temperatures, Ps atoms are expected to ionize resulting in a classical pair plasma; and at high densities, a Mott transition is expected in which Ps atoms transform into a quantum pair liquid. To date, achievable positron densities have only been sufficient to create and study Ps_2 , while near-term goals include the creation of a Ps BEC and classical electron-positron plasmas.

b. Experimental studies: spin polarized positrons and the positronium molecule. Study of the two-electron, one positron system Ps^- was enabled by the relative availability of electrons (Mills, 1981). However, the formation and study of the di-positronium molecule, Ps_2 , presented a considerably greater challenge (Cassidy and Mills, 2007). The experiment is shown schematically in Fig. 42 (Cassidy *et al.*, 2006a). A ^{22}Na source ($\sim 25\text{--}50$ mCi) and solid neon moderator provide the positrons that feed a BGT, and positron pulses from the trap are shuttled into a separate accumulation stage in a magnetic field 0.05 T. Rotating wall compression is used both in the buffer-gas trap and in the accumulator, with the former in the single-particle regime and the latter in the strong-drive, plasma regime (Sec.VI.A.2).

Bursts of $\sim 10^8$ positrons from the accumulator are compressed in time to 1 ns, using a harmonic buncher and accelerated to $\sim 1\text{--}4$ keV before impinging upon a solid sample [i.e., porous silica or an Al (1,1,1) surface]. The (line-integrated) areal density of these pulses is $n_{2D} \sim 1 \times 10^{13} \text{ m}^{-2}$. To achieve higher areal densities, the sample is placed in a region of (pulsed) magnetic field up to $B \sim 2.3$ T, producing areal positron densities up to $\sim 10^{15} \text{ m}^{-2}$. The dependence of the Ps-Ps interactions on areal positron density n_{2D} in the sample was studied by adjusting the rotating wall electric field in the accumulator, while keeping all other parameters of the experiment constant.

Plans to study the quantum electron-positron system rely on a source of spin-polarized positrons to take advantage of the relatively long lifetime of triplet, $s = 1$, $m = 0$ state Ps, which is $0.14 \mu\text{s}$, set by three-gamma annihilation, even in tesla-strength fields. While positrons from radioisotope sources have spins preferentially aligned along the direction of the particle's momentum (cf. Sec. III.A.5) and could be used for this purpose, an important question is whether trapping and other manipulation techniques destroy this alignment.

To address this question, Cassidy and co-workers used the experimental arrangement described above and studied the delayed annihilation from a porous silica sample as a function of n_{2D} (Cassidy *et al.*, 2010a). After Ps is formed, the $m_z = 1$ component remains after the $s = 0$ Ps atoms and $s = 1$, $m_z = 0$ atoms have decayed. Data for a quenching parameter Q (defined as the delayed fraction of the annihilation, normalized to the delayed fraction at $n_{2D} = 0$), is shown in Fig. 43. The asymptotic value for large n_{2D} indicates that 28% of the positrons from the ^{22}Na source that strike the sample are spin aligned. This important result validates the positron-trap approach to studying the quantum electron-positron system.

Studies of Ps_2 also exploit the properties of Ps in microscopic cavities to increase the Ps-Ps interactions. The repulsive energy associated with quantum confinement of a Ps atom in a cavity of characteristic dimension l is proportional to $1/l^2$. Thus Ps implanted in a porous material (e.g., porous silica) will diffuse to the larger cavities and be confined there. The dependence of Q on n_{2D} and sample temperature provided the first experimental evidence of Ps_2 formation (Cassidy and Mills, 2007).

Using these and complimentary techniques, Mills and collaborators have made considerable progress in studying important Ps-Ps interactions: They have

- Created a spin-polarized Ps gas (Cassidy *et al.*, 2010a).
- Created the first di-positronium molecules, Ps₂ (Cassidy and Mills, 2007).
- Investigated Ps₂ formation in porous samples and at crystal surfaces (Cassidy *et al.*, 2012b).
- Studied optically the Ps₂ electronically excited state (Cassidy *et al.*, 2012b).

Mills and collaborators were able to make the first optical studies of Ps₂ (Cassidy *et al.*, 2012b; Cassidy and Mills, 2007). Shown in Fig. 44 are data for the one excited “electronic” state of Ps₂ (Cassidy *et al.*, 2012b). The observed shift in the resonance relative to that expected in vacuum is believed to be due to the surrounding environment. Those and related optical experiments were conducted to study Ps and Ps₂ in solids and in proximity to solid surfaces. They addressed important issues relevant to the creation of a Ps BEC.

c. Work towards a Ps BEC. The Ps–Ps interaction potential for triplet positronium is known to be repulsive. Thus it inhibits recombination and facilitates the formation of a relatively high-density gas of (long-lived) triplet Ps atoms. This is crucial for the formation of a Ps BEC. The critical density (n_c in m⁻³) for Bose condensation of Ps atoms is

$$n_c \sim 10^{24} \left[\frac{T}{14.6 \text{ K}} \right]^{3/2} \text{ m}^{-3}, \quad (85)$$

where T is the temperature (Landau, 1941; Mills *et al.*, 2004). This is approximately two orders of magnitude beyond current capabilities. However, numerous techniques can be used to increase n_{2D} , including

- Improved RW compression.
- Use of multiple PM traps (e.g., in series) to increase n_{2D} .
- Specially tailored porous structures to concentrate the Ps atoms.
- Non-adiabatic B -field extraction and electrostatic focusing to increase n_{2D} .

d. An annihilation gamma-ray laser. The possibility of stimulated emission at 511 keV has been considered by numerous authors (Bertolotti and Sibilia, 1979; Dirac, 1930; Liang and Dermer, 1988; Loeb and Eliezer, 1986; Platzman, 1986; Varma, 1977). Among other requirements to achieve appreciable gain, the linewidth must be sufficiently small. However, a pair plasma at the required density would be degenerate, leading to an unacceptably broad linewidth (i.e., due to the Fermi momentum). To circumvent this, it was proposed that stimulated emission might be achieved using a collection of Ps atoms (Liang and Dermer, 1988; Loeb and Eliezer, 1986).

Platzman and Mills (1994) proposed an experimental arrangement to accomplish this using a long, rod-shaped cavity 0.5 μm in diameter by 0.02 m long, just below the surface of a solid. The cavity would be filled with triplet Ps atoms, then the triplet Ps converted to singlet atoms by an intense microwave pulse (Mills, 2002; Yamazaki *et al.*, 2012). Mills has estimated that, for 3×10^{11} singlet Ps atoms in the cavity, the stimulated emission will be one standard deviation above background. Achieving such a large number of singlet Ps in such a small, pencil-shaped cavity will be exceedingly challenging. The tools and expected future improvement outlined above (i.e., to achieve a Ps BEC) are directly relevant to this type of experiment.

Given estimated losses, one would like to use larger bursts of positrons (e.g., $N \geq 10^{12}$). A multicell trap (cf. Sec. IV.D.2) could potentially be useful for this purpose, assuming a method can be developed to deliver such positron bursts in an acceptably short time (e.g., ≤ 100 ns).

2. Classical electron-positron (pair) plasmas

From a fundamental perspective, an (electrically neutral) equal-mass plasma is expected to exhibit qualitatively different properties than conventional electron-ion plasmas. Electron-positron plasmas of this type have been the subject of extensive theoretical investigation. Linear aspects of the system have been considered in several studies (Iwamoto, 1993; Stewart and Laing, 1992; Zank and Greaves, 1995). Nonlinear processes have been a particularly rich area including such aspects as solitary waves (Dubinov *et al.*, 2006; El-Shamy *et al.*, 2010; Ghosh *et al.*, 2012; Gordienko and Dubinov, 2008; Roy *et al.*, 2012; Sabry, 2009), solitons (Cattaert and Kourakis, 2005; Sabry *et al.*,

2009; Zank and Greaves, 1995), double layers (Alterkop *et al.*, 2007; Mishra *et al.*, 2007), collisionless reconnection processes (Bessho and Bhattacharjee, 2005; Hosseinpour and Vekstein, 2008) electrostatic and electromagnetic wave phenomena (El-Taibany and Mamun, 2012; Ghosh *et al.*, 2012; Gordienko and Dubinov, 2007; Kourakis *et al.*, 2007; Mushtaq and Khan, 2008), and vortices (Shukla *et al.*, 2003).

A system that approximates an equal-mass plasma has been studied using positive and negative ions (Oohara *et al.*, 2005; Oohara and Hatakeyama, 2003, 2007; Schermann and Major, 1978; Wexler *et al.*, 1983). However, experimental studies of such systems can suffer from the fact that the positive and negative ions (e.g., of C_{60}) are not exactly equal in mass, and that electron contamination can act to screen underlying equal-mass plasma response.

For an equal-density, equal-mass plasma, both the linear and non-linear plasma properties are expected to be fascinating. Interest in the latter is due to the fact that the electron and positron contributions to the nonlinear response, which are quadratic in the fields, are cubic in the charge; and hence they cancel. Properties include:

- Electromagnetic waves will be linearly, as opposed to circularly polarized (i.e., Faraday rotation is absent).
- Three-wave interactions, including Raman and Brillouin scattering, are absent.
- Non-linear Landau damping is larger than in conventional plasmas by the ion-electron mass ratio.
- Solitary wave phenomena dominate (i.e., due to large ion-acoustic wave damping, solitary-wave decay is weak).

Thus these novel properties offer the possibility of studying many interesting phenomena in pair plasmas.

The second motivation to study pair plasmas is that relativistic pair plasmas are expected to be important in many astrophysical settings, such as the magnetospheres of pulsars. Consequently, relativistic pair plasmas have been the subject of enormous theoretical activity. See, for example, papers by Berezhiani *et al.* (1993); Bessho and Bhattacharjee (2005); Blackman and Field (1994); Cattaert and Kourakis (2005) and Yin *et al.* (2008).

A range of physical situations have been considered, as well as linear and nonlinear phenomena in a variety of settings, including mixtures of pair plasma and ordinary electron-ion plasma. Such considerations provide strong motivation to study pair plasmas in the laboratory. Topics include, for example, nonlinear effects (Asenjo *et al.*, 2012; Liu and Liu, 2011), wave phenomena (Alinejad, 2012; Keston *et al.*, 2003), solitary waves (Berezhiani *et al.*, 1993; Tribeche and Boukhalfa, 2011), solitons (Pakzad and Kurosh, 2011; Saeed *et al.*, 2010; Verheest and Cattaert, 2005) and shock waves (Gallant *et al.*, 1992; Hussain *et al.*, 2013; Masood and Rizvi, 2010; Shah and Saeed, 2009; Tsintsadze, 1995).

The challenge of creating classical pair plasmas, as with achieving a Ps BEC, lies in large part in finding efficient methods to furnish sufficient numbers of positrons. In particular, one must confine the plasma long enough to study the particular plasma phenomena of interest. In addition, for a given source flux, the shorter the confinement time, the slower data can be accrued. Good confinement of neutral plasma is very generally problematic; this, and the lack of strong positron sources represent major constraints on the ability to study pair plasma phenomena. A second important consideration is that the positron-electron gas will exhibit plasma phenomena only if the characteristic dimension L of the charge cloud is such that $L \gg \lambda_D$. This favors high plasma densities and low temperatures.

On a positive note, pair plasmas are not particularly susceptible to annihilation. As per Eq. (78), the characteristic annihilation time $\Gamma_D^{-1} \sim 100$ s for an electron density $n_e = 10^{18} \text{ m}^{-3}$, which is more than sufficient to conduct many useful experiments. Similarly, the three-body recombination rate (i.e., for Ps formation, followed by annihilation) turns out to be negligible at all but cryogenic temperatures (Murphy, 1987).

a. Beam-plasma experiments. Considering that a major difficulty in studying pair plasma phenomena is providing the necessary number of positrons, a simple experiment to study pair plasma instabilities is to pass an electron beam through positron plasma. This was done in two geometries: using positrons trapped in a cylindrical PM trap and in a quadrupole trap (Gilbert *et al.*, 2001; Greaves and Surko, 1995). In the cylindrical trap, plasma heating was observed that depends on the electron-beam velocity. The data shown in Fig. 45 provide evidence of a two-stream instability, and the observed positron-plasma heating rate as a function of beam velocity matches reasonably well the predicted instability growth rate.

In the quadrupole trap, oscillations were observed due to the coherent excitation of the center-of-mass motion of the positron plasma in the confining well (the “transit-time” instability). The growth and then decay of the signal as a function of time coincided with observation of annihilation gamma rays, providing evidence of particle loss. In both experiments, no attempt was made to monitor *in situ* fluctuations in the plasma. This will be a crucial, albeit difficult, step in studying the pair plasma system in greater detail.

b. Pair plasmas in a stellerator. A number of approaches have either been proposed, attempted, or are in the process of being attempted, to study confined pair plasmas.

Pedersen and collaborators proposed an experiment to study such plasmas (Pedersen *et al.*, 2003, 2012). As described in Sec. IV.D.2.d, they constructed a device (the Columbia Nonneutral Torus, CNT, shown in Fig. 15). To do this, they conducted experiments with single-component electron plasmas and studied confinement in the CNT (Pedersen *et al.*, 2006). A disadvantage of the CNT is the relatively large plasma volume, that in turn, would require a large quantity of positrons. Consequently they proposed to build a new device (named “A Positron-Electron eXperiment”, APEX) using superconducting coils ($B \sim 2$ T). This will improve confinement and reduce the plasma volume, as well as decrease the cyclotron cooling time to ~ 1 s, which is expected to be less than or equal to the plasma confinement time (Pedersen *et al.*, 2012).

The arrangement of confining magnetic fields will be created by two intertwined circular field coils, similar to those of CNT. The APEX device will be a factor of two smaller in size and a factor of ten larger in field strength as compared with CNT (Pedersen *et al.*, 2012). The anticipated operating parameters for the APEX experiment are: $N \sim 10^{11}$; major and minor radii, 0.15 and 0.07 m; T : 0.2 – 2 eV; and λ_D : 0.001 – 0.03 m (Pedersen *et al.*, 2012).

The required positrons will be delivered in bursts from a multi-cell trap. Unlike the Ps BEC application, plasma confinement times are long enough so that the MCT can be dumped serially, one line of cells at a time. This is expected to be within present capabilities (i.e., \sim milliseconds per line of cells).

Two methods are proposed to fill APEX with positrons (Pedersen *et al.*, 2012). One involves drift-orbit injection using pulsed electrostatic fields. A second, more challenging approach involves magnetically guiding the positrons to a single-crystal Si surface where they will produce 0.16 eV Ps atoms (Cassidy *et al.*, 2011b). The Ps atoms will be optically excited to the $n = 2$ state, then excited by a second laser into a higher Rydberg state to further increase their lifetime. After the Ps atoms drift across the magnetic field into the confinement volume, they can be photo-ionized by a third, infrared laser or using microwaves. In this scheme, the plasma will automatically be “born neutral,” since the photo-ionized Ps will provide both the electrons and the positrons in equal numbers. A further advantage of this scenario is that the plasma temperature can be varied by adjusting the wavelength of the second laser.

c. Confinement using a magnetic dipole. A second proposed magnetic geometry for studying pair plasma phenomena is to use a (magnetically) levitated superconducting magnetic dipole. The RT-1 device, shown in Fig. 46 has recently demonstrated good confinement for single-component electron plasmas (Saitoh *et al.*, 2013; Yoshida *et al.*, 2010). Specifically, an electron plasma of density 10^{11} m^{-3} was confined for 300 s. This device could be filled with positrons from an MCT using the methods described above for the APEX stellarator.

An experiment was conducted placing a ^{22}Na positron source directly in the confinement region of the RT-1 device (Saitoh *et al.*, 2013). Simulations showed that the fast positrons follow chaotic orbits in the confinement region. Annihilation was monitored on a target plate in the confinement region. The data indicate 4% of the fast positrons annihilated on the target, verifying fast-positron confinement. For a pair plasma experiment, applied azimuthal electric fields could be used to induce inward diffusion of the positrons to the stronger field part of the confinement region (Saitoh *et al.*, 2013). Alternatively, the laser scheme described above could also be used to fill the dipole.

d. Magnetic mirror confinement. As discussed in Sec. IV.D.2, the concept of positron and pair-plasma trapping in magnetic mirror devices has a long history beginning with the seminal positron confinement experiments of Gibson *et al.* (1960, 1963) (cf. Fig. 1). While such experiments have not yet demonstrated pair plasma confinement, magnetic mirrors have considerable promise for studying *relativistic* pair plasmas. One could fill the mirror trap and then cyclotron-heat the particles (i.e., done relatively efficiently for electron-mass particles) to achieve good confinement.

Nevertheless, a major impediment to studying relativistic pair plasmas is still in furnishing sufficient numbers of positrons. This is accentuated by the fact that the particle energy will be high. For example, for a plasma with temperature of 300 keV (mildly relativistic), $\lambda_D = 0.01\text{m}$ will require a positron density $\sim 10^{17} \text{ m}^{-3}$. Thus a plasma with characteristic dimension of $10 \lambda_D$ will require $N \geq 10^{14}$ positrons per discharge. This, for example, is near the outer boundary of what is currently thought possible using an MCT.

e. Confinement in a Penning-Paul trap. A different approach was proposed for the study of pair plasmas that relies on Paul-trapping technology. As illustrated in Fig. 47, a cylindrical PM trap was proposed, but with rf on the confining end electrodes (as opposed to potentials) to provide the repulsive potential to confine particles with both sign of charge (Greaves and Surko, 2002b). Positive dc potentials could also be applied to the electrodes to aid in positron confinement, in this case using the electrons sacrificially.

Parameters of the experiment are listed in Table V. The particles would be cooled by inelastic vibrational collisions with a molecule such as CO₂. Details of the cooling process are discussed by Greaves and Surko (2002b), and additional considerations, including heating due to lepton-neutral collisions, are discussed in Surko *et al.* (2014). A limitation of the Penning-Paul approach is that practical rf field amplitudes restrict the confining potential to ≤ 10 V, which restricts studies to relatively cool, low-density plasmas.

D. Atomic and molecular physics with positrons

Historically, understanding electron interactions with matter began with experimental electron-atom and electron-molecule studies. They led to many important physical insights and first-principles connections with theory. While this same approach is relevant to positron-matter interactions, progress has been hindered by the relative lack of experimental tools. In recent years, positron traps and trap-based beams have helped remedy this situation.

1. *In situ* annihilation studies

Early low-energy positron experiments, such as those in which the Ps atom was discovered, were conducted with a radioisotope source in close proximity to a test gas (Deutsch, 1951; Heyland *et al.*, 1982). The gas was typically at 300 K and amagat-scale densities, the latter to ensure that the positrons stopped in the sample. The lifetimes of the positrons were measured as a function of density and test-gas species, sometimes varying the test-gas pressure, or in the presence of an external electric field. Those annihilation rate studies led to better understanding of numerous processes such as annihilation on noble gas atoms. However, the drawbacks of that type of experiment include ensuring that the positrons are thermalized before annihilation, the inability to study low-vapor-pressure materials, and quantifying the effects of many-body interactions. Such considerations highlighted the need for additional technology.

The invention of the BGT immediately provided new opportunities for annihilation studies (Surko *et al.*, 1988). With the positron trap, low-density test gases could be placed in contact with trapped positrons that were verified to be at a known temperature (e.g., the ambient, 300 K). This technique permitted study of a wide range of molecular species, including relatively large molecules, and low-vapor pressure materials (Iwata *et al.*, 1995; Murphy and Surko, 1991). The effect of positron temperature T_p was also studied by measuring both T_p and the annihilation rate as a function of time following heating with rf noise (Kurz *et al.*, 1996).

For a simple collision of a positron with an atomic or molecular target, the benchmark annihilation rate is expected to be approximately the Dirac rate Γ_D for annihilation in a free electron gas. The measured rates λ are converted to a normalized rate

$$Z_{\text{eff}} \equiv \frac{\lambda}{\Gamma_D}, \quad (86)$$

where Γ_D is given by Eq. (78) using for n the atomic or molecular number density. Thus for a simple collision, it is expected that $Z_{\text{eff}} \sim Z$, where Z is the total electronic charge on the target. Typically this is observed for atoms. However, a perplexing result, dating from the first studies of annihilation on molecules by Deutsch (1951), is that $Z_{\text{eff}} \gg Z$ for many molecular species.

Figure 48 shows Z_{eff} data for a wide variety of molecular species measured *in situ* in a BGT. Generally $Z_{\text{eff}} \gg Z$ for molecules, and large variations in Z_{eff} are observed depending upon the chemical composition of the target. As discussed below, this is related to the fact that positrons bind to atomic and molecular species; and for molecules, the positron can become attached *via* the excitation of a vibrational Feshbach resonance.

The annihilation rate measurements were augmented by study of the Doppler broadening of the annihilation gamma rays (Iwata *et al.*, 1997a,b; Tang *et al.*, 1992). The gamma-ray energies are shifted by the Doppler effect arising from the center of mass velocity of the annihilating electron-positron pair. Since the positron energy is low (e.g., 300 K), these shifts come predominantly from the momentum distribution of the bound electrons. Key results from those measurements included precision comparisons with state-of-the-art calculations of the gamma ray spectrum from helium atoms (Van Reeth *et al.*, 1996), and benchmark spectra for atoms and molecules.

As shown in Fig. 49, similar experiments were able to distinguish annihilation from inner-shell electrons from the dominant contribution of that from the valence shell that agreed well with contemporary theoretical calculations (Iwata *et al.*, 1997a). Recent theoretical studies aim to provide a more complete understanding of the contribution of the positron wave function to the spectra from molecules (Green *et al.*, 2012).

2. Scattering studies

Experiments with positron beams produced using radioisotope sources and metallic positron moderators elucidated many aspects of positron atomic and molecular physics and motivated complementary theoretical studies. They were, however, hindered by a lack of energy resolution (e.g., typical resolution > 0.1 eV FWHM) and low beam fluxes due to the lack of efficient moderators. As described in Sec. VII.A, about a decade after the development of the BGT, a trap-based positron beam was developed, using a solid neon moderator, that had an energy resolution of $\simeq 40$ meV FWHM total energy spread, comprised of $\Delta\epsilon_{\parallel} = 18$ meV FWHM in energy spread in motion parallel to the magnetic field and $\Delta\epsilon_{\perp} = 25$ meV FWHM (i.e., $k_B T$ at 300 K) in the cyclotron motion perpendicular to the field (Gilbert *et al.*, 1997).

The experimental arrangement is illustrated in Fig. 28. The beam is passed through a cell filled with the test species in the gas phase (Gilbert *et al.*, 2002; Sullivan *et al.*, 2002) in a magnetic field ~ 0.01 – 0.1 T. In fields of this strength, the quantity ϵ_{\perp}/B is an adiabatic invariant, where ϵ_{\perp} is the particle energy in the cyclotron motion. Since a scattering event takes place on length scales small compared with the positron gyroradius, it can change parallel energy ϵ_{\parallel} into ϵ_{\perp} and vice versa. Transporting the scattered positrons to a much lower field after a scatter transfers ϵ_{\perp} to ϵ_{\parallel} , and so the total energy (i.e., now $\epsilon \approx \epsilon_{\parallel}$) can be measured using a retarding potential analyzer (Gilbert *et al.*, 2002; Sullivan *et al.*, 2002).

This and related techniques enabled a number of new positron scattering studies, such as:

- First state-resolved measurements of the vibrational excitation of molecules (Gilbert *et al.*, 1999)
- First state-resolved measurements of the electronic excitation of molecules (Caradonna *et al.*, 2009; Sullivan *et al.*, 2001)
- Improved cross sections for atoms and molecules (Chiari *et al.*, 2013; Jones *et al.*, 2011; Makochekanwa *et al.*, 2011; Marler *et al.*, 2005; Marler and Surko, 2005a)

Ionization studies included both “direct” ionization (i.e., $A + e^+ \rightarrow A^+ + e^+ + e^-$, where A is an atom or molecule) and ionization via Ps-atom formation (Laricchia *et al.*, 2008; Marler *et al.*, 2005; Marler and Surko, 2005a). Cross section measurements for atoms led to new theoretical calculations. Agreement between theory and experiment for noble gas atoms is generally good below the threshold for Ps formation, while theoretical description of Ps formation continues to be challenging (Jones *et al.*, 2011; Makochekanwa *et al.*, 2011).

Beyond their importance in developing a more complete understanding of positron interactions, some of the results led to a better understanding of the efficient operation of the BGT (Sec. IV.B). Shown in Fig. 50 are the electronic excitation and positronium formation cross sections for positron scattering from molecular N_2 (Marler *et al.*, 2005). The trapping efficiency on N_2 benefits from the fact that at energies ~ 10 eV, electronic excitation has a larger cross section than positronium formation (i.e., the latter a potent positron loss process).

Another important contribution to positron-trap physics was measurement of the (unusually large) inelastic vibrational excitation cross section of CF_4 , shown in Fig. 51. This is used in the BGT to cool the positrons to 300 K (Sec. IV.C).

3. Annihilation as a function of positron energy

A highlight of the positron-atomic physics results was the discovery that the large annihilation rates on molecules imply that molecules can support positron bound states (Barnes *et al.*, 2003, 2006; Danielson *et al.*, 2010, 2012; Gilbert *et al.*, 2002; Gribakin *et al.*, 2010; Young and Surko, 2008; Young *et al.*, 2008). As illustrated in Fig. 52, annihilation was found to occur by the excitation of vibrational Feshbach resonances (Gribakin and Lee, 2006a; Gribakin *et al.*, 2010). An incident positron at energy $\epsilon_{\nu} = \omega_{\nu} - \epsilon_b$, where ω_{ν} is the energy of a vibration and ϵ_b is the positron-molecule binding energy, excites vibration ω_{ν} and populates the bound state, thus leading to an enhanced annihilation rate. Shown in Fig. 53 is the effect of increased molecular size on the Z_{eff} spectrum for alkane molecules ($C_n H_{2n+2}$). The Z_{eff} values increase and the spectrum downshifts in energy as molecular size (and ϵ_b) increase. The amplitudes of the resonant annihilation peaks are limited by the subsequent ejection of the positron due to de-excitation of a vibration. A focus of current research is the understanding of the vibrational dynamics that leads to this ejection (Jones *et al.*, 2013).

Binding energies for over 75 molecular species have now been measured. They range from a few millielectron volts to ≥ 300 meV (Gribakin *et al.*, 2010). Table VI shows a comparison of positron and analogous electron binding to selected molecules (Danielson *et al.*, 2012). Electron binding is typically weaker by a factor ranging from 10 to 100. One reason for this is illustrated in Fig. 54 for the molecule acetonitrile (CH_3CN), which has a relatively large electric

dipole moment μ . Both leptons are excluded from penetrating the molecule. However, the positron can come closer to the electric dipole, since the negative end of the dipole is closer to the periphery of the molecule, and this leads to larger ϵ_b . Theoretical predictions for ϵ_b for positrons for this and similar molecules are now within 30% of the measurements (Tachikawa *et al.*, 2011).

It is fair to say that understanding positron binding to molecules is now at a more advanced stage than positron binding to atoms. While there are more accurate theories for positron-atom binding (Mitroy and Ivanov, 2002), they do not possess low-lying excitations, such as vibrational modes, so that the attached state cannot be populated in a two-body positron-atom collision. It has recently been proposed to use a laser to photo-induce positron-atom recombination to do this (Surko *et al.*, 2012). The success of such an experiment will likely hinge on exploiting the positron plasma and beam manipulation techniques described in Sec. VI.

4. Laser spectroscopy of positronium

As discussed in Sec. VIII.C.1, trap-based beams have enabled new studies of the Ps many body system. While laser spectroscopy is one of the most important tools for studying physical systems, there have been few optical studies of Ps [for example, see (Chu and Mills, 1982; Fee *et al.*, 1993; Ziock *et al.*, 1990)]. This is due, in considerable part, to the relative unavailability of techniques to produce large bursts of Ps atoms that can be probed with pulsed laser light. The development of pulsed, trap-based positron beams has gone a long way toward mitigating this problem.

Exploiting this technology, recent laser studies of atomic positronium include probing paramagnetic centers (Cassidy *et al.*, 2007), optical measurement of the Ps hyperfine interval (Cassidy *et al.*, 2012c), spectroscopic observation of the Ps₂ molecule (Cassidy *et al.*, 2012b), and the efficient production of Rydberg positronium (Cassidy *et al.*, 2012a). This technology opens the door to other experiments, such as Ps laser cooling (e.g., to create a Ps BEC [Sec. VIII.C.1, (Liang and Dermer, 1988)] and improved spectroscopy of Ps to test QED theory (Karshenboim, 2002, 2005). It will also facilitate the development of advanced materials to be used as positron-to-Ps converters, such as the newly discovered Ps production mechanism involving a semiconductor surface state (Cassidy *et al.*, 2011a,b).

5. Selective ionization of molecules

When a positron is incident upon a neutral molecule, it can produce a spectrum of secondary ions (Hulett *et al.*, 1993; Passner *et al.*, 1989). At least three processes appear to be involved: annihilation on the molecule (either nonresonant or resonant), Ps formation, and so-called direct ionization.

In each case, there can be a spectrum of ion fragments, presumably accompanied by a complementary set of neutral fragments. A key result is that the spectrum of secondary ions depends upon the incident positron energy (Hulett *et al.*, 1993, 1996). Intriguingly, at least in some molecules, positrons with incident energies near the threshold for Ps formation, produce an un-fragmented ion (i.e., the ion corresponding to the parent molecule with one electron removed), which could be used for mass spectrometry. While a number of species have been studied, this approach to selective ionization has yet to be investigated in detail. Scientific questions of interest include whether the pre-dominance of the parent ion near the Ps threshold is a general phenomenon and how this effect depends upon beam energy resolution.

6. Laboratory modeling of astrophysical processes

There are numerous questions regarding the behavior of positrons in astrophysical settings, and several involve atomic and molecular processes. Positron traps and trap-based beams can be used to address questions such as study of the slowing and annihilation spectra of energetic positrons in various gaseous and plasma media (Brown and Leventhal, 1986; Brown *et al.*, 1984; Iwata *et al.*, 1996). Important considerations include the dependence on the composition, density, temperature and ionization state of the medium. Specific goals include modeling positron annihilation in the interstellar medium and studying annihilation on dust grains and clusters. While a relatively wide range of tools are now available to study such processes, very few of these questions have been addressed (Guessoum, 2014; Guessoum *et al.*, 2006, 2010).

7. Trapping and cooling highly charged ions

There is considerable interest in studying atomic processes involving highly charged ions (Bernard *et al.*, 2004; Mohri *et al.*, 2002; Oshima *et al.*, 2003, 2005; Zwicknagel, 2006). Plasma applications include study of radiation from so-called high- Z impurities in magnetically confined fusion plasmas and understanding the behavior of high-temperature plasmas in astrophysical settings. A convenient way to do this is to confine highly charged ions in an electromagnetic trap and study absorption and emission spectra. To accomplish this, one needs an energy loss mechanism, first to trap the ions, and then to provide a cooling mechanism to prevent ion losses and to produce cold ions for improved precision in spectroscopy. It has been pointed out that positrons can be used effectively for this purpose. While electrons can recombine and thus reduce the ion's charge state, positrons will not. Further, given the positive charge of the positron, positron-ion collisions can transfer energy efficiently without electron-positron overlap; hence annihilation is not a problem. More efficient and intense positron sources and efficient positron moderators would facilitate such experiments (Oshima *et al.*, 2005).

E. Materials studies

Positron probes have been extensively employed to characterize materials. Specific capabilities include the ability to measure the concentration and size distribution of voids in materials as well as measure the elemental composition at surfaces.

These techniques can be implemented using unmoderated positrons from a radioactive source but their utility is greatly increased when implemented using moderated positrons. Desirable characteristics for such beams include short pulses and finely focused beams.

1. Positron annihilation lifetime spectroscopy

a. Single photon techniques. Positron annihilation spectroscopy (PALS) is a useful technique, for example, for probing local electron density (Puska and Nieminen, 1994; Schultz and Lynn, 1988; Tuomisto and Makkonen, 2013). This technique is based on the fact that positrons injected into materials can become trapped in voids where the annihilation time is increased due to the reduced electron density. By measuring the positron lifetime, both the density and size distribution of the voids can be measured (Gidley *et al.*, 2006, 2000). The technique is applicable to a wide range of void distributions from single atom vacancies to mesoporous materials. Applications include studying metal fatigue, aging of polymers, and characterizing low- k dielectric films for integrated circuit fabrication (Gidley *et al.*, 2006, 2000).

Measurement of the positron lifetime spectra requires knowledge of both the time of injection of the positron into the sample and the time of annihilation. Several techniques have been developed for obtaining this timing information. The time of annihilation is conveniently measured by detecting the 511-keV annihilation gamma ray using fast scintillation detectors. The time of injection can be obtained by detecting secondary electrons emitted at the surface when the positron is injected (Lynn *et al.*, 1984). Alternatively, the incoming positrons can be bunched and the bunching signal can provide the required timing information (Mills, 1980c). Bunchers based on rf sine-waves are commonly used for bunching positrons from a moderator, but the technique is complex to implement in practice.

Positron traps provide a simpler alternative using the bunching techniques described in Sec. VII.D. Sullivan *et al.* (2010) described a positron lifetime system based on a compact two-stage trap. Bunching is obtained by applying a tailored waveform generated by an arbitrary waveform generator to the ring electrode of the trap during the dump. They obtained time resolution of ~ 800 ps. Figure 55 shows an example of the lifetime spectrum for a biopolymer (Chaudhary *et al.*, 2010).

b. Single shot measurements. Cassidy and coworkers developed a complementary method for measuring positron lifetime spectra that is particularly useful when intense positron bursts impinge on a sample. The anode signal from a photomultiplier attached to a fast scintillator or Cherenkov radiation detector is recorded with a fast digital storage oscilloscope following the deposition of an intense, time-bunched positron pulse from a trap (Cassidy *et al.*, 2006c). Data for porous silica is shown in Fig. 56. This technique permits the measurement of transitory effects as well as high density positronium interactions.

If a finely focused positron beam (“microbeam”) is available, *spatially resolved* lifetime information can be obtained by scanning the beam across the sample to act as a positron microscope. A further refinement can be obtained by varying the implantation energy of the beam to resolve subsurface features. The conventional technique for producing positron microbeams is based on repeated application of the remoderation brightness enhancement technique described in Sec. III.D together with electrostatic focusing. David *et al.* (2001) described a scanning positron microprobe with a 2 μm diameter beam and a 200 ps pulse width.

However, remoderation brightness enhancement has the disadvantage of significant losses (70% or more at each stage), and so long data acquisition times are required to obtain detailed images using this technique. On the other hand, positron traps have the potential to achieve the same result with greatly reduced losses. For example, rotating wall compression (Sec. VI.A) can reduce the diameter of the incoming beam by a factor of ten or more, while extraction of positrons from the center of the plasma (Sec. VII.B) can reduce the beam diameter by another order of magnitude. When combined with extraction of the positrons from the magnetic field of the trap (Sec. VII.E) and electrostatic focusing, it should be possible to produce microbeams with much higher throughputs.

IX. SUMMARY AND CONCLUDING REMARKS

We have presented a review of the plasma tools that have been developed to accumulate, store and manipulate antimatter. Emphasis has been placed upon techniques involving positrons. Since they are easier to produce, much more work has been done with them than with antiprotons, and hence the knowledge base is greater. Emphasis is also placed upon those techniques that have proven to be most useful to date. Additional discussion was focused in areas where the potential for further development appears to be significant. Finally we discussed briefly the related techniques and regimes that might be considered for future development as the need and opportunity arises.

As research and technology goals for antimatter expand to confront, for example, new antimatter phases and regimes, further development will be required. Some topics on the “technological wish list” have been outstanding needs from the very beginning of low-energy antimatter research. For example, there continues to be a generic need for more intense sources of antiparticles, both positrons and antiprotons. A related challenge is to devise more efficient positron moderators and analogous methods to slow fast antiprotons for low-energy applications. Indeed, in the case of positrons, progress has arguably been painfully slow since the invention of the solid rare gas moderator three decades ago.

As antimatter research and technology focuses more intently on high-density states of antiparticles (e.g., to study and exploit many body effects), a natural objective is further development of the rotating wall technique or a similar active method to compress antiparticle plasmas. An outstanding challenge with regard to the rotating wall is to understand what currently limits the maximum density and to overcome this limit if possible.

There is also a generic need for improved antiparticle cooling techniques. Many manipulation techniques and applications either benefit from, or require, efficient methods to cool antiparticles. Examples include efficient operation of the rotating wall technique and the creation of positron beams with good energy resolution, both of which require efficient cooling.

Often rapid, and/or large bursts of positrons are desired. Thus another challenge is the development of improved methods to deliver such bursts (e.g., $\geq 10^{12}$ positrons delivered in milliseconds for a classical pair plasma and in tens of nanoseconds for a Ps BEC).

The development of a practical portable positron trap would be transformative. It would enable much more widespread use of positrons without the need for co-located radioisotopes or a particle accelerator or nuclear reactor. The good news is that, while challenging, none of these technological goals is obviously beyond reach, and progress in several of these areas is quite likely in the next few years.

The second dimension of this review is a discussion of areas in which these antimatter manipulation techniques have proven particularly useful. These applications provide a glimpse of the forefront of low-energy antimatter research, and they naturally highlight the present outstanding goals and challenges. In the area of positron beams used to study ordinary matter, for example, there is a continuing need for specially tailored beams: finely focused for microscopy, improved energy resolution for spectroscopy, and shorter pulses for lifetime spectroscopy.

The continuing challenge in antihydrogen research is to create colder antiparticle plasmas and beams and to develop methods to combine the constituents efficiently while avoiding additional heating. Finally, we are arguably at the cusp in the effort to study antiparticle many-body effects, such as the nature of a Ps BEC and the behavior of classical pair plasmas. In the latter area, a further goal will be to create and study a *relativistic* pair plasma. Progress in all of these areas provides an exciting array of interesting challenging problems for both the experimenter and the theorist.

ACKNOWLEDGMENTS

We wish to acknowledge helpful conversations with John Bollinger, David Cassidy, Mike Charlton, Joel Fajans, Thomas Pedersen and Francis Robicheaux. D. D. wishes to acknowledge support from the NSF, grant PHY0903877 and the DOE, grant DE-SC0002451. J. D. and C. S. wish to acknowledge support from the NSF atomic physics program, grants PHY10-68023 and PHY14-01794; as well as previous support from the NSF/DOE Plasma Partnership and the Defense Threat Reduction Agency.

REFERENCES

- Akahane, T (1994), “Extraction of slow positrons from the magnetic field,” in *Slow Positron Beam Techniques For Solids And Surfaces: Fifth International Workshop*, AIP Conference Proceedings, Vol. 303, edited by E. Ottewitte and A. H. Weiss (AIP Press, Melville, NY) pp. 437–40.
- Al-Qaradawi, I Y, P. A. Sellin, and P. G. Coleman (2002), “Tests of a diamond field-assisted positron moderator,” *Appl. Surf. Sci.* **194**, 29–31.
- Alinejad, H (2012), “Effect of nonthermal electrons on oblique electrostatic excitations in a magnetized electron-positron-ion plasma,” *Phys. Plasmas* **19**, 052302–6.
- Alterkop, B A, I. D. Dubinov, and A. E. Dubinov (2007), “Charged double layer at the boundary between a symmetric plasma and a wall,” *Tech. Phys.* **52**, 884–91.
- Amole, C, G. B. Andresen, M. D. Ashkezari, M. Baquero-Ruiz, W. Bertsche, P. D. Bowe, E. Butler, A. Capra, P. T. Carpenter, C. L. Cesar, S. Chapman, M. Charlton, A. Deller, S. Eriksson, J. Escallier, J. Fajans, T. Friesen, M. C. Fujiwara, D. R. Gill, A. Gutierrez, J. S. Hangst, W. N. Hardy, R. S. Hayano, M. E. Hayden, A. J. Humphries, J. L. Hurt, R. Hydromako, C. A. Isaac, M. J. Jenkins, S. Jonsell, L. V. Jørgensen, S. J. Kerrigan, L. Kurchaninov, N. Madsen, A. Marone, J. T. K. McKenna, S. Menary, P. Nolan, K. Olchanski, A. Olin, B. Parker, A. Povilus, P. Pusa, F. Robicheaux, E. Sarid, D. Seddon, S. Seif El Nasr, D. M. Silveira, C. So, J. W. Storey, R. I. Thompson, J. Thornhill, D. Wells, D. P. van der Werf, J. S. Wurtele, and Y. Yamazaki (2014), “The alpha antihydrogen trapping apparatus,” *Nucl. Instrum. Methods A* **735**, 319–40.
- Amole, C, M. D. Ashkezari, M. Baquero-Ruiz, W. Bertsche, P. D. Bowe, E. Butler, A. Capra, C. L. Cesar, M. Charlton, A. Deller, P. H. Donnan, S. Eriksson, J. Fajans, T. Friesen, M. C. Fujiwara, D. R. Gill, A. Gutierrez, J. S. Hangst, W. N. Hardy, M. E. Hayden, A. J. Humphries, C. A. Isaac, S. Jonsell, L. Kurchaninov, A. Little, N. Madsen, J. T. K. McKenna, S. Menary, S. C. Napoli, P. Nolan, K. Olchanski, A. Olin, P. Pusa, C. Ø. Rasmussen, F. Robicheaux, E. Sarid, C. R. Shields, D. M. Silveira, S. Stracka, C. So, R. I. Thompson, D. P. van der Werf, and J. S. Wurtele (2012), “Resonant quantum transitions in trapped antihydrogen atoms,” *Nature* **483**, 439–44.
- Amole, C, M. D. Ashkezari, M. Baquero-Ruiz, W. Bertsche, E. Butler, A. Capra, C. L. Cesar, M. Charlton, S. Eriksson, J. Fajans, T. Friesen, M. C. Fujiwara, D. R. Gill, A. Gutierrez, J. S. Hangst, W. N. Hardy, M. E. Hayden, C. A. Isaac, S. Jonsell, L. Kurchaninov, A. Little, N. Madsen, J. T. K. McKenna, S. Menary, S. C. Napoli, P. Nolan, A. Olin, P. Pusa, C. Ø. Rasmussen, F. Robicheaux, E. Sarid, D. M. Silveira, C. So, R. I. Thompson, D. P. van der Werf, J. S. Wurtele, and A. I. Zhmoginov (2013), “Description and first application of a new technique to measure the gravitational mass of antihydrogen,” *Nature Comm.* **4**, 1785–9.
- Amoretti, M, C. Amsler, G. Bonomi, A. Bouchta, P. Bowe, C. Carraro, C. L. Cesar, M. Charlton, M. Collier, M. Doser, V. Filippini, K. S. Fine, A. Fontana, M. C. Fujiwara, R. Funakoshi, P. Genova, J. S. Hangst, R. S. Hayano, M. H. Holzschleiter, L. V. Jørgensen, V. Lagomarsino, R. Landua, D. Lindelöf, E. Lodi Rizzini, M. Macrì, N. Madsen, G. Manuzio, M. Marchesotti, P. Montagna, H. Pruys, C. Regenfus, P. Riedler, J. Rochet, A. Rotondi, G. Rouleau, G. Testera, A. Variola, T. L. Watson, and D. P. van der Werf (2002), “Production and detection of cold antihydrogen atoms,” *Nature* **419**, 456–9.
- Amoretti, M, C. Amsler, G. Bonomi, A. Bouchta, P. D. Bowe, C. Carraro, C. L. Cesar, M. Charlton, M. Doser, V. Filippini, A. Fontana, M. C. Fujiwara, R. Funakoshi, P. Genova, J. S. Hangst, R. S. Hayano, L. V. Jørgensen, V. Lagomarsino, R. Landua, D. Lindelöf, E. Lodi Rizzin, M. Macrì, N. Madsen, G. Manuzio, P. Montagna, H. Pruys, C. Regenfus, A. Rotondi, G. Testera, A. Variola, and D. P. van der Werf (2003a), “Positron plasma diagnostics and temperature control for antihydrogen production,” *Phys. Rev. Lett.* **91**, 055001–5.
- Amoretti, M, G. Bonomi, A. Bouchta, P. D. Bowe, C. Carraro, C. L. Cesar, M. Charlton, M. Doser, A. Fontana, M. C. Fujiwara, R. Funakoshi, P. Genova, J. S. Hangst, R. S. Hayano, L. V. Jørgensen, V. Lagomarsino, R. Landua, E. L. Rizzini, M. Macrì, N. Madsen, G. Manuzio, G. Testera, A. Variola, and D. P. van der Werf (2003b), “Complete nondestructive diagnostic of nonneutral plasmas based on the detection of electrostatic modes,” *Phys. Plasmas* **10**, 3056–64.
- Anderegg, F, E. M. Hollmann, and C. F. Driscoll (1998), “Rotating field confinement of pure electron plasmas using Trivelpiece-Gould modes,” *Phys. Rev. Lett.* **81**, 4875–8.
- Anderegg, F, N. Shiga, J. R. Danielson, D. H. E. Dubin, C. F. Driscoll, and R. W. Gould (2003), “Thermally excited modes in a pure electron plasma,” *Phys. Rev. Lett.* **90**, 115001–4.
- Anderson, C D (1932), “The apparent existence of easily deflectable positives,” *Science* **76**, 238–9.
- Andresen, G B, M. D. Ashkezari, M. Baquero-Ruiz, W. Bertsche, P. D. Bowe, E. Butler, P. T. Carpenter, C. L. Cesar, S. Chapman, M. Charlton, J. Fajans, T. Friesen, M. C. Fujiwara, D. R. Gill, J. S. Hangst, W. N. Hardy, M. E. Hayden, A. J. Humphries, J. L. Hurt, R. Hydromako, S. Jonsell, N. Madsen, S. Menary, P. Nolan, K. Olchanski, A. Olin, A. Povilus,

- P. Pusa, F. Robicheaux, E. Sarid, D. M. Silveira, C. So, J. W. Storey, R. I. Thompson, D. P. van der Werf, J. S. Wurtele, and Y. Yamazaki (2011a), “Autoresonant excitation of antiproton plasmas,” *Phys. Rev. Lett.* **106**, 025002–5.
- Andresen, G B, M. D. Ashkezari, M. Baquero-Ruiz, W. Bertsche, P. D. Bowe, E. Butler, C. L. Cesar, S. Chapman, M. Charlton, J. Fajans, T. Friesen, M. C. Fujiwara, D. R. Gill, J. S. Hangst, W. N. Hardy, R. S. Hayano, M. E. Hayden, A. Humphries, R. Hydromako, S. Jonsell, L. Kurchaninov, R. Lambo, N. Madsen, S. Menary, P. Nolan, K. Olchanski, A. Olin, A. Povilus, P. Pusa, F. Robicheaux, E. Sarid, D. M. Silveira, C. So, J.W. Storey, R. I. Thompson, D. P. van der Werf, D. Wilding, J. S. Wurtele, and Y. Yamazaki (2010), “Evaporative cooling of antiprotons to cryogenic temperatures,” *Phys. Rev. Lett.* **105**, 013003–5.
- Andresen, G B, M. D. Ashkezari, M. Baquero-Ruiz, W. Bertsche, P. D. Bowe, E. Butler, C. L. Cesar, M. Charlton, A. Deller, S. Eriksson, J. Fajans, T. Friesen, M. C. Fujiwara, D. R. Gill, A. Gutierrez, J. S. Hangst, W. N. Hardy, R. S. Hayano, M. E. Hayden, A. J. Humphries, R. Hydromako, S. Jonsell, S. L. Kemp, L. Kurchaninov, N. Madsen, S. Menary, P. Nolan, K. Olchanski, A. Olin, P. Pusa, C. Ø. Rasmussen, F. Robicheaux, E. Sarid, D. M. Silveira, C. So, J.W. Storey, R. I. Thompson, D. P. van der Werf, J. S. Wurtele, and Y. Yamazaki (2011b), “Confinement of antihydrogen for 1,000 seconds,” *Nature Physics* **7**, 558–64.
- Andresen, G B, W. Bertsche, P. D. Bowe, C. C. Bray, E. Butler, C. L. Cesar, S. Chapman, M. Charlton, J. Fajans, M. C. Fujiwara, R. Funakoshi, D. R. Gill, J. S. Hangst, W. N. Hardy, R. S. Hayano, M. E. Hayden, R. Hydromako, M. J. Jenkins, L.V. Jørgensen, L. Kurchaninov, R. Lambo, N. Madsen, P. Nolan, K. Olchanski, A. Olin, A. Povilus, P. Pusa, F. Robicheaux, E. Sarid, S. Seif El Nasr, D. M. Silveira, J.W. Storey, R. I. Thompson, D. P. van der Werf, J. S. Wurtele, and Y. Yamazaki (2008), “Compression of antiproton clouds for antihydrogen trapping,” *Phys. Rev. Lett.* **100**, 203401–5.
- Andresen, G B, W. Bertsche, P. D. Bowe, C. C. Bray, E. Butler, C. L. Cesar, S. Chapman, M. Charlton, J. Fajans, M. C. Fujiwara, D. R. Gill, J. S. Hangst, W. N. Hardy, R. S. Hayano, M. E. Hayden, A. J. Humphries, R. Hydromako, L. V. Jørgensen, S. J. Kerrigan, L. Kurchaninov, R. Lambo, N. Madsen, P. Nolan, K. Olchanski, A. Olin, A. P. Povilus, P. Pusa, E. Sarid, S. Seif El Nasr, D. M. Silveira, J. W. Storey, R. I. Thompson, D. P. van der Werf, and Y. Yamazaki (2009), “Antiproton, positron, and electron imaging with a microchannel plate/phosphor detector,” *Rev. Sci. Instrum.* **80**, 123701–5.
- Aoki, J, Y. Kiwamoto, and Y. Kawai (2006), “Determination of equilibrium density distribution and temperature of a pure electron plasma confined in a Penning trap,” *Phys. Plasmas* **13**, 112109–8.
- Asenjo, F A, F. A. Borotto, A. C.-L. Chian, V. Muñoz, J. Alejandro Valdivia, and E. L. Rempel (2012), “Self-modulation of nonlinear waves in a weakly magnetized relativistic electron-positron plasma with temperature,” *Phys. Rev. E* **85**, 046406–6.
- Baker, C J, J. Jennings, A. Verma, J. Xu, M. H. Weber, and K. G. Lynn (2012), “Progress toward the long time confinement of large positron numbers,” *Euro. Phys. J. D* **66**, 109–6.
- Baker, C J, D. P. van der Werf, D. C. S. Beddows, P. R. Watkeys, C. A. Isaac, M. Charlton, and H. H. Telle (2008), “Weakly bound positron-electron pairs in a strong magnetic field,” *J. Phys. B* **41**, 245003–6.
- Banković, A, J. P. Marler, M. Šuvakov, G. Maiović, and Z. L. Petrović (2008), “Transport coefficients for positron swarms in nitrogen,” *Nucl. Instrum. Methods B* **266**, 462–5.
- Barnes, L D, S. J. Gilbert, and C. M. Surko (2003), “Energy-resolved positron annihilation for molecules,” *Phys. Rev. A* **67**, 032706–11.
- Barnes, L D, J. A. Young, and C. M. Surko (2006), “Energy-resolved annihilation rates for molecules,” *Phys. Rev. A* **74**, 012706–10.
- Baur, G, G. Boero, A. Brauksiepe, A. Buzzo, W. Eyrich, R. Geyer, D. Grzonka, J. Hauffe, K. Kiliana, M. LoVetere, M. Macrì, M. Moosburger, R. Nellen, W. Oelert, S. Passaggio, A. Pozzo, K. Röhrich, K. Sachs, G. Schepers, T. Seifick, R. S. Simon, R. Stratmann, F. Stinzing, and M. Wolke (1996), “Production of antihydrogen,” *Phys. Lett. B* **368**, 251–8.
- Beck, B R (1990), *Measurement of the Magnetic and Temperature Dependence of the Electron-Electron Anisotropic Temperature Relaxation Rate*, Ph.D. thesis, unpublished (University of California, San Diego).
- Beck, B R, J. Fajans, and J. H. Malmberg (1996), “Temperature and anisotropic-temperature relaxation measurements in cold, pure-electron plasmas,” *Phys. Plasmas* **3**, 1250–8.
- Beling, C D, R. I. Simpson, M. Charlton, F. M. Jacobsen, T. C. Griffith, P. Moriarty, and S. Fung (1987), “A field-assisted moderator for low-energy positrons,” *Appl. Phys. A* **42**, 111–6.
- Berezhiani, V I, V. Skarka, and S. Mahajan (1993), “Relativistic solitary wave in an electron-positron plasma,” *Phys. Rev. E* **48**, 3252–5.
- Bergeman, T, G. Erez, and H. J. Metcalf (1987), “Magnetostatic trapping fields for neutral atoms,” *Phys. Rev. A* **35**, 1535–46.
- Bernard, J, J. Alonso, T. Beier, M. Block, S. Djekić, H.-J. Kluge, C. Kozhuharov, W. Quint, S. Stahl, T. Valenzuela, J. Verdú, M. Vogel, and G. Werth (2004), “Electron and positron cooling of highly charged ions in a cooler Penning trap,” *Nucl. Instrum. Methods A* **532**, 224–8.
- Bernstein, I B (1956), “Waves in a plasma in a magnetic field,” *Phys. Rev.* **109**, 10–21.
- Bertolotti, M, and C. Sibia (1979), “Coherent γ emission by stimulated annihilation of electron-positron pairs,” *Appl. Phys.* **19**, 127–30.
- Bessho, N, and A. Bhattacharjee (2005), “Collisionless reconnection in an electron-positron plasma,” *Phys. Rev. Lett.* **95**, 245001–4.
- Bettega, G, F. Cavaliere, M. Cavenago, F. De Luca, A. Illiberi, R. Pozzoli, and M. Romé (2006), “Active control of the ion resonance instability by ion removing fields,” *Phys. Plasmas* **13**, 112102–6.
- Bettega, G, F. Cavaliere, B. Paroli, M. Cavenago, R. Pozzoli, and M. Romé (2007), “Excitation of the $l = 2$ azimuthal mode in a pure electron plasma,” *Phys. Plasmas* **14**, 102103–6.
- Bettega, G, F. Cavaliere, B. Paroli, R. Pozzoli, M. Romé, and M. Cavenago (2008), “Excitation of the $l = 2$ diocotron mode

- with a resistive load,” *Phys. Plasmas* **15**, 032102–5.
- Bettega, G, B. Paroli, R. Pozzoli, and M. Romé (2009), “Excitation of the $l = 3$ diocotron mode in a pure electron plasma by means of a rotating electric field,” *J. Appl. Phys.* **105**, 053303–4.
- Blackman, E G, and G. B. Field (1994), “Kinematics of relativistic magnetic reconnection,” *Phys. Rev. Lett.* **72**, 494–7.
- Blanford, G, D. C. Christian, K. Gollwitzer, M. Mandelkern, C. T. Munger, J. Schultz, and G. Zioulas (1998), “Observation of atomic antihydrogen,” *Phys. Rev. Lett.* **80**, 3037–40.
- Boehmer, H, M. Adams, and N. Rynn (1995), “Positron trapping in a magnetic mirror configuration,” *Phys. Plasmas* **2**, 4369–71.
- Bollinger, J J, D. J. Heinzen, F. L. Moore, and W. M. Itano (1993), “Electrostatic modes of ion-trap plasmas,” *Phys. Rev. A* **48**, 525–45.
- Bollinger, J J, D. J. Wineland, and D. H. E. Dubin (1994), “Non-neutral ion plasmas and crystals, laser cooling, and atomic,” *Physics of Plasmas* **1**, 1403–14.
- Brandes, G R, K. Canter, A. Krupyshev, R. Xie, and A. P. Mills, Jr. (1997), “Diamond field-assisted moderator,” *Mat. Sci. Forum* **255-257**, 653–5.
- Brenner, P W, and T. S. Pedersen (2012), “Pure electron plasmas confined for 90ms in a stellarator without electron sources or internal objects,” *Phys. Plasmas* **19**, 050701–4.
- Brillouin, L (1945), “A theorem of Larmor and its importance for electrons in magnetic fields,” *Phys. Rev.* **67**, 260–6.
- Brown, B L, and M. Leventhal (1986), “Laboratory simulation of direct positron annihilation in a neutral-hydrogen galactic environment,” *Phys. Rev. Lett.* **57**, 1651–4.
- Brown, B L, M. Leventhal, A. P. Mills, and D. W. Gidley (1984), “Positron annihilation in a simulated low-density galactic environment,” *Phys. Rev. Lett.* **53**, 2347–50.
- Brown, L S, and G. Gabrielse (1986), “Geonium theory: physics of a single electron or ion in a Penning trap,” *Rev. of Mod. Phys.* **58**, 233–313.
- Byrne, J, and P. S. Farago (1965), “On production of polarized electron beams by spin exchange collisions,” *Proc. Phys. Soc. London* **86**, 801–15.
- Canali, C, C. Carraro, D. Krasnický, V. Lagomarsino, L. Di Noto, G. Testera, and S. Zavatarelli (2011), “Off-axial plasma displacement suitable for antihydrogen production in AEGIS experiment,” *Eur. Phys. J. D* **65**, 499–504.
- Caradonna, P, J. P. Sullivan, A. Jones, C. Makochekanwa, D. Slaughter, D. W. Mueller, and S. J. Buckman (2009), “Excitation of the $n = 2$ states of helium by positron impact,” *Phys. Rev. A* **80**, 060701–4 (R).
- Carraro, C, M. Amoretti, C. Amsler, G. Bonomi, A. Bouchta, P. D. Bowe, C. L. Cesar, M. Charlton, M. Doser, V. Filippini, A. Fontana, M. C. Fujiwara, R. Funakoshi, P. Genova, J. S. Hangst, R. S. Hayano, L. V. Jørgensen, V. Lagomarsino, R. Landua, D. Lindelöf, E. Lodi Rizzini, M. Macrì, N. Madsen, G. Manuzio, P. Montagna, H. Pruijs, C. Regenfus, A. Rotondi, G. Testera, A. Variola, and D. P. van der Werf (2004), “Real-time detector for plasma diagnostic in antimatter experiment,” *Nucl. Instrum. Methods A* **518**, 249–51.
- Cassidy, D B, P. Crivelli, T. H. Hisakado, L. Liskay, V. E. Meline, P. Pérez, H. W. K. Tom, and A. P. Mills, Jr. (2010a), “Positronium cooling in porous silica measured via Doppler spectroscopy,” *Phys. Rev. A* **81**, 012715–12.
- Cassidy, D B, S. H. M. Deng, R. G. Greaves, T. Maruo, N. Nishiyama, J. B. Snyder, H. K. M. Tanaka, and A. P. Mills, Jr. (2005), “Experiments with a high-density positronium gas,” *Phys. Rev. Lett.* **95**, 195006–4.
- Cassidy, D B, S. H. M. Deng, R. G. Greaves, and A. P. Mills, Jr. (2006a), “Accumulator for the production of intense positron pulses,” *Rev. Sci. Instrum.* **77**, 073106–8.
- Cassidy, D B, S. H. M. Deng, and A. P. Mills, Jr. (2006b), “Noisy emission of a slowly released single component plasma,” *Nucl. Instrum. Methods B* **248**, 121–6.
- Cassidy, D B, S. H. M. Deng, H. K. M. Tanaka, and A. P. Mills, Jr. (2006c), “Single shot positron annihilation lifetime spectroscopy,” *Appl. Phys. Lett.* **88**, 194105–3.
- Cassidy, D B, R. G. Greaves, V. E. Meline, and A. P. Mills, Jr. (2010b), “Strong drive compression of a gas-cooled positron plasma,” *Appl. Phys. Lett.* **96**, 101502–3.
- Cassidy, D B, T. H. Hisakado, H. W. K. Tom, and A. P. Mills, Jr. (2011a), “New mechanism for positronium formation on a silicon surface,” *Phys. Rev. Lett.* **106**, 133401–4.
- Cassidy, D B, T. H. Hisakado, H. W. K. Tom, and A. P. Mills, Jr. (2011b), “Positronium formation via excitonlike states on Si and Ge surfaces,” *Phys. Rev. B* **84**, 195312–12.
- Cassidy, D B, T. H. Hisakado, H. W. K. Tom, and A. P. Mills, Jr. (2012a), “Efficient production of Rydberg positronium,” *Phys. Rev. Lett.* **108**, 043401–5.
- Cassidy, D B, T. H. Hisakado, H. W. K. Tom, and A. P. Mills, Jr. (2012b), “Optical spectroscopy of molecular positronium,” *Phys. Rev. Lett.* **108**, 133402–5.
- Cassidy, D B, T. H. Hisakado, H. W. K. Tom, and A. P. Mills, Jr. (2012c), “Positronium hyperfine interval measured via saturated absorption spectroscopy,” *Phys. Rev. Lett.* **109**, 173401–5.
- Cassidy, D B, V. E. Meline, and A. P. Mills, Jr. (2010c), “Production of a fully spin-polarized ensemble of positronium atoms,” *Phys. Rev. Lett.* **104**, 173401–4.
- Cassidy, D B, and A. P. Mills, Jr. (2007), “The production of molecular positronium,” *Nature* **449**, 195–7.
- Cassidy, D B, K. T. Yokoyama, S. H. M. Deng, D. L. Griscom, H. Miyadera, H. W. K. Tom, C. M. Varma, and A. P. Mills, Jr. (2007), “Positronium as a probe of transient paramagnetic centers in α -SiO₂,” *Phys. Rev. B* **75**, 085415–6.
- Castelli, F, I. Boscolo, S. Cialdi, M. G. Giammarchi, and D. Comparat (2008), “Efficient positronium laser excitation for antihydrogen production in a magnetic field,” *Phys. Rev. A* **78**, 052512–7.
- Cattaert, T, and I. Kourakis (2005), “Envelope solitons associated with electromagnetic waves in a magnetized pair plasma,”

- Phys. Plasmas **12**, 012319–6.
- Charlton, M (1985), “Experimental studies of positrons scattering in gases,” Rep. Prog. Phys. **48**, 737–793.
- Charlton, M (1990), “The attachment of positrons to molecules,” Comments At. Mol. Phys. **24**, 53–64.
- Charlton, M, and J. W. Humberston (2001), *Positron Physics*, Positron Physics (Cambridge Univ. Press, Cambridge, U. K.).
- Chaudhary, D, M. R. Went, K. Nakagawa, S. Buckman, and J. P. Sullivan (2010), “Molecular pore size characterization within chitosan biopolymer using positron annihilation lifetime spectroscopy,” Mater. Lett. **64**, 2635–7.
- Chen, F F (1984), *Introduction to Plasma Physics and Controlled Fusion, Volume I: Plasma Physics*, 2nd ed. (Springer, New York).
- Chen, H, S. C. Wilks, J. D. Bonlie, E. P. Liang, J. Myatt, D. F. Price, D. D. Meyerhofer, and P. Beiersdorfer (2009), “Relativistic positron creation using ultra-intense short pulse lasers,” Phys. Rev. Lett. **102**, 105001–4.
- Chiari, L, P. Paliawadana, J. R. Machacek, C. Makochekanwa, G. García, F. Blanco, R. P. McEachran, M. J. Brunger, S. J. Buckman, and J. P. Sullivan (2013), “Experimental and theoretical cross sections for positron collisions with 3-hydroxy-tetrahydrofuran,” J. Chem. Phys. **138**, 074302–11.
- Chu, S, and A. P. Mills, Jr. (1982), “Excitation of the positronium $1^3S_1 - 2^3S_1$ two-photon transition,” Phys. Rev. Lett. **48**, 1333–7.
- Clarke, J, D. P. van der Werf, B. Griffiths, D. C. S. Beddows, M. Charlton, H. H. Telle, and P. R. Watkeys (2006), “Design and operation of a two-stage positron accumulator,” Rev. Sci. Instrum. **77**, 063302–5.
- Cluggish, B P, J. R. Danielson, and C. F. Driscoll (1998), “Resonant particle heating of an electron plasma by oscillating sheaths,” Phys. Rev. Lett. **81**, 353–6.
- Cluggish, B P, and C. F. Driscoll (1995), “Measurement of transport and damping from rotational pumping,” AIP Conference Proceedings **331**, 14–9.
- Coleman, P G (2000), *Positron beams and their applications* (World Scientific, Singapore).
- Coleman, P G, and N. R. Potter (2008), “Back to the future: Polarised positron beams,” Appl. Surf. Sci. **255**, 101–3.
- Comeau, D, A. Dror, D. W. Fitzakerley, M. C. George, E. A. Hessels, C. H. Storry, M. Weel, D. Grzonka, W. Oelert, G. Gabrielse, R. Kalra, W. S. Kolthammer, R. McConnell, P. Richerme, A. Müllers, and J. Walz (2012), “Efficient transfer of positrons from a buffer-gas-cooled accumulator into an orthogonally oriented superconducting solenoid for antihydrogen studies,” New J. Phys. **14**, 045006–10.
- Conti, R S, B. Ghaffari, and T. D. Steiger (1990), “A positron accumulator,” Nucl. Instrum. Methods A **299**, 420–4.
- Crane, W S, and A. P. Mills (1985), “Subnanosecond bunching of a positron beam,” Rev. Sci. Instrum. **56**, 1723–6.
- CRC, (2008), *CRC Handbook of Chemistry and Physics*, Vol. 89th edition (CRC Press/Taylor & Francis, Boca Raton, FL).
- Danielson, J R, F. A. Anderegg, and C. F. Driscoll (2004), “Measurement of Landau damping and the evolution to a BGK equilibrium,” Phys. Rev. Lett. **92**, 245003–4.
- Danielson, J R, and C. F. Driscoll (1999), “Measurement of plasma mode damping in pure electron plasmas,” in *Nonneutral Plasma Physics III*, AIP Conference Proceedings, Vol. 498, edited by J. J. Bollinger, R. L. Spencer, and R. C. Davidson (AIP Press, Melville, NY) pp. 214–9.
- Danielson, J R, J. J. Gosselin, and C. M. Surko (2010), “Dipole enhancement of positron binding to molecules,” Phys. Rev. Lett. **104**, 233201–4.
- Danielson, J R, N. C. Hurst, and C. M. Surko (2013), “Progress towards a practical multicell positron trap,” in *Nonneutral Plasmas VIII*, AIP Conference Proceedings, Vol. 1521, edited by X. Sarasola, L. Schweikhard, and T. S. Pedersen (AIP Press, Melville, NY) pp. 101–12.
- Danielson, J R, A. C. L. Jones, J. J. Gosselin, M. R. Natisin, and C. M. Surko (2012), “Interplay between permanent dipole moments and polarizability in positron-molecule binding,” Phys. Rev. A **85**, 022709–9.
- Danielson, J R, and C. M. Surko (2005), “Torque-balanced high-density steady states of single component plasmas,” Phys. Rev. Lett. **95**, 035001–4.
- Danielson, J R, and C. M. Surko (2006a), “Plasma compression using rotating electric fields - the strong drive regime,” in *Non-Neutral Plasma Physics VI*, AIP Conference Proceedings, Vol. 862, edited by M. Drewsen, U. Uggerhøj, and H. Knudsen (AIP Press, Melville, NY) pp. 19–28.
- Danielson, J R, and C. M. Surko (2006b), “Radial compression and torque-balanced steady states of single-component plasmas in Penning-Malmberg traps,” Phys. Plasmas **13**, 055706–10.
- Danielson, J R, C. M. Surko, and T. M. O’Neil (2007a), “High-density fixed point for radially compressed single-component plasmas,” Phys. Rev. Lett. **99**, 135005–4.
- Danielson, J R, T. R. Weber, and C. M. Surko (2006), “Plasma manipulation techniques for positron storage,” Phys. Plasmas **13**, 123502–10.
- Danielson, J R, T. R. Weber, and C. M. Surko (2007b), “Extraction of small-diameter beams from single-component plasmas,” Appl. Phys. Lett. **90**, 081503–3.
- Danielson, J R, T. R. Weber, and C. M. Surko (2009), “Next generation trap for positron storage,” in *Nonneutral Plasma Physics VII*, Vol. 1114, edited by J. R. Danielson and T. S. Pedersen (AIP Press, Melville, NY) pp. 171 – 178.
- David, A, G. Kögel, P. Sperr, and W. Triftshäuser (2001), “Lifetime measurements with a scanning positron microscope,” Phys. Rev. Lett. **87**, 067402–4.
- Davidson, R C (1990), *Physics of Nonneutral Plasmas* (Addison-Wesley, Reading, MA).
- Davidson, R C, and N. A. Krall (1970), “Vlasov equilibria and stability of an electron gas,” Phys. Fluids **13**, 1543–55.
- Debu, P (2013), “Status report on the GBAR Cern experiment,” in *Sixth Symposium on Large TCPs for Low Energy Rare Event Detection*, Journal of Physics Conference Series, Vol. 460 (IOP Press) pp. 012008–7.
- DeGrassie, J S, and J. H. Malmberg (1977), “Wave-induced transport in pure electron-plasma,” Phys. Rev. Lett. **39**, 1077–80.

- DeGrassie, J S, and J. H. Malmberg (1980), “Waves and transport in the pure electron plasma,” *Phys. Fluids* **23**, 63–81.
- Dehmelt, H (1990), “Experiments with an isolated subatomic particle at rest,” *Rev. Mod. Phys.* **62**, 525–30.
- Dehmelt, H G, P. B. Schwinberg, and R. S. Van Dyck (1978), “Proposed scheme to catch positrons in a Penning trap,” *Int. J. Mass Spectrom. Ion Phys.* **26**, 107–8.
- Deller, A, T. Mortensen, C. A. Isaac, D. P. van der Werf, and M. Charlton (2014), “Radially selective inward transport of positrons in a penning-malmberg trap,” *New J. Phys.* **16**, 073028–10.
- Deutsch, M (1951), “Evidence for the formation of positronium in gases,” *Phys. Rev.* **83**, 455–6.
- Dirac, P A M (1930), “On the annihilation of electrons and protons,” *Proc. Cambridge Phil. Soc.* **26**, 361–75.
- DiSciaccia, J, M. Marshall, K. Marable, and G. Gabrielse (2013a), “Resolving an individual one-proton spin flip to determine a proton spin state,” *Phys. Rev. Lett.* **110**, 140406–5.
- DiSciaccia, J, M. Marshall, K. Marable, G. Gabrielse, S. Ettenauer, E. Tardiff, R. Kalra, D. W. Fitzakerley, M. C. George, E. A. Hessels, C. H. Storry, M. Weel, D. Grzonka, W. Oelert, T. Sefzick, and the ATRAP collaboration (2013b), “One-particle measurement of the antiproton magnetic moment,” *Phys. Rev. Lett.* **110**, 130801–5.
- Doser, M, C. Amsler, A. Belov, G. Bonomi, P. Bräunig, J. Bremer, R. Brusa, G. Burkhart, L. Cabaret, C. Canali, F. Castelli, K. Chlouba, S. Cialdi, D. Comparat, G. Consolati, L. Di Noto, A. Donzella, A. Dudarev, T. Eisel, R. Ferragut, G. Ferrari, A. Fontana, P. Genova, M. Giammarchi, A. Gligorova, S. Gninenko, S. Haider, J. P. Hansen, S. Hogan, L. Jørgensen, T. Kaltenbacher, A. Kellerbauer, D. Krasnicky, V. Lagomarsino, S. Mariazzi, V. Matveev, F. Merkt, F. Moia, G. Nebbia, P. Nedelec, M. Oberthaler, D. Perini, V. Petracek, F. Prelz, M. Prevedelli, C. Regenfus, C. Riccardi, O. Rohne, A. Rotondi, M. Sacerdoti, H. Sandaker, M. Spacek, J. Storey, G. Testera, A. Tokareva, D. Trezzi, R. Vaccarone, F. Villa, Z. Zavatarelli, and A. Zenoni (2012), “Exploring the WEP with a pulsed cold beam of antihydrogen,” *Class. Quantum Gravity* **29**, 184009–11.
- Driscoll, C F (2004), “Comment on ‘Driven production of cold antihydrogen and the first measured distribution of antihydrogen states’,” *Phys. Rev. Lett.* **92**, 149303–1.
- Driscoll, C F, A. A. Kabantsev, T. J. Hilsabeck, and T. M. O’Neil (2003), “Trapped-particle-mediated damping and transport,” in *Non-Neutral Plasma Physics V*, AIP Conference Proceedings, Vol. 692, edited by M. Schauer, T. Mitchell, and R. Nebel (AIP Press, Melville, NY) pp. 3–14.
- Driscoll, C F, and J. H. Malmberg (1983), “Length-dependent containment of a pure electron-plasma column,” *Phys. Rev. Lett.* **50**, 167–70.
- Dubin, D H E (1991), “Theory of electrostatic fluid modes in a cold spheroidal non-neutral plasma,” *Phys. Rev. Lett.* **66**, 2076–9.
- Dubin, D H E (1993), “Equilibrium and dynamics of uniform density ellipsoidal nonneutral plasmas,” *Phys. Fluids B* **5**, 295–324.
- Dubin, D H E (2005), “Displacement eigenmodes for cold-fluid and warm-fluid magnetized plasma oscillations,” *Phys. Plasmas* **12**, 042107–13.
- Dubin, D H E (2008), “Theory and simulations of electrostatic field error transport,” *Phys. Plasmas* **15**, 072112–26.
- Dubin, D H E, and T. M. O’Neil (1999), “Trapped nonneutral plasmas, liquids, and crystals (the thermal equilibrium states),” *Rev. Mod. Phys.* **71**, 87–172.
- Dubin, D H E, and Yu. A. Tsidulko (2011), “Neoclassical transport and plasma mode damping caused by collisionless scattering across an asymmetric separatrix,” *Phys. Plasmas* **18**, 062114–17.
- Dubinov, A E, I. D. Dubinova, and V. A. Gordienko (2006), “Solitary electrostatic waves are possible in unmagnetized symmetric pair plasmas,” *Phys. Plasmas* **13**, 082111–6.
- Durkin, D, and J. Fajans (2000), “Experiments on two-dimensional vortex patterns,” *Phys. Plasmas* **12**, 289–93.
- Eggleston, D L, C. F. Driscoll, B. R. Beck, A. W. Hyatt, and J. H. Malmberg (1992), “Parallel energy analyzer for pure electron plasma devices,” *Phys. Fluids B* **4**, 3432–9.
- Eggleston, D L, T. M. O’Neil, and J. H. Malmberg (1984), “Collective enhancement of radial transport in a nonneutral plasma,” *Phys. Rev. Lett.* **53**, 982–4.
- El-Shamy, E F, R. Sabry, W. M. Moslem, and P. K. Shukla (2010), “Head-on collision of ion-acoustic solitary waves in multicomponent plasmas with positrons,” *Phys. Plasmas* **17**, 082311–7.
- El-Taibany, W F, and A. A. Mamun (2012), “Nonlinear electromagnetic perturbations in a degenerate ultrarelativistic electron-positron plasma,” *Phys. Rev. E* **85**, 026406–7.
- Enomotom, Y, N. Kuroda, K. Michishio, C. H. Kim, H. Higaki, Y. Nagata, Y. Kanai, H. A. Torii, M. Corradini, M. Leali, E. Lodi-Rizzini, V. Mascagna, L. Venturelli, N. Zurlo, K. Fujii, M. Ohtsuka, K. Tanaka, H. Imao, Y. Nagashima, Y. Matsuda, B. Juhász, A. Mohri, and Y. Yamazaki (2010), “Synthesis of cold antihydrogen in a cusp trap,” *Phys. Rev. Lett.* **105**, 243401–4.
- Eseev, M K, A. G. Kobets, I. N. Meshkov, A. Yu. Rudakov, and S. L. Yakovenko (2013), “Study of nonneutral plasma storage in a magnetic trap with a rotating electric field at the lepta facility,” *Plasma Physics Reports* **39**, 787–94.
- Estrada, J, T. Roach, J. N. Tan, P. Yesley, and G. Gabrielse (2000), “Field ionization of strongly magnetized Rydberg positronium: A new physical mechanism for positron accumulation,” *Phys. Rev. Lett.* **84**, 859–62.
- Fajans, J (1993), “Transient ion resonance instability,” *Phys. Plasmas* **5**, 3127–35.
- Fajans, J, and L. Friedland (2001), “Autoresonant (non stationary) excitation of a pendulum, plutinos, plasmas and other nonlinear oscillators,” *Am. J. Phys.* **69**, 1096–1102.
- Fajans, J, E. Gilson, and L. Friedland (1999a), “Autoresonant excitation of a collective nonlinear mode,” *Phys. Plasmas* **6**, 4497–503.
- Fajans, J, E. Gilson, and L. Friedland (1999b), “Autoresonant excitation of the diocotron mode in non-neutral plasmas,” *Phys. Rev. Lett.* **82**, 4444–7.

- Fajans, J, E. Gilson, and L. Friedland (2000), “Second harmonic autoresonant control of the $l = 1$ diocotron mode in pure-electron plasmas,” *Phys. Rev. E* **62**, 4131–6.
- Fajans, J, E. Gilson, and L. Friedland (2001), “The effect of damping on autoresonant (nonstationary) excitation,” *Phys. Plasmas* **8**, 423–7.
- Falub, C V, S. W. H. Eijt, P. E. Mijnders, H. Schut, and A. van Veen (2002), “Magnetic focusing of an intense slow positron beam for enhanced depth-resolved analysis of thin films and interfaces,” *Nucl. Instrum. Methods A* **488**, 478–92.
- Fee, M S, S. Chu, A. P. Mills, Jr., R. Chichester, D. M. Zuckerman, E. D. Shaw, and K. Danzhan (1993), “Measurement of the positronium $1^3S_1 - 2^3S_1$ interval by continuous-wave two-photon excitation,” *Phys. Rev. Lett.* **70**, 1397–1400.
- Feng, X, M. H. Holzschneider, M. Charlton, F. Cverna, T. Ichioka, N. S. P. King, R. A. Lewis, L. Morgan, J. Rochet, and Y. Yamazaki (1996), “Ultralow-energy antiprotons for antihydrogen spectroscopy and antimatter gravity,” *Physics of Atomic Nuclei* **59**, 1551–5.
- Fine, K S (1988), *Experiments with the $l = 1$ diocotron mode*, Ph.D. thesis, unpublished (University of California, San Diego).
- Fine, K S, A. C. Cass, W. G. Flynn, and C. F. Driscoll (1995), “Relaxation of 2D turbulence to vortex crystals,” *Phys. Rev. Lett.* **75**, 3277–80.
- Fine, K S, and C. F. Driscoll (1998), “The finite length diocotron mode,” *Phys. Plasmas* **5**, 601–7.
- Fitzakerley, D W, M. C. George, E. A. Hessels, C. H. Storry, M. Weel, D. Grzonka, W. Oelert, G. Gabrielse, W. S. Kolthammer, R. McConnell, P. Richerme, A. Mullers, and J. Walz (2013), “Electron cooling and accumulation of 4×10^9 positrons in a system for long term storage of antihydrogen atoms,” *Bull. Am. Phys. Soc.* **58**, 176.
- Friedland, L, J. Fajans, and E. Gilson (2000), “Subharmonic autoresonance of the diocotron mode,” *Phys. Plasmas* **7**, 1712–8.
- Funakoshi, R, M. Amoretti, G. Bonomi, P. D. Bowe, C. Canali, C. Carraro, C. L. Cesar, M. Charlton, M. Doser, A. Fontana, M. C. Fujiwara, P. Genova, J. S. Hangst, R. S. Hayano, L. V. Jørgensen, A. Kellerbauer, V. Lagomarsino, R. Landua, E. Lodi Rizzini, M. Macri, N. Madsen, G. Manuzio, D. Mitchard, P. Montagna, L. G. C. Posada, A. Rotondi, G. Testera, A. Variola, L. Venturelli, D. P. van der Werf, Y. Yamazaki, and N. Zurlo (2007), “Positron plasma control techniques for the production of cold antihydrogen,” *Phys. Rev. A* **76**, 012713–8.
- Gabrielse, G (1983), “Relaxation calculation of the electrostatic properties of compensated Penning traps with hyperbolic electrodes,” *Phys. Rev. A* **27**, 2277–90.
- Gabrielse, G (2001), “Comparing the antiproton and proton, and opening the way to cold antihydrogen,” *Adv. At. Mol. Opt. Phys.* **45**, 1 – 39.
- Gabrielse, G (2010), “Slow antihydrogen,” *Physics Today* **63**, 68–9.
- Gabrielse, G, N. S. Bowden, P. Oxley, A. Speck, C. H. Storry, J. Tan, M. Wessels, D. Grzonka, W. Oelert, G. Schepers, T. Sefzick, J. Walz, H. Pittner, T. Hänsch, and E. A. Hessels (2002), “Driven production of cold antihydrogen and the first measured distribution of antihydrogen states,” *Phys. Rev. Lett.* **89**, 233401–5.
- Gabrielse, G, N. S. Bowden, P. Oxley, A. Speck, C. H. Storry, J. N. Tan, M. Wessels, D. Grzonka, W. Oelert, G. Schepers, T. Sefzick, J. Walz, H. Pittner, T. W. Hänsch, and E. A. Hessels (2004a), “Driven production of cold antihydrogen and the first measured distribution of antihydrogen states - reply,” *Phys. Rev. Lett.* **92**, 149304.
- Gabrielse, G, X. Fei, K. Helmerson, S. L. Rolston, R. Tjoelker, T. A. Trainor, H. Kalinowsky, J. Haas, and W. Kells (1986), “First capture of antiprotons in a Penning trap: A kiloelectronvolt source,” *Phys. Rev. Lett.* **57**, 2504–7.
- Gabrielse, G, X. Fei, L. A. Orozco, and S. L. Rolston (1989a), “Barkas effect observed with antiprotons and protons,” *Phys. Rev. A* **40**, 481–4.
- Gabrielse, G, L. Haarsma, and S. L. Rolston (1989b), “Open-endcap Penning traps for high precision experiments,” *Int. J. Mass Spectrom. Ion Proc.* **88**, 319–32.
- Gabrielse, G, R. Kalra, W. S. Kolthammer, R. McConnell, P. Richerme, D. Grzonka, W. Oelert, T. Sefzick, M. Zielinski, D. W. Fitzakerley, M. C. George, E. A. Hessels, C. H. Storry, M. Weel, A. Müllers, and J. Walz (2012), “Trapped antihydrogen in its ground state,” *Phys. Rev. Lett.* **108**, 113002–4.
- Gabrielse, G, W. S. Kolthammer, R. McConnell, P. Richerme, R. Kalra, E. Novitski, D. Grzonka, W. Oelert, T. Sefzick, M. Zielinski, D. Fitzakerley, M. C. George, E. A. Hessels, C. H. Storry, M. Weel, A. Müllers, and J. Walz (2011), “Adiabatic cooling of antiprotons,” *Phys. Rev. Lett.* **106**, 073002–4.
- Gabrielse, G, and F. C. Mackintosh (1984), “Cylindrical Penning traps with orthogonalized anharmonicity compensation,” *Int. J. Mass Spectrom. Ion Proc.*, **57**, 1–17.
- Gabrielse, G, A. Speck, C. H. Storry, D. LeSage, N. Guise, D. Grzonka, W. Oelert, G. Schepers, T. Sefzick, H. Pittner, J. Walz, T.W. Hänsch, D. Comeau, and E. A. Hessels (2004b), “First measurement of the velocity of slow antihydrogen atoms,” *Phys. Rev. Lett.* **93**, 073401–4.
- Gallant, Y A, M. Hoshino, A. B. Langdon, J. Arons, and C. E. Max (1992), “Relativistic, perpendicular shocks in electron-positron plasmas,” *Astrophys. J.* **391**, 73–101.
- Gerola, D, W. B. Waeber, M. Shi, and S. J. Wang (1995), “Quasidivergency-free extraction of a slow positron beam from high magnetic fields,” *Rev. Sci. Instrum.* **66**, 3819–25.
- Ghaffari, B, and R. S. Conti (1995), “Experimental evidence for chaotic transport in a positron trap,” *Phys. Rev. Lett.* **75**, 3118–21.
- Ghosh, D K, P. Chatterjee, and B. Sahu (2012), “Nonplanar ion acoustic solitary waves with superthermal electrons and positrons,” *Astron. Space Sci.* **341**, 559–65.
- Gibson, G, W. C. Jordan, and E. J. Lauer (1960), “Containment of positrons in a mirror machine,” *Phys. Rev. Lett.* **5**, 141–4.
- Gibson, G, W. C. Jordan, and E. J. Lauer (1963), “Particle behavior in static, axially symmetric magnetic mirror,” *Phys. Fluids* **6**, 116–33.
- Gidley, D W, D. Z. Chi, W. D. Wang, and R. S. Vallery (2006), “Positron annihilation as a method to characterize porous

- materials,” *Ann. Rev. Mat. Sci.* **36**, 49–79.
- Gidley, D W, W. E. Frieze, T. L. Dull, J. Sun, A. F. Yee, C. V. Nguyen, and D. Y. Yoon (2000), “Determination of pore-size distribution in low-dielectric thin films,” *Appl. Phys. Lett.* **76**, 1282–4.
- Gilbert, S J, L. D. Barnes, J. P. Sullivan, and C. M. Surko (2002), “Vibrational resonance enhancement of positron annihilation in molecules,” *Phys. Rev. Lett.* **88**, 043201–4.
- Gilbert, S J, D. H. E. Dubin, R. G. Greaves, and C. M. Surko (2001), “An electron-positron beam-plasma instability,” *Phys. Plasmas* **8**, 4982–94.
- Gilbert, S J, R. G. Greaves, and C. M. Surko (1999), “Positron scattering from atoms and molecules at low energies,” *Phys. Rev. Lett.* **82**, 5032–5.
- Gilbert, S J, C. Kurz, R. G. Greaves, and C. M. Surko (1997), “Creation of a monoenergetic pulsed positron beam,” *Appl. Phys. Lett.* **70**, 1944–6.
- Glinsky, M E, and T. M. O’Neil (1991), “Guiding center atoms: three-body recombination in a strongly magnetized plasma,” *Phys. Fluids B* **3**, 1279–93.
- Gordienko, V A, and A. E. Dubinov (2007), “The gas-dynamic approach in the nonlinear theory of electrostatic waves in symmetric plasma,” *High Temp.* **45**, 740–50.
- Gordienko, V A, and A. E. Dubinov (2008), “Principle of charge-mass invariance of motion and possibility of steady-state solitary electrostatic waves in a nearly symmetric plasma,” *Tech. Phys.* **53**, 43–8.
- Gramsch, E, J. Throwe, and K. G. Lynn (1987), “Development of transmission positron moderators,” *Appl. Phys. Lett.* **51**, 1862–4.
- Greaves, R G, S. J. Gilbert, and C. M. Surko (2002), “Trap-based positron beams,” *Appl. Surf. Sci.* **194**, 56–60.
- Greaves, R G, and J. Moxom (2003), “Design and performance of a trap-based positron beam source,” in *Non-Neutral Plasma Physics V*, AIP Conference Proceedings, Vol. 692, edited by M. Schauer, T. Mitchell, and R. Nebel (AIP Press, Melville, NY) pp. 140–8.
- Greaves, R G, and J. M. Moxom (2008), “Compression of trapped positrons in a single particle regime by a rotating electric field,” *Phys. Plasmas* **15**, 072304–6.
- Greaves, R G, and C. M. Surko (1995), “An electron-positron beam-plasma experiment,” *Phys. Rev. Lett.* **75**, 3846–9.
- Greaves, R G, and C. M. Surko (2000), “Inward transport and compression of a positron plasma by a rotating electric field,” *Phys. Rev. Lett.* **85**, 1883–6.
- Greaves, R G, and C. M. Surko (2001), “Radial compression and inward transport of positron plasmas using a rotating electric field,” *Phys. Plasmas* **8**, 1879–85.
- Greaves, R G, and C. M. Surko (2002a), “Positron trapping and the creation of high-quality trap-based positron beams,” *Nucl. Instrum. Methods B* **192**, 90–6.
- Greaves, R G, and C. M. Surko (2002b), “Practical limits on positron accumulation and the creation of electron-positron plasmas,” in *Non-Neutral Plasma Physics IV*, AIP Conference Proceedings, Vol. 606, edited by F. Anderegg, L. Schweikhard, and C. Driscoll (AIP Press, Melville, NY) pp. 10–23.
- Greaves, R G, M. D. Tinkle, and C. M. Surko (1994), “Creation and uses of positron plasmas,” *Phys. Plasmas* **1**, 1439–46.
- Green, D G, S. Saha, F. Wang, G. F. Gribakin, and C. M. Surko (2012), “Effect of positron-atom interactions on the annihilation gamma spectra of molecules,” *New J. Phys.* **14**, 035021–26.
- Gribakin, G F, and C. M. R. Lee (2006a), “Application of the zero-range potential model to positron annihilation on molecules,” *Nucl. Instrum. Methods B* **247**, 31–7.
- Gribakin, G F, and C. M. R. Lee (2006b), “Positron annihilation in molecules by capture into vibrational feshbach resonances of infrared-active modes,” *Phys. Rev. Lett.* **97**, 193201–4.
- Gribakin, G F, J. A. Young, and C. M. Surko (2010), “Positron-molecule interactions: Resonant attachment, annihilation, and bound states,” *Rev. Mod. Phys.* **82**, 2557–607.
- Griffith, T C, G. R. Heyland, K. S. Lines, and T. R. Twomey (1978), “The production of slow positron beams from magnesium oxide-coated moderators,” *Phys. Lett. A* **69**, 169–71.
- Guessoum, N (2014), “Positron astrophysics and areas of relation to low-energy positron physics,” *Euro. Phys. J. D* **68**, 137–6.
- Guessoum, N, P. Jean, and W. Gillard (2006), “Relevance of slow positron beam research to astrophysical studies of positron interactions and annihilation in the interstellar medium,” *Appl. Surf. Sci.* **252**, 3352–61.
- Guessoum, N, P. Jean, and W. Gillard (2010), “Positron annihilation on polycyclic aromatic hydrocarbon molecules in the interstellar medium,” *Mon. Not. R. Astron. Soc.* **402**, 1171–78.
- Haarsma, L, K. Abdullah, and G. Gabrielse (1995), “Extremely cold positrons accumulated electronically in ultra-high vacuum,” *Phys. Rev. Lett.* **75**, 806–9.
- Hammer, N I, K. Diri, K. D. Jordan, C. Desfrancois, and R. N. Compton (2003), “Dipole-bound anions of carbonyl, nitrile and sulfoxide containing molecules,” *J. Chem. Phys.* **119**, 3650–60.
- Hansen, J P (1973), “Statistical-mechanics of dense ionized matter I: equilibrium properties of classical one-component plasma,” *Phys. Rev. A* **8**, 3096–109.
- Hart, G W, and B. G. Peterson (2006), “Finding the radial parallel temperature profile of a non-neutral plasma using equilibrium calculations on experimental data,” *Phys. Plasmas* **13**, 022101–8.
- Heinzen, D J, J. J. Bollinger, and F. L. Moore (1991), “Rotational equilibria and low-order modes of a non-neutral ion plasma,” *Phys. Rev. Lett.* **66**, 2080–3.
- Heyland, G R, M. Charlton, T. C. Griffith, and G. L. Wright (1982), “Positron lifetime spectra for gases,” *Can. J. Phys.* **60**, 503–16.
- Higaki, H, N. Kuroda, T. Ichioka, K. Franzen, Z. Wang, K. Komaki, Y. Yamazaki, M. Hori, N. Oshima, and A. Mohri (2002),

- “Electron cooling of high-energy protons in a multiring trap with a tank circuit monitoring the electron-plasma oscillations,” *Phys. Rev. E* **65**, 046410–5.
- Higaki, H, and A. Mohri (1997), “Experiment on diocotron oscillations of spheroidal non-neutral electron plasmas in a multi-ring-electrode trap,” *Phys. Lett. A* **235**, 504–7.
- Higaki, H, S. Sakurai, K. Ito, and H. Okamoto (2012), “Nonneutral electron plasmas confined in a compact magnetic mirror trap,” *Appl. Phys. Express* **5**, 106001–3.
- Hirose, M, M. Washio, and K. Takahashi (1995), “Production of an intense slow positron beam using a compact cyclotron,” *Appl. Surf. Sci.* **85**, 111–17.
- Hollmann, E M, F. Anderegg, and C. F. Driscoll (2000), “Confinement and manipulation of non-neutral plasmas using rotating wall electric fields,” *Phys. Plasmas* **7**, 2776–89.
- Holzscheiter, M H, and M. Charlton (1999), “Ultra-low energy antihydrogen,” *Rep. Prog. Phys.* **62**, 1 – 60.
- Hori, M, and J. Walz (2013), “Physics at CERN’s antiproton decelerator,” *Prog. in Part. Nucl. Phys.* **72**, 206–53.
- Hosseinpour, M, and G. Vekstein (2008), “Collisionless forced magnetic reconnection in an electron-positron plasma,” *Phys. Plasmas* **15**, 022904–6.
- Howell, R H, I. J. Rosenberg, and M. J. Fluss (1987), “Production and use of low-energy, monoenergetic positron beams from electron LINACS,” *Appl. Phys. A* **43**, 247–55.
- Hsu, T, and J. L. Hirshfield (1976), “Electrostatic energy analyzer using a nonuniform axial magnetic field,” *Rev. Sci. Instrum.* **47**, 236–8.
- Huang, X P, F. Anderegg, E. M. Hollmann, C. F. Driscoll, and T. M. O’Neil (1997), “Steady state confinement of nonneutral plasma by rotating electric fields,” *Phys. Rev. Lett.* **78**, 875–8.
- Huang, X P, J. J. Bollinger, T. B. Mitchell, and W. M. Itano (1998), “Phase-locked rotation of crystallized non-neutral plasmas by rotating electric fields,” *Phys. Rev. Lett.* **80**, 73–6.
- Huang, X P, K. S. Fine, and C. F. Driscoll (1995), “Coherent vorticity holes from 2D turbulence decaying in a background shear flow,” *Phys. Rev. Lett.* **74**, 4424–7.
- Hugenschmidt, C, C. Piochacz, M. Reiner, and Klaus Schreckenbach (2012), “The NEPOMUC upgrade and advanced positron beam experiments,” *New J. Phys.* **14**, 055027–22.
- Hulet, L D, D. L. Donohue, and T. A. Lewis (1991), “A quadratic potential time-of-flight mass spectrometer,” *Rev. Sci. Instrum.* **62**, 2131–7.
- Hulet, L D, D. L. Donohue, Jun Xu, T. A. Lewis, S. A. McLuckey, and G. L. Glish (1993), “Mass spectrometry studies of the ionization of organic molecules by low-energy positrons,” *Chem. Phys. Lett.* **216**, 236–40.
- Hulet, L D, Jun Xu, S.A. McLuckey, T. A. Lewis, and D. M. Schrader (1996), “The ionization of organic molecules by slow positrons,” *Can. J. Phys.* **74**, 411–19.
- Hunt, A W, L. Pilant, D. B. Cassidy, R. Tjossem, M. Shurtliff, M. H. Weber, and K. G. Lynn (2002), “The development of the intense positron beam at Washington State University,” *Appl. Surf. Sci.* **194**, 296–300.
- Hussain, S, S. Mahmood, and A. Mushtaq (2013), “Magnetoacoustic solitons in dense astrophysical electron-positron-ion plasmas,” *Astrophys. Space Sci.* **346**, 359–66.
- Hyatt, A W, C. F. Driscoll, and J. H. Malmberg (1987), “Measurement of the anisotropic temperature relaxation rate in a pure electron plasma,” *Phys. Rev. Lett.* **59**, 2975–8.
- Ichimaru, S (1982), “Strongly coupled plasmas - high-density classical plasmas and degenerate electron liquids,” *Rev. Mod. Phys.* **54**, 1017–59.
- Isaac, C A (2013), “Motional sideband excitation using rotating electric fields,” *Phys. Rev. A* **87**, 043415–7.
- Isaac, C A, C. J. Baker, T. Mortensen, D. P. van der Werf, and M. Charlton (2011), “Compression of positron clouds in the independent particle regime,” *Phys. Rev. Lett.* **107**, 033201–4.
- Iwamoto, N (1993), “Collective modes in nonrelativistic electron-positron plasmas,” *Phys. Rev. E* **47**, 604–11.
- Iwata, K, R. G. Greaves, T. J. Murphy, M. D. Tinkle, and C. M. Surko (1995), “Measurements of positron-annihilation rates on molecules,” *Phys. Rev. A* **51**, 473–87.
- Iwata, K, R. G. Greaves, and C. M. Surko (1996), “Positron annihilation in a simulated interstellar medium,” *Can. J. Phys.* **51**, 407–10.
- Iwata, K, G. Gribakin, R. G. Greaves, and C. M. Surko (1997a), “Positron annihilation with inner-shell electrons in noble gas atoms,” *Phys. Rev. Lett.* **79**, 39–42.
- Iwata, Koji, R. G. Greaves, and C. M. Surko (1997b), “Gamma-ray spectra from positron annihilation on atoms and molecules,” *Phys. Rev. A* **55**, 3586–3604.
- Jackson, J D, S. B. Treiman, and H. W. Wyld (1957), “Possible tests of time reversal invariance in beta decay,” *Phys. Rev.* **106**, 517–21.
- Jacobsen, F M, M. Petkov, and K. G. Lynn (1998), “Electric-field-assisted moderator for generation of intense low-energy positron beams,” *Phys. Rev. B* **57**, 6998–7003.
- Jelenković, B M, A. S. Newbury, J. Bollinger, W. M. Itano, and T. B. Mitchell (2003), “Sympathetically cooled and compressed positron plasma,” *Phys. Rev. A* **67**, 063406–9.
- Jelenković, B M, A. S. Newbury, J. J. Bollinger, T. B. Mitchell, and W. M. Itano (2002), “Sympathetically laser-cooled positrons,” *Nucl. Instrum. Methods B* **192**, 117–27.
- Jennings, J K, R. L. Spencer, and K. C. Hansen (1995), “Numerical-calculation of axisymmetrical electrostatic modes for cold finite-length nonneutral plasmas,” *Phys. Plasmas* **2**, 2630–9.
- Jones, A C L, J. R. Danielson, M. R. Natisin, and C. M. Surko (2013), “Role of vibrational dynamics in resonant positron annihilation on molecules,” *Phys. Rev. Lett.* **110**, 223201–5.

- Jones, A C L, C. Makochekanwa, P. Caradonna, D. S. Slaughter, J. R. Machacek, R. P. McEachran, J. P. Sullivan, S. J. Buckman, A. D. Stauffer, I. Bray, and D. V. Fursa (2011), “Positron scattering from neon and argon,” *Phys. Rev. A* **83**, 032701–12.
- Jørgensen, L V, M. Amoretti, G. Bonomi, P. D. Bowe, C. Canali, C. Carraro, C. L. Cesar, M. Charlton, M. Doser, A. Fontana, M. C. Fujiwara, R. Funakoshi, P. Genova, J. S. Hangst, R. S. Hayano, A. Kellerbauer, V. Lagomarsino, R. Landua, E. Lodi Rizzini, M. Macrì, N. Madsen, D. Mitchard, P. Montagna, A. Rotondi, G. Testera, A. Variola, L. Venturelli, D. P. van der Werf, and Y. Yamazaki (2005), “New source of dense, cryogenic positron plasmas,” *Phys. Rev. Lett.* **95**, 025002–5.
- Jørgensen, L V, and H. Schut (2008), “GaN - a new material for positron moderation,” *Appl. Surf. Sci.* **255**, 231–3.
- Jungmann, M, J. Haeberle, R. Krause-Rehberg, W. Anwand, M. Butterling, A. Wagner, J. M. Johnson, and T. E. Cowan (2013), “First experiments with MePS,” *J. Phys: Conf. Series* **443**, 012088–4.
- Kabantsev, A A, and C. F. Driscoll (2010), “Experiments on neoclassical asymmetric superbanana ripple transport in electron plasmas,” *Prob. of Atomic Sci. Tech.* **6**, 26–30.
- Kabantsev, A A, D. H. E. Dubin, C. F. Driscoll, and Yu. A. Tsidulko (2010), “Chaotic transport and damping from theta-ruffled separatrices,” *Phys. Rev. Lett.* **105**, 205001–4.
- Kabantsev, A A, J. H. Yu, R. B. Lynch, and C. F. Driscoll (2003), “Trapped particles and asymmetry-induced transport,” *Phys. Plasmas* **10**, 1628–35.
- Karshenboim, S G (2002), “Precision study of positronium and precision tests of the bound state quantum electrodynamics,” *Appl. Surf. Sci.* **194**, 307–11.
- Karshenboim, S G (2005), “Precision physics of simple atoms: QED tests, nuclear structure and fundamental constants,” *Phys. Rep.* **422**, 1–63.
- Keinigs, R (1981), “Effect of magnetic field errors on low-frequency waves in a pure electron plasma,” *Phys. Fluids* **27**, 860–3.
- Keinigs, R (1984), “Field-error induced transport in a pure electron plasma column,” *Phys. Fluids* **27**, 1427–33.
- Keston, D A, E. W. Laing, and D. A. Diver (2003), “Bernstein modes in a weakly relativistic electron-positron plasma,” *Phys. Rev. E* **67**, 036403–10.
- Khatri, R, M. Charlton, P. Sferlazzo, K. G. Lynn, A. P. Mills, Jr., and L. O. Roellig (1990), “Improvement of rare-gas solid moderators by using conical geometry,” *Appl. Phys. Lett.* **57**, 2374–6.
- Kiwamoto, Y, Y. Soga, and J. Aoki (2005), “Radial transport in magnetized non-neutral plasma driven by rotating wave,” *Phys. Plasmas* **12**, 094501–4.
- Kourakis, I, F. Verheest, and N. F. Cramer (2007), “Nonlinear perpendicular propagation of ordinary mode electromagnetic wave packets in pair plasmas and electron-positron-ion plasmas,” *Phys. Plasmas* **14**, 022306–10.
- Krause-Rehberg, R, G. Brauer, M. Jungmann, A. Krille, A. Rogov, and K. Noack (2008), “Progress of the intense positron beam project EPOS,” *Appl. Surf. Sci.* **255**, 22–4.
- Krause-Rehberg, R, N. van der Walt, L. Büttner, and F. Börner (2004), “A ^{22}Na positron source for use in UHV,” *Nucl. Instrum. Methods B* **221**, 165–7.
- Kuroda, N, A. Mohri, H. A. Torii, Y. Nagata, and M. Shibata (2014a), “First observation of a (1,0) mode frequency shift of an electron plasma at antiproton beam injection,” *Phys. Rev. Lett.* **113**, 025001–5.
- Kuroda, N, H. A. Torii, M. Shibata, Y. Nagata, D. Barna, M. Hori, D. Horváth, A. Mohri, J. Eades, K. Komaki, and Y. Yamazaki (2008), “Radial compression of an antiproton cloud for production of intense antiproton beams,” *Phys. Rev. Lett.* **100**, 203402–4.
- Kuroda, N, S. Ulmer, D. J. Murtagh, S. Van Gorp, Y. Nagata, M. Diermaier, S. Federmann, M. Leali, C. Malbrunot, V. Mascagna, O. Massiczek, K. Michishio, T. Mizutani, A. Mohri, H. Nagahama, M. Ohtsuka, B. Radics, S. Sakurai, C. Sauerzopf, K. Suzuki, M. Tajima, H. A. Torii, L. Venturelli, B. Wünschek, J. Zmeskal, N. Zurlo, H. Higaki, Y. Kanai, E. Lodi Rizzini, Y. Nagashima, Y. Matsuda, E. Widmann, and Y. Yamazaki (2014b), “A source of antihydrogen for in-flight hyperfine spectroscopy,” *Nature Commun.* **5**, 3089–6.
- Kurz, C, R. G. Greaves, and C. M. Surko (1996), “Temperature dependence of positron annihilation rates in noble gases,” *Phys. Rev. Lett.* **77**, 2929–32.
- Landau, L (1941), “Theory of the superfluidity of helium II,” *Phys. Rev. A* **60**, 356–8.
- Landau, L D, and E. M. Lifshitz (1976), *Mechanics* (Pergamon, Oxford).
- Laricchia, G, S. Armitage, A. Köver, and D.J. Murtagh (2008), “Ionizing collisions by positrons and positronium impact on the inert atoms,” *Adv. At. Mol. Phys.* **56**, 1–47.
- Levy, R H, J. D. Daugherty, and O. Buneman (1969), “Ion resonance instability in grossly nonneutral plasmas,” *Phys. Fluids* **12**, 2616–29.
- Liang, E P, and C. D. Dermer (1988), “Laser cooling of positronium,” *Opt. Comm.* **65**, 419–24.
- Liszskay, L, P. Comini, C. Corbel, P. Debu, P. Dupré, P. Grandemange, P. Pérez, J.-M. Rey, N. Ruiz, and Y. Sacquin (2013), “Linac-based positron source and generation of a high density positronium cloud for the gbar experiment,” in *16th International Conference on Positron Annihilation*, Journal of Physics Conference Series, Vol. 443, edited by A. Alam, P. Coleman, S. Dugdale, and M. Roussanova (IOP Press) pp. 012006–5.
- Liu, Y, and S. Q. Liu (2011), “Nonlinear behavior of electromagnetic waves in ultra-relativistic electron-positron plasmas,” *Contrib. Plasma Phys.* **51**, 698–706.
- Loeb, A, and S. Eliezer (1986), “A gamma-ray laser based on induced annihilation of electron-positron pairs,” *Laser and Particle Beams* **4**, 577–87.
- Loewe, B, K. Schreckenbach, and C. Hugenschmidt (2008), “Gas moderation of positrons,” *Appl. Surf. Sci.* **255**, 96–7.
- Loewe, B, K. Schreckenbach, and C. Hugenschmidt (2010), “Positron remoderation by gas cooling within an electric drift field,” *Nucl. Instrum. Methods B* **268**, 529–32.

- Lynn, K G, W. E. Frieze, and P. J. Schultz (1984), “Measurement of the positron surface-state lifetime for Al,” *Phys. Rev. Lett.* **52**, 1137–40.
- Lynn, K G, B. Nielsen, and J. H. Quateman (1985), “Development and use of a thin-film transmission positron moderator,” *Appl. Phys. Lett.* **47**, 239–40.
- Lynn, K G, M. Weber, L. O. Roellig, A. P. Mills, and A. R. Moodenbaugh (1987), “A high intensity positron beam at the brookhaven reactor,” in *Atomic Physics with Positrons*, edited by J. W. Humbertston and E. A. G. Armour (Plenum, New York, NY, USA) pp. 161–74.
- Madsen, N, S. Jonsell, and F. Robicheaux (2013), “Antihydrogen trapping assisted by sympathetically cooled positrons,” *Bull. Am. Phys. Soc.* **58**, 314.
- Maekawa, M, Y. Fukaya, A. Yabuuchi, I. Mochizuki, and A. Kawasuso (2013), “Development of spin-polarized slow positron beam using a ^{68}Ge - ^{68}Ga positron source,” *Nucl. Instrum. Methods B* **308**, 9–14.
- Makochekanwa, C, J. R. Machacek, A. C. L. Jones, P. Caradonna, D. S. Slaughter, R. P. McEachran, J. P. Sullivan, S. J. Buckman, S. Belim, B. Lohmann, D. V. Fursa, I. Bray, D. W. Mueller, A. D. Stauffer, and M. Hoshino (2011), “Low-energy positron interactions with krypton,” *Phys. Rev. A* **83**, 032721–12.
- Malmberg, J H, and J. S. DeGrassie (1975), “Properties of nonneutral plasma,” *Phys. Rev. Lett.* **35**, 577–80.
- Malmberg, J H, and C. F. Driscoll (1980), “Long-time containment of a pure electron plasma,” *Phys. Rev. Lett.* **44**, 654–7.
- Malmberg, J H, C. F. Driscoll, and W. D. White (1982), “Experiments with pure electron plasmas,” *Phys. Scr.* **T2**, 288–92.
- Malmberg, J H, and T. M. O’Neil (1977), “Pure electron plasma, liquid and crystal,” *Phys. Rev. Lett.* **39**, 1333–6.
- Marjanović, S, M. Šuvakov, A. Banković, M. Savić, G. Malović, S. Buckman, and Z. Lj. Petrović (2011), “Numerical modeling of thermalization of positrons in gas-filled Surko traps,” *IEEE Trans. Plas. Sci.* **39**, 2614–15.
- Marler, J P, and M. R. Stoneking (2008), “Confinement time exceeding one second for a toroidal electron plasma,” *Phys. Rev. Lett.* **100**, 155001–4.
- Marler, J P, J. P. Sullivan, and C. M. Surko (2005), “Ionization and positronium formation in noble gases,” *Phys. Rev. A* **71**, 022701–12.
- Marler, J P, and C. M. Surko (2005a), “Positron-impact ionization, positronium formation and electronic excitation cross sections for diatomic molecules,” *Phys. Rev. A* **72**, 062713–10.
- Marler, J P, and C. M. Surko (2005b), “Systematic comparison of positron and electron impact excitation of the ν_3 vibrational mode of CF_4 ,” *Phys. Rev. A* **72**, 062702–6.
- Masood, W, and H. Rizvi (2010), “Two dimensional electrostatic shock waves in relativistic electron positron ion plasmas,” *Phys. Plasmas* **17**, 052314–6.
- Merrison, J P, M. Charlton, P. Aggerholm, H. Knudsen, D. P. van der Werf, J. Clarke, and M. R. Poulsen (2003), “Development and applications of time-bunched and velocity-selected positron beams,” *Rev. Sci. Instrum.* **74**, 3284–92.
- Merrison, J P, M. Charlton, B. I. Deutch, and L. V. Jørgensen (1992), “Field assisted positron moderation by surface charging of rare gas solids,” *J. Phys. Condens. Matter* **4**, 207–12.
- Meshkov, I N (2004), “LEPTA project: generation and study of positronium in directed fluxes,” *Nucl. Instrum. Methods B* **221**, 168–73.
- Michishio, K, T. Tachibana, R. H. Suzuki, K. Wada, A. Yagishita, T. Hyodo, and Y. Nagashima (2012), “An energy-tunable positronium beam produced using the photodetachment of the positronium negative ion,” *Appl. Phys. Lett.* **100**, 254102–4.
- Mills, Jr, A P (1980a), “Brightness enhancement of slow positron beams,” *Appl. Phys.* **23**, 189–91.
- Mills, Jr, A P (1980b), “Further improvements in the efficiency of low-energy positron moderators,” *Appl. Phys. Lett.* **37**, 667–8.
- Mills, Jr, A P (1980c), “Time bunching of slow positrons for annihilation lifetime and pulsed laser photon-absorption experiments,” *Appl. Phys.* **22**, 273–76.
- Mills, Jr, A P (1981), “Observation of the positronium negative ion,” *Phys. Rev. Lett.* **46**, 717–20.
- Mills, Jr, A P (1982), “Surface analysis and atomic physics with slow positron beams,” *Science* **218**, 335–40.
- Mills, Jr, A P (1992), “Suitability of ^{79}Kr as a reactor-based source of slow positrons,” *Nucl. Sci. Eng.* **110**, 165–7.
- Mills, Jr, A P (2002), “Positronium molecule formation, bose-einstein condensation and stimulated annihilation,” *Nucl. Instrum. Methods B* **192**, 107–116.
- Mills, Jr, A P (2010), “Physics with many positrons,” in *Physics with Many Positrons*, edited by A. P. Mills, Jr. and A. Dupasquier (IOS Press, Amsterdam) pp. 77–187.
- Mills, Jr, A P, G. R. Brandes, D. M. Zuckerman, W. Liu, and S. Berko (1992), “Positron mobility in natural diamond,” *Mat. Sci. Forum* **105–110**, 763–6.
- Mills, Jr, A P, D. B. Cassidy, and R. G. Greaves (2004), “Prospects for making a Bose-Einstein-condensed positronium annihilation gamma ray laser,” *Mat. Sci. Forum* **445–446**, 424–9.
- Mills, Jr, A P, and E. M. Gullikson (1986), “Solid neon moderator for producing slow positrons,” *Appl. Phys. Lett.* **49**, 1121–3.
- Mills, Jr, A P, and M. Leventhal (2002), “Can we measure the gravitational free fall of cold Rydberg state positronium?” *Nucl. Instrum. Methods B* **192**, 102–6.
- Mills, Jr, A P, E. D. Shaw, R. J. Chichester, and D. M. Zuckerman (1989), “Production of slow positron bunches using a microtron accelerator,” *Rev. Sci. Instrum.* **60**, 825–30.
- Mills, Jr, A P, S. S. Voris, and T. S. Andrew (1994), “Solid Kr moderator for producing slow positrons,” *J. Appl. Phys.* **76**, 2556–8.
- Mishra, M K, R. S. Tiwari, and S. K. Jain (2007), “Small amplitude ion-acoustic double layers in multicomponent plasma with positrons,” *Phys. Rev. E* **76**, 036401–7.
- Mitchell, T R (1993), *Experiments on Electron Vortices in Malmberg-Penning Trap*, Ph.D. thesis (University of California San

- Diego).
- Mitchell, T.B., J.J. Bollinger, X.-P. Huang, and W.M. Itano (1999), “Mode and transport studies of laser-cooled ion plasmas in a Penning trap,” in *Trapped Charged Particles and Fundamental Physics*, AIP Conference Proceedings, Vol. 457, edited by D. H. E. Dubin and D. Schneider (AIP Press, Melville, NY) p. 309.
- Mitroy, J., and I. A. Ivanov (2002), “Semi-empirical model of positron scattering and annihilation,” *Phys. Rev. A* **65**, 042705–15.
- Mohamed, T., A. Mohri, and Y. Yamazaki (2013), “Comparison of non-neutral electron plasma confinement in harmonic and rectangular potentials in a very dense regime,” *Phys. Plasmas* **20**, 012502–6.
- Mohri, A., H. Higaki, H. Tanaka, Y. Yamazawa, and M. Aoyagi (1998), “Confinement of nonneutral spheroidal plasmas in multi-ring electrode traps,” *Japanese J. Appl. Phys.* **37**, 664–70.
- Mohri, A., T. M. Kojima, N. Oshima, M. Niigaki, and Y. Yamazaki (2002), “System of slow highly charged ion beam generation using a cold positron plasma trap at riken,” in *Nonneutral Plasmas IV*, AIP Conference Proceedings, Vol. 606, edited by F. Anderegg, L. Schweikhard, and C. F. Driscoll (AIP Press, Melville, NY) pp. 634–40.
- Moxom, J., A. G. Hathaway, E. W. Bodnaruk, A. I. Hawari, and J. Xu (2007), “Performance analysis of the intense slow-positron beam at the N. C. State University PULSTAR,” *Nucl. Instrum. Methods A* **579**, 534–7.
- Murphy, T. J. (1987), “Positron deposition in plasmas by positronium beam ionization and transport of positrons in tokamak plasmas,” *Plasma Phys. Control. Fusion* **29**, 549–63.
- Murphy, T. J., and C. M. Surko (1991), “Annihilation of positrons on organic molecules,” *Phys. Rev. Lett.* **67**, 2954–7.
- Murphy, T. J., and C. M. Surko (1992), “Positron trapping in an electrostatic well by inelastic collisions with nitrogen molecules,” *Phys. Rev. A* **46**, 5696–705.
- Mushtaq, A., and R. Khan (2008), “Linear and nonlinear studies of two-stream instabilities in electron-positron-ion plasmas with quantum corrections,” *Phys. Scripta* **78**, 015501–5.
- Natisin, M. R., N. C. Hurst, J. R. Danielson, and C. M. Surko (2013), “Recent progress in tailoring trap-based positron beams,” in *Nonneutral Plasmas VIII*, AIP Conference Proceedings, Vol. 1521, edited by X. Sarasola, L. Schweikhard, and T. S. Pedersen (AIP Press, Melville, NY) pp. 154–164.
- O’Neil, T. (1995), “Plasmas with a single sign of charge (an overview),” *Phys. Scr.* **T59**, 341–51.
- O’Neil, T. M. (1980a), “Cooling of a pure electron plasma by cyclotron radiation,” *Phys. Fluids* **23**, 725–31.
- O’Neil, T. M. (1980b), “Nonneutral plasmas have exceptional confinement properties,” *Comments Plasma Phys. Controlled Fusion* **5**, 213–17.
- Oohara, W., D. Date, and R. Hatakeyama (2005), “Electrostatic waves in a paired fullerene-ion plasma,” *Phys. Rev. Lett.* **95**, 175003–4.
- Oohara, W., and R. Hatakeyama (2003), “Pair-ion plasma generation using fullerenes,” *Phys. Rev. Lett.* **91**, 205005–4.
- Oohara, W., and R. Hatakeyama (2007), “Basic studies of the generation and collective motion of pair-ion plasmas,” *Phys. Plasmas* **14**, 055704–7.
- O’Rourke, B. E., N. Hayashizaki, A. Kinomura, R. Kuroda, E. J. Minehara, T. Ohdaira, N. Oshima, and R. Suzuki (2011), “Simulations of slow positron production using a low-energy electron accelerator,” *Rev. Sci. Instrum.* **82**, 063302–10.
- Oshima, N., T. M. Kojima, M. Niigaki, A. Mohri, K. Komaki, Y. Iwai, and Y. Yamazaki (2003), “Development of a cold HCl source for ultra-slow collisions,” *Nucl. Instrum. Methods B* **205**, 178–82.
- Oshima, N., T. M. Kojima, M. Niigaki, A. Mohri, K. Komaki, and Y. Yamazaki (2004), “New scheme for positron accumulation in ultrahigh vacuum,” *Phys. Rev. Lett.* **93**, 195001–4.
- Oshima, N., M. Niigaki, M. Lebois, A. Mohri, K. Komaki, and Y. Yamazaki (2005), “Simultaneous cooling of highly charged ions with electrons and positrons,” *Nucl. Instrum. Methods B* **235**, 504–8.
- Oxley, P., N. S. Bowden, R. Parrott, A. Speck, C. Storry, J. N. Tan, M. Wessels, G. Gabrielse, and D. Grzonka (2004), “Aperture method to determine the density and geometry of antiparticle plasmas,” *Phys. Lett. B* **595**, 60–7.
- Pakzad, H. R., and J. Kurosh (2011), “Energy of ion acoustic solitons in electron-positron-ion plasmas with high relativistic ions,” *Astro. Space Sci.* **2011**, 257–61.
- Parthey, C. G., A. Matveev, J. Alnis, B. Bernhardt, A. Beyer, R. Holzwarth, A. Maistrou, R. Pohl, K. Predehl, T. Udem, T. Wilken, N. Kolachevsky, M. Abgrall, D. Rovera, C. Salomon, P. Laurent, and T. W. Hänsch (2011), “Improved measurement of the hydrogen 1S-2S transition frequency,” *Phys. Rev. Lett.* **107**, 203001–5.
- Passner, A., C. M. Surko, M. Leventhal, and A. P. Mills, Jr. (1989), “Ion production by positron-molecule resonances,” *Phys. Rev. A* **39**, 3706–9.
- Paul, W. (1990), “Electromagnetic traps for charged and neutral particles,” *Rev. Mod. Phys.* **62**, 531–40.
- Pedersen, T. S., A. H. Boozer, W. Dorland, J. P. Kremer, and R. Schmitt (2003), “Prospects for the creation of positron-electron plasmas in a non-neutral stellarator,” *J. Phys. B* **36**, 1029–39.
- Pedersen, T. S., J. R. Danielson, C. Hugenschmidt, G. Marx, X. Sarasola, F. Schauer, L. Schweikhard, C. M. Surko, and E. Winkler (2012), “Plans for the creation and studies of electron-positron plasmas in a stellarator,” *New J. Phys.* **14**, 035010–13.
- Pedersen, T. S., J. P. Kremer, R. G. Lefrancois, Q. Marksteiner, X. Sarasola, and N. Ahmad (2006), “Experimental demonstration of a compact stellarator magnetic trap using four circular coils,” *Phys. Plasmas* **13**, 102502–6.
- Penning, F. M. (1936), “Die glimmladung bei niedrigem druck zwischen koaxialen zylindern in einem axialen magnetfeld,” *Physica* **3**, 873–94.
- Petrović, Z. Lj., A. Banković, S. Dujko, S. Marjanović, G. Malović, J. P. Sullivan, and S. J. Buckman (2013), “Data for modeling of positron collisions and transport in gases,” in *Eighth International Conference on Atomic and Molecular Data and Their Applications (ICAMDATA-2012)*, Conference Proceedings, Vol. 1545, edited by J. D. Gillaspay, W. L. Wiese, and Y. A. Podpaly (American Institute of Physics Press, Melville, NY) pp. 115–31.
- Peurrung, A. J., and J. Fajans (1993), “A pulsed microchannel-plate-based non-neutral plasma imaging system,” *Rev. Sci.*

- Instrum. **64**, 52–5.
- Pfluger, T, M. Holzwarth, A. Senfleben, X. Ren, A. Dorn, J. Ullrich, L. R. Hargreaves, B. Lohmann, D. S. Slaughter, J. P. Sullivan, J. C. Lower, and S. J. Buckman (2011), “Kinematically complete experiments for positron-impact ionization of helium atoms at the NEPOMUC facility,” *J. Phys: Conf. Series* **262**, 012047–6.
- Pierce, J R (1954), *Theory and Design of Electron Beams* (D. Van Nostrand Company, Inc., New York, NY).
- Platzman, P M (1986), “Surface positrons and the many-positron many-electron system,” in *Positrons in Atoms, Solids and Surfaces*, edited by A. P. Mills, Jr., K. F. Canter, and W. S. Crane (World Scientific, Singapore).
- Platzman, P M, and A. P. Mills, Jr. (1994), “Possibilities for Bose condensation of positronium,” *Phys. Rev. B* **49**, 454–8.
- Pohl, T, H. R. Sadeghpour, and G. Gabrielse (2006), “New interpretations of measured antihydrogen velocities and field ionization spectra,” *Phys. Rev. Lett.* **97**, 143401–4.
- Prasad, S A, and T. M. O’Neil (1979), “Finite length thermal equilibria of a pure electron plasma column,” *Phys. Fluids* **22**, 278–81.
- Prasad, S A, and T. M. O’Neil (1983), “Waves in a cold pure electron plasma of finite length,” *Phys. Fluids* **26**, 665–74.
- Pritchard, D E (1983), “Cooling neutral atoms in a magnetic trap for precision spectroscopy,” *Phys. Rev. Lett.* **51**, 1336–9.
- Puska, M J, and R. M. Nieminen (1994), “Theory of positrons in solids and on solid surfaces,” *Rev. Mod. Phys.* **66**, 841–97.
- Rey, J M, G. Coulloux, P. Debu, H. Dzitko, P. Hardy, L. Liskay, P. Lotrus, T. Muranaka, C. Noel, P. Pérez, O. Pierret, N. Ruiz, and Y. Sacquin (2013), “Status of the linac based positron source at Saclay,” in *16th International Conference on Positron Annihilation*, Journal of Physics Conference Series, Vol. 443, edited by A. Alam, P. Coleman, S. Dugdale, and M. Roussanova (IOP Press) pp. 012077–4.
- Robicheaux, F (2004), “Simulations of antihydrogen formation,” *Phys. Rev. A* **70**, 022510–5.
- Robicheaux, F (2008), “Atomic processes in antihydrogen experiments: a theoretical and computational perspective,” *J. Phys. B* **41**, 192001–15.
- Roy, N, S. Tasnim, and A. A. Mamun (2012), “Solitary waves and double layers in an ultra-relativistic degenerate dusty electron-positron-ion plasma,” *Phys. Plasmas* **19**, 033705–5.
- Sabry, R (2009), “Large amplitude ion-acoustic solitary waves and double layers in multicomponent plasma with positrons,” *Phys. Plasmas* **16**, 072307.
- Sabry, R, W. M. Moslem, P. K. Shukla, and H. Saleem (2009), “Cylindrical and spherical ion-acoustic envelope solitons in multicomponent plasmas with positrons,” *Phys. Rev. E* **79**, 056402–6.
- Saeed, R, A. Shah, and M. Noaman-Ul-Haq (2010), “Nonlinear Korteweg-de Vries equation for soliton propagation in relativistic electron-positron-ion plasma with thermal ions,” *Phys. Plasmas* **17**, 102301–6.
- Saito, F, Y. Nagashima, T. Kurihara, I. Fujiwara, R. Iwata, N. Suzuki, Y. Itoh, A. Goto, and T. Hyodo (2000), “Spot ^{18}F positron source electro-deposited on a graphite rod,” *Nucl. Instrum. Methods A* **450**, 491–4.
- Saito, F, Y. Nagashima, L. Wei, Y. Itoh, A. Goto, and T. Hyodo (2002), “A high-efficiency positron moderator using electro-polished tungsten meshes,” *Appl. Surf. Sci.* **194**, 13–5.
- Saitoh, H, Z. Yoshida, J. Morikawa, Y. Yano, N. Kasaoka, W. Sakamoto, and T. Nogami (2013), “Stable confinement of electron plasma and initial results on positron injection in RT-1,” in *Non-neutral Plasma Physics VIII*, AIP Conference Proceedings, Vol. 1521 (AIP Press, Melville, NY) pp. 63–72.
- Sarasola, X, and T. S. Pedersen (2012), “First experimental studies of the physics of plasmas of arbitrary degree of neutrality,” *Plasma Phys. Control. Fusion* **54**, 1–8.
- Schermann, J P, and F. G. Major (1978), “Characteristics of electron-free confinement in an rf quadrupole field,” *Appl. Phys.* **16**, 225–30.
- Schultz, P J, and K. G. Lynn (1988), “Interaction of positrons beams with surfaces, thin films, and interfaces,” *Rev. Mod. Phys.* **60**, 701–79.
- Schwinberg, P B, R. S. Van Dyck, and H. G. Dehmelt (1981), “Trapping and thermalization of positrons for geonium spectroscopy,” *Phys. Lett.* **81A**, 119–20.
- Segers, D, J. Paridaens, M. Dorikens, and L. Dorikens-Vanpraet (1994), “Beam handling with a Penning trap of a LINAC-based slow positron beam,” *Nucl. Instrum. Methods A* **337**, 246–52.
- Shah, A, and F. Saeed (2009), “Ion acoustic shock waves in a relativistic electron-positron-ion plasmas,” *Phys. Lett. A* **373**, 4164–8.
- Shan, Y Y, H. L. Au, C. C. Ling, T. C. Lee, B. K. Panda, S. Fung, C. D. Beling, Y. Y. Wang, and H. M. Weng (1994), “Semiinsulating GaAs - a possible substrate for a field-assisted positron moderator,” *Appl. Phys. A* **59**, 259–73.
- Shi, M, D. Gerola, W. B. Waeber, and U. Zimmermann (1995), “Slow positron beam extraction from high magnetic fields,” *Appl. Surf. Sci.* **85**, 143–8.
- Shiga, N, F. Anderegg, D. H. E. Dubin, C. F. Driscoll, and R. W. Gould (2006), “Thermally excited fluctuations as a pure electron plasma temperature diagnostic,” *Phys. Plasmas* **13**, 022109–12.
- Shukla, P K, A. A. Mamun, and L. Stenflo (2003), “Vortices in a strongly magnetized electron-positron-ion plasma,” *Phys. Scr.* **68**, 295–7.
- Simons, J (2008), “Molecular anions,” *J. Phys. Chem. A* **112**, 6401–11.
- Skalsey, M, and J. Vanhouse (1988), “Proposed new reactor-activated positron source for intense slow e^+ -beam production,” *Nucl. Instrum. Methods B* **30**, 211–6.
- Soga, Y, Y. Kiwamoto, and N. Hashizume (2006), “Transport processes of a non-neutral plasma coupled to an external rotating wave,” *Phys. Plasmas* **13**, 052105–7.
- Speck, A, G. Gabrielse, P. Larochele, D. Le Sage, B. Levitt, W. S. Kolthammer, R. McConnell, J. Wrubel, D. Grzonka, W. Oelert, T. Seifick, Z. Zhang, D. Comeau, M. C. George, E. A. Hessels, C. H. Storry, M. Weel, and J. Walz (2007),

- “Density and geometry of single component plasmas,” *Phys. Lett. B* **650**, 119–23.
- Spencer, R L, S. N. Rasband, and R. R. Vanfleet (1993), “Numerical-calculation of axisymmetrical nonneutral plasma equilibria,” *Phys. Fluids B* **5**, 4267–72.
- Stein, T S, W. E. Kauppila, and L. O. Roellig (1974), “Production of a monochromatic, low-energy positron beam using $^{11}\text{B}(p,n)^{11}\text{C}$ reaction,” *Rev. Sci. Instrum.* **45**, 951–3.
- Stewart, G A, and E. W. Laing (1992), “Wave propagation in equal-mass plasmas,” *J. Plasma Phys.* **47**, 295–319.
- Stoneking, M R, J. W. Darrell, S. A. Exarhos, A. S. Patterson, M. J. Price, and A. H. Wright (2013), “Diocotron and Trivelpiece-Gould mode behavior in toroidal plasma,” in *Nonneutral Plasma Physics VIII*, AIP Conference Proceedings, Vol. 1521, edited by T. S. Pedersen X. Sarasola, L. Schweikhard (AIP Press, Melville, NY) pp. 82–88.
- Stoneking, M R, P. W. Fontana, and R. L. Sampson (2002), “Electron plasmas in a ‘partial’ torus,” *Phys. Plasmas* **9**, 766–71.
- Stoneking, M R, J. P. Marler, B. N. Ha, and J. Smoniewski (2009), “Experimental realization of nearly steady-state toroidal electron plasma,” *Phys. Plasmas* **16**, 055708–7.
- Stormer, J, A. Goodyear, W. Anwand, G. Brauer, P. G. Coleman, and W. Triftshäuser (1996), “Silicon carbide: a new positron moderator,” *J. Phys. Condens. Matter* **8**, L89–94.
- Storry, C H, A. Speck, D. Le Sage, N. Guise, G. Gabrielse, D. Grzonka, W. Oelert, G. Schepers, T. Sefzick, H. Pittner, M. Herrmann, J. Walz, T. W. Hänsch, D. Comeau, and E. A. Hessels (2004), “First laser-controlled antihydrogen production,” *Phys. Rev. Lett.* **93**, 263401–4.
- Sullivan, J, S. J. Gilbert, and C. M. Surko (2001), “Excitation of molecular vibrations by positron impact,” *Phys. Rev. Lett.* **86**, 1494–7.
- Sullivan, J, J. Roberts, R. Weed, M. Went, D. Newman, and S. Buckman (2010), “A trap-based beamline for the study of materials,” *Meas. Sci. Tech.* **21**, 085702–7.
- Sullivan, J P, S. J. Gilbert, J. P. Marler, R. G. Greaves, S. J. Buckman, and C. M. Surko (2002), “Positron scattering from atoms and molecules using a magnetized beam,” *Phys. Rev. A* **66**, 042708–12.
- Sullivan, J P, A. Jones, P. Caradonna, C. Makochekanwa, and S. J. Buckman (2008), “A positron trap and beam apparatus for atomic and molecular scattering experiments,” *Rev. Sci. Instrum.* **79**, 113105–5.
- Surko, C M, J. R. Danielson, G. F. Gribakin, and R. E. Continetti (2012), “Measuring positron-atom binding energies through laser-assisted photo-recombination,” *New J. Phys.* **14**, 065004–6.
- Surko, C M, J. R. Danielson, and T. R. Weber (2010), “Accumulation, storage and manipulation of large numbers of positrons in traps II.—Selected topics,” in *Physics with Many Positrons*, edited by A. P. Mills, Jr. and A. Dupasquier (IOS press, Amsterdam) pp. 545–74.
- Surko, C M, J. R. Danielson, and T. R. Weber (2014), “Accumulation, storage and manipulation of large numbers of positrons in traps II - selected topics,” in *Physics with Trapped Charged Particles*, edited by M. Kroop, N. Madsen, and R. C. Thompson (Imperial College Press, London, U. K.) pp. 129–72.
- Surko, C M, S. J. Gilbert, and R. G. Greaves (1999), “Progress in creating low-energy positron plasmas and beams,” in *Non-Neutral Plasma Physics*, edited by J. J. Bollinger, R. L. Spencer, and R. C. Davidson (American Institute of Physics, New York) pp. 3–12.
- Surko, C M, and R. G. Greaves (2003), “A multi-cell trap to confine large numbers of positrons,” *Rad. Chem. and Phys.* **68**, 419–25.
- Surko, C M, and R. G. Greaves (2004), “Emerging science and technology of antimatter plasmas and trap-based beams,” *Phys. Plasmas* **11**, 2333–48.
- Surko, C M, G. F. Gribakin, and S. J. Buckman (2005), “Low-energy positron interactions with atoms and molecules,” *J. Phys. B* **38**, R57–R126.
- Surko, C M, M. Leventhal, W. S. Crane, A. Passner, and F. Wysocki (1986), “Use of positrons to study transport in tokamak plasmas,” *Rev. Sci. Instrum.* **57**, 1862–7.
- Surko, C M, M. Leventhal, and A. Passner (1989), “Positron plasma in the laboratory,” *Phys. Rev. Lett.* **62**, 901–4.
- Surko, C M, A. Passner, M. Leventhal, and F. J. Wysocki (1988), “Bound states of positrons and large molecules,” *Phys. Rev. Lett.* **61**, 1831–4.
- Tachikawa, M, Y. Kita, and R. N. Buenker (2011), “Bound states of the positron with nitrile species with a configuration interaction multi-component molecular orbital approach,” *Phys. Chem. Chem. Phys.* **13**, 2701–5.
- Tang, S, M. D. Tinkle, R. G. Greaves, and C. M. Surko (1992), “Annihilation gamma-ray spectra from positron-molecule interactions,” *Phys. Rev. Lett.* **68**, 3793–6.
- Tinkle, M D, R. G. Greaves, C. M. Surko, R. L. Spencer, and G. W. Mason (1994), “Low-order modes as diagnostics of spheroidal non-neutral plasmas,” *Phys. Rev. Lett.* **72**, 352–5.
- Tribeche, M, and S. Boukhalfa (2011), “Ion-acoustic solitary waves in a fully relativistic ion-electron-positron plasma,” *Astro. Space Sci.* **332**, 279–86.
- Trivelpiece, A W, and R. W. Gould (1959), “Space charge waves in a cylindrical plasma column,” *J. Appl. Phys.* **30**, 1784–93.
- Tseng, C H, and G. Gabrielse (1993), “Portable trap carries particles 5000 kilometers,” *Hyperfine Interact.* **76**, 381–6.
- Tsintsadze, L N (1995), “Relativistic shock-waves in an electron-positron plasma,” *Phys. Plasmas* **2**, 4462–9.
- Tsyтович, V, and C. B. Wharton (1978), “Laboratory electron-positron plasma—a new research object,” *Comments Plasma Phys. Controlled Fusion* **4**, 91–100.
- Tuomisto, F, and I. Makkonen (2013), “Defect identification in semiconductors with positron annihilation: Experiment and theory,” *Rev. Mod. Phys.* **85**, 1583–1631.
- Vallery, R S, P. A. Encarnacion, W. E. Frieze, D. W. Gidley, H. C. Griffin, M. Ludington, and M. Skalsey (1994), “Fabrication of ^{58}Co positron sources,” *Nucl. Instrum. Methods A* **353**, 16–9.

- van der Walt, T N, and C. Vermeulen (2004), “Thick targets for the production of some radionuclides and the chemical processing of these targets at iThemba LABS,” Nucl. Instrum. Methods A **521**, 171–5.
- Van Dyck, R S, P. B. Schwinberg, and H. G. Dehmelt (1977), “Precise measurements of axial, magnetron, cyclotron, and spin-cyclotron-beat frequencies on an isolated 1-mev electron,” Phys. Rev. Lett. **38**, 310–4.
- Van Reeth, P, J. W. Humberston, K. Iwata, R. G. Greaves, and C. M. Surko (1996), “Annihilation in low-energy positron-helium scattering,” J. Phys. B **29**, L465–71.
- Varma, C M (1977), “Stimulated gamma-ray emission from the pulsar in the Crab,” Nature **267**, 686–7.
- Vehanen, A, K. G. Lynn, P. J. Schultz, and M. Eldrup (1983), “Improved slow-positron yield using a single-crystal tungsten moderator,” Appl. Phys. A **32**, 163–7.
- Verheest, F, and G. Cattaert (2005), “Parallel propagating electromagnetic solitons and oscillitons in space plasmas and in relativistic electron-positron plasmas,” Phys. Scr. **T116**, 62–6.
- Vrinceanu, D, B. E. Granger, R. Parrott, H. R. Sadeghpour, L. Cederbaum, A. Mody, J. Tan, and G. Gabrielse (2004), “Strongly magnetized antihydrogen and its field ionization,” Phys. Rev. Lett. **92**, 133402–4.
- Wada, K, T. Hyodo, A. Yagishita, M. Ikeda, S. Ohsawa, T. Shidara, K. Michishio, T. Tachibana, Y. Nagashima, Y. Fukaya, M. Maekawa, and A. Kawasuso (2012), “Increase in the beam intensity of the linac-based slow positron beam and its application at the slow positron facility, KEK,” Euro. Phys. J. D **66**, 37.
- Wang, B Y, Y. Y. Ma, P. Wang, X. Z. Cao, X. B. Qin, Z. Zhang, R. S. Yu, and L. Wei (2008), “Development and application of the intense slow positron beam at IHEP,” Chin. Phys. C **32**, 156–59.
- Weber, T R (2010), *Tailored Charged Particle Beams from Single-Component Plasmas*, Ph.D. thesis, unpublished (University of California, San Diego).
- Weber, T R, J. R. Danielson, and C. M. Surko (2008), “Creation of finely focused particle beams from single-component plasmas,” Phys. Plasmas **15**, 012106–10.
- Weber, T R, J. R. Danielson, and C. M. Surko (2009), “Energy spectra of tailored particle beams from trapped single-component plasmas,” Phys. Plasmas **16**, 057105–8.
- Weber, T R, J. R. Danielson, and C. M. Surko (2010), “Electrostatic beams from tailored plasmas in a Penning-Malmberg trap,” Phys. Plasmas **17**, 123507–10.
- Weimer, C S, J. J. Bollinger, F. L. Moore, and D. J. Wineland (1994), “Electrostatic modes as a diagnostic in Penning trap experiments,” Phys. Rev. A **49**, 3842–53.
- Wexler, S, E. K. Parks, C. E. Young, and R. A. Bennett (1983), “Behavior of CS^+ - UF_6 ion-pair plasmas in radio frequency quadrupole-dipole fields: I. experiment,” J. Appl. Phys. **54**, 1730–54.
- Wheeler, J A (1946), “Polyelectrons,” Ann. New York Acad. Sci. **48**, 219–38.
- White, W D, J. H. Malmberg, and C. F. Driscoll (1982), “Resistive-wall destabilization of diocotron waves,” Phys. Rev. Lett. **49**, 1822–6.
- Williams, A I, Á. Kövér, D. J. Murtagh, and G. Laricchia (2010), “Progress towards a positron reaction microscope,” J. Phys: Conf. Series **199**, 012025–4.
- Wineland, D J, and H. G. Dehmelt (1975), “Principles of the stored ion calorimeter,” J. Appl. Phys. **46**, 919–30.
- Wineland, D J, W. M. Itano, J. C. Bergquist, and R. G. Hulet (1987), “Laser-cooling limits and single-ion spectroscopy,” Phys. Rev. A **36**, 2220–32.
- Witteborn, F C, and W. M. Fairbank (1967), “Experimental comparison of the gravitational force,” Phys. Rev. Lett. **19**, 1049–52.
- Wuerker, R F, H. Shelton, and R. V. Langmuir (1959), “Electrodynamic containment of charged particles,” J. Appl. Phys. **30**, 342–9.
- Xie, R, M. Petkov, D. Becker, K. Canter, F. M. Jacobsen, K. G. Lynn, R. Mills, and L. O. Roellig (1994), “Production of a low energy positron beam using the $^{12}C(d,n)^{13}N$ reaction,” Nucl. Instrum. Methods B **93**, 98–102.
- Yabu, H (2004), “Many positron and positronium interactions,” Nuc. Instrum. Methods B **221**, 144–8.
- Yamazaki, T, A. Miyazaki, T. Suehara, T. Namba, S. Asai, T. Kobayashi, H. Saito, I. Ogawa, T. Idehara, and S. Sabchevski (2012), “Direct observation of the hyperfine transition of ground-state positronium,” Phys. Rev. Lett. **108**, 253401–5.
- Yang, L, C. R. Brome, J. S. Butterworth, S. N. Dzhosyuk, Mattoni C. E. H, D. N. McKinsey, R. A. Michniak, J. M. Doyle, R. Golub, E. Korobkina, C. M. O’Shaughnessy, G. R. Palmquist, P.-N. Seo, P. R. Huffman, K. J. Coakley, H. P. Mumm, A. K. Thompson, G. L. Yang, and S. K. Lamoreaux (2008), “Development of high-field superconducting ioffe magnetic traps,” Rev. Sci. Instrum. **79**, 031301–11.
- Yin, L, W. Daughton, H. Karimabadi, B. J. Albright, K. J. Bowers, and J. Margulies (2008), “Three-dimensional dynamics of collisionless magnetic reconnection in large-scale pair plasmas,” Phys. Rev. Lett. **101**, 125001–4.
- Yoshida, Z, H. Saitoh, J. Morikawa, Y. Yano, S. Watanabe, and Ogawa Y. (2010), “Magnetospheric vortex formation: Self-organized confinement of charged particles,” Phys. Rev. Lett. **104**, 235004–4.
- Yoshida, Z, H. Saitoh, Y. Yano, H. Mikami, N. Kasaoka, W. Sakamoto, J. Morikawa, M. Furukawa, and S M Mahajan (2013), “Self-organized confinement by magnetic dipole: recent results from RT-1 and theoretical modeling,” Plasma Phys. Control. Fusion **55**, 014018–8.
- Young, J A, and C. M. Surko (2006), “Charged particle motion in spatially varying electric and magnetic fields,” Nucl. Instrum. Methods B **247**, 147–154.
- Young, J A, and C. M. Surko (2008), “Feshbach-mediated annihilation in positron interactions with large molecules,” Phys. Rev. A **77**, 052704–14.
- Young, J A, C. M. Surko, G. F. Gribakin, and C. M. R. Lee (2008), “Role of combination vibrations in resonant positron annihilation,” Phys. Rev. A **77**, 060702–4(R).

- Zafar, N, J. Chevallier, G. Laricchia, and M. Charlton (1989), "Single-crystal nickel foils as positron transmission-mode moderators," *J. Phys. D* **22**, 868–70.
- Zank, G P, and R. G. Greaves (1995), "Linear and nonlinear modes in nonrelativistic electron-positron plasmas," *Phys. Rev. E* **51**, 6079–90.
- Zecca, A, L. Chiari, A. Sarkar, S. Chattopadhyay, and M. J. Brunger (2010), "Procedures for conditioning W- and Ni-moderators for application in positron-scattering measurements," *Nucl. Instrum. Methods B* **268**, 533–6.
- Ziock, K P, C. D. Dermer, R. H. Howell, F. Magnotta, and K. M. Jones (1990), "Optical saturation of the 1^3S - 2^3P transition in positronium," *J. Phys. B* **23**, 329–36.
- Zwicky, G (2006), "Electron cooling of highly charged ions in Penning traps," in *Nonneutral Plasma Physics VI*, AIP Conference Proceedings, Vol. 862, edited by M. Drewsen, U. Uggerhøj, and H. Knudsen (AIP Press, Melville, NY) pp. 281–91.

FIGURES

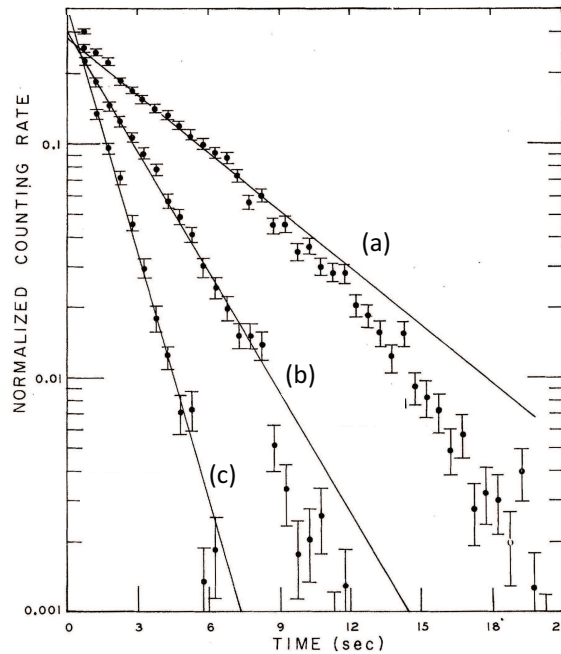


FIG. 1 Early positron trapping experiment using a magnetic mirror trap. Shown is the flux as a function of time of relativistic (mega-electron volt) positrons exiting the trap when increasing pressures [(a)–(c)] of neon gas are used to induce de-confinement. Confinement times of 10 s were observed. Adapted from Gibson *et al.* (1960); see this reference for details.

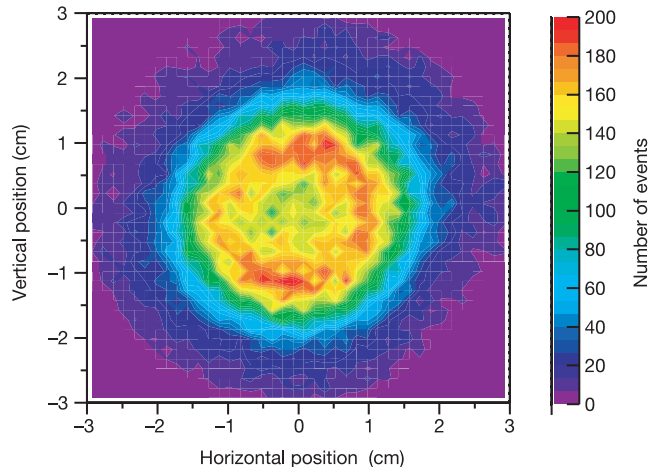


FIG. 2 (color online) First glimpse of stable, neutral antimatter at low energies. Image of antihydrogen atoms annihilating at the inner surface of electrodes used to confine and merge cold antiproton and positron plasmas. See Sec. VIII.A for details. Adapted from Amoretti *et al.* (2002).

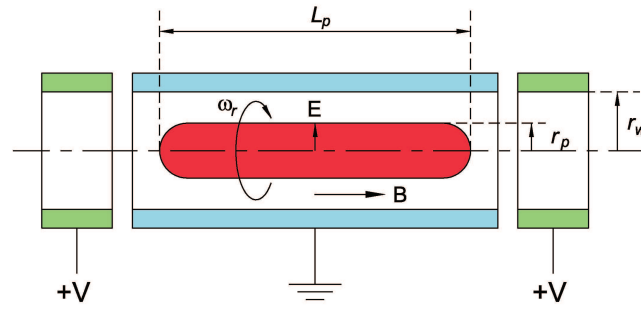


FIG. 3 (Color online) Schematic of a cylindrical Penning-Malmberg trap for positive charges.

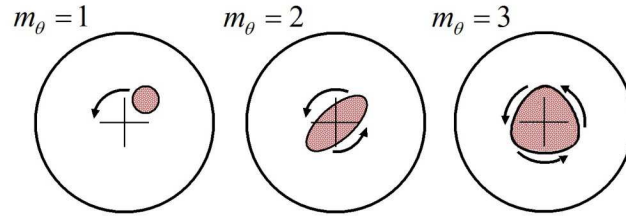


FIG. 4 (color online) Schematic picture of $\delta n(r, \theta)$ for several $k_z = 0$ diocotron modes. The magnetic field B is oriented into the page. The direction of rotation assumes the charge $q > 0$ and corresponds to $\theta < 0$.

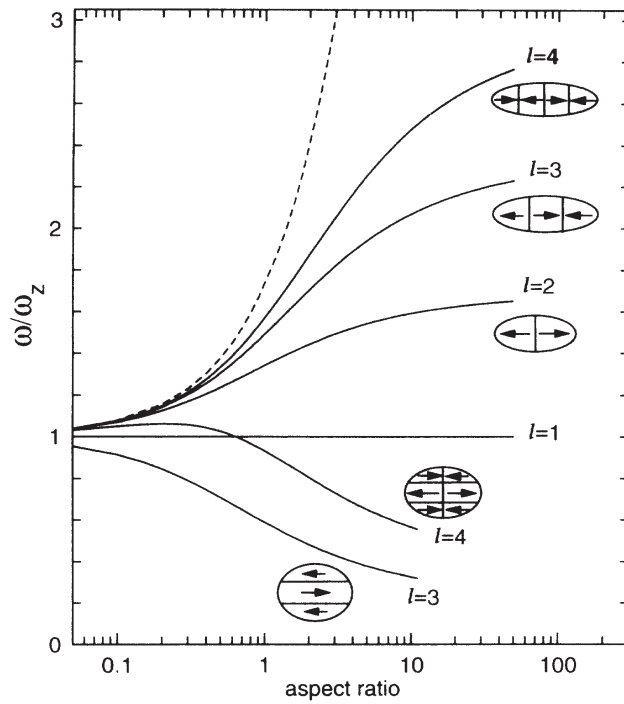


FIG. 5 Dispersion relation for $m_\theta = 0$ modes in spheroidal plasmas [Eq. (55)], from Tinkle *et al.* (1994). Only the lowest-order azimuthally symmetric modes are shown; the dashed line is the plasma frequency. For the $l = 3$ and $l = 4$ modes, there are two branches. The sketches indicate the fluid motion for each mode.

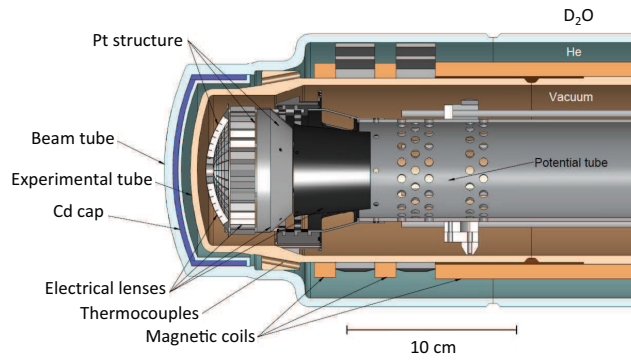


FIG. 6 (color online) Cross section of the NEPOMUC converter showing the cadmium shell, platinum production and moderation foils and magnetic beam transport elements (Hugenschmidt *et al.*, 2012).

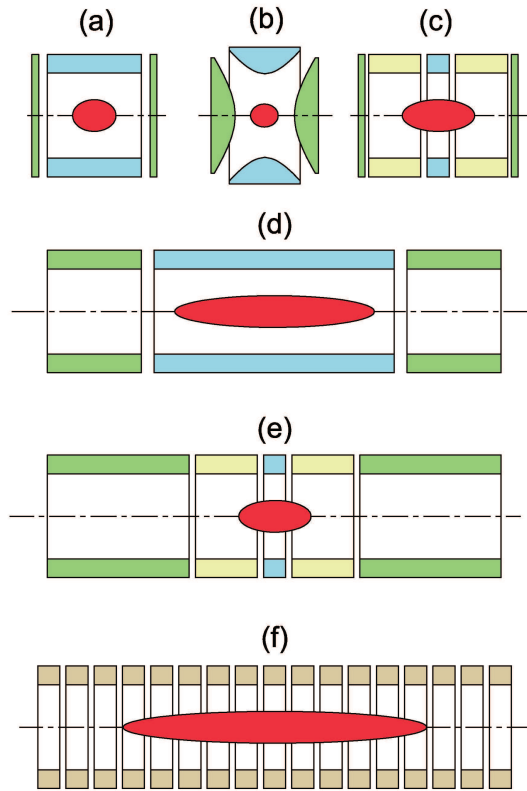


FIG. 7 (color online) Geometries for Penning traps: (a) cylindrical trap with closed endcaps; (b) trap with hyperboloidal electrodes (“harmonic trap”); (c) orthogonalized cylindrical trap; (d) open endcap cylindrical trap (i.e., the Penning-Malmberg trap); (e) orthogonalized open endcap design; and (f) multi-ring trap. Color code: (blue) ring electrode; (green) endcaps; (yellow) compensation electrode; (red) confined charge cloud; and (brown) multi-ring electrodes.

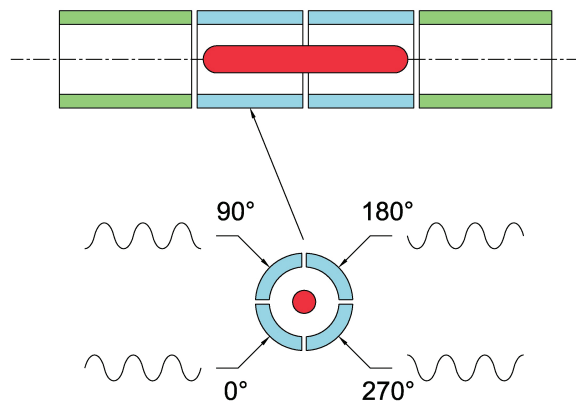


FIG. 8 (color online) Typical layout for a PM trap for RW compression. Phased sine waves applied to azimuthal segments create the rotating electric field. The RW field is applied along only part of the length of the plasma. The color coding is the same as Fig. 7.

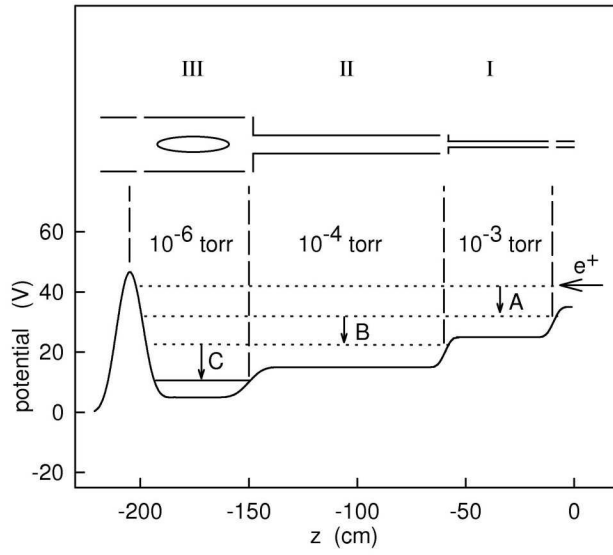


FIG. 9 Buffer gas trap for positron trapping. Above: electrode structure showing the three stages. Below: electrostatic potential profile.

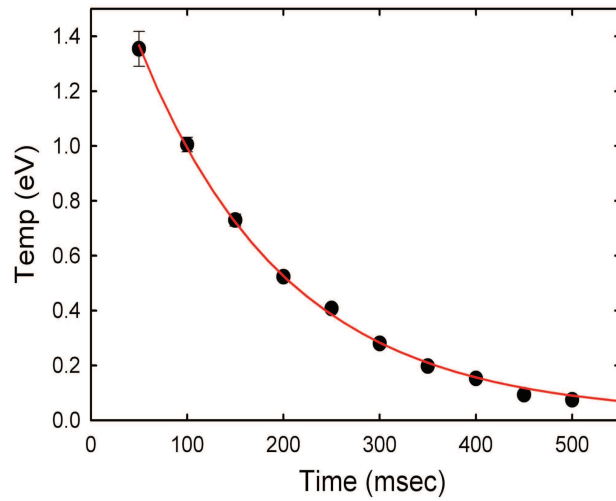


FIG. 10 (color online) Cyclotron cooling of an electron plasma in a magnetic field of 4.8 T, following heating with rf noise. Equation (67) yields $\Gamma_c = 6.5 \text{ s}^{-1}$, as compared with a predicted value of 5.9 s^{-1} . Courtesy of T. R. Weber, unpublished.

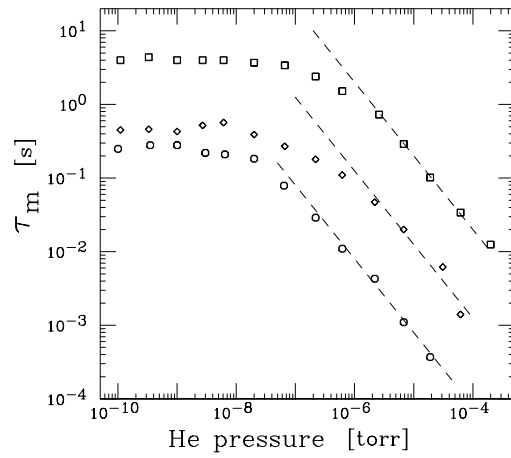


FIG. 11 Radial confinement time of a pure electron plasma versus pressure of the helium gas for magnetic fields of (\square) 0.067; (\diamond) 0.017; and (\circ) 0.0042 T. Adapted from Fig. 3 of Malmberg and Driscoll (1980), courtesy of C. F. Driscoll.

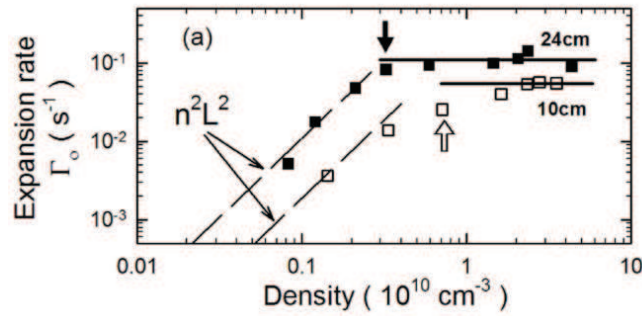


FIG. 12 Outward asymmetry-induced transport vs plasma density for two different plasma lengths, $L_p=24 \text{ cm}$, and 10 cm . Vertical arrows correspond to the densities at which $\nu_c = 3f_b$, where ν_c is the Coulomb collision frequency and f_b is the axial bounce frequency. See Danielson and Surko (2006b) for details.

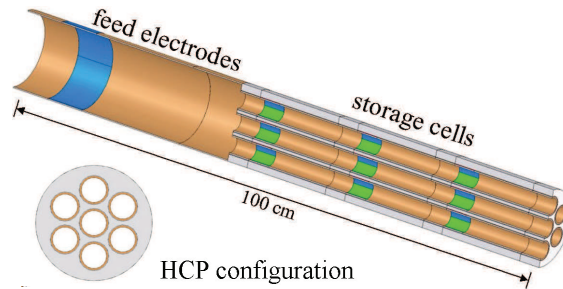


FIG. 13 (color online) Schematic diagram of the design of a 21-cell multicell PM trap for 10^{12} positrons. It consists of a set of feed electrodes and three banks of 7 storage cells in a hexagonally closed packed (HCP) arrangement. A RW electrode (blue/green) is incorporated in each cell. Autoresonant excitation of the diocotron mode (Sec. VI.B.2) will be used to move plasmas across B for off-axis storage.

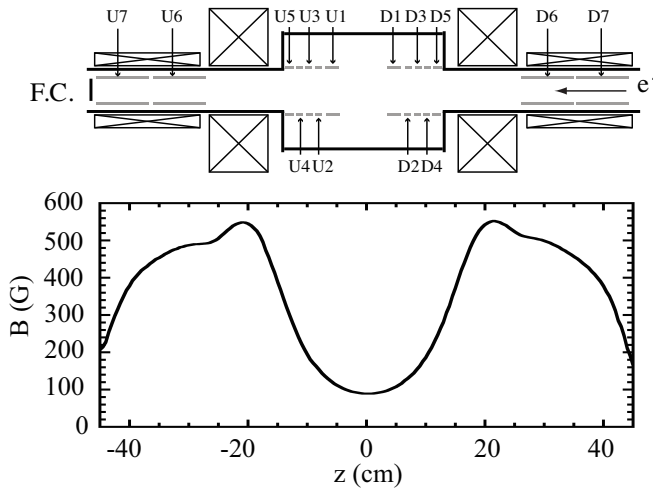


FIG. 14 (above) magnetic mirror arrangement for the experiments to study electron-plasma confinement, and (below) the on-axis magnetic field strength as a function of position. Two inner coils provide magnetic mirror confinement field with a mirror ratio of 5, while an outer pair of coils guide the filling beam from an electron gun and extracted beams to a Faraday cup (labelled F.C. in the upper panel). Reprinted from Higaki *et al.* (2012), copyrighted by the Japan Society of Applied Physics.

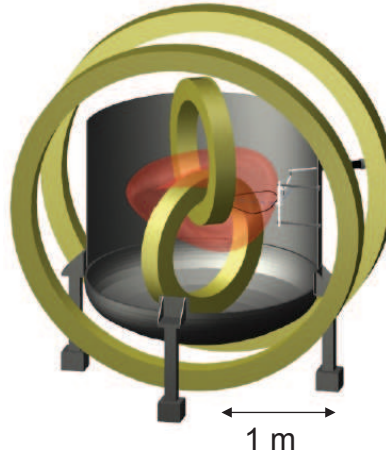


FIG. 15 (color online) The Columbia Nonneutral Torus (CNT) showing a cut-away of the vacuum vessel, the four circular magnetic field coils used to produce the stellarator field, and the calculated magnetic surfaces (faint deformed donut). Figure courtesy of T. S. Pedersen.

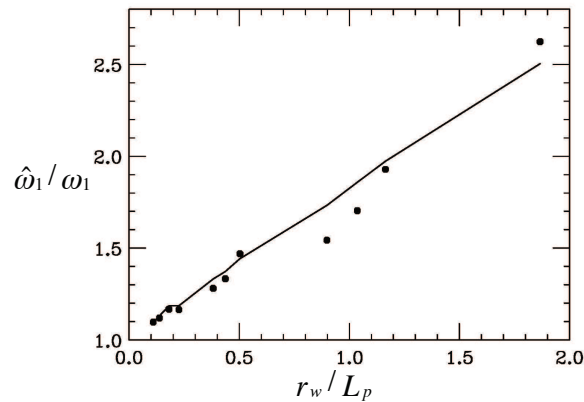


FIG. 16 Measured $m_\theta = 1$ diocotron mode frequency as a function of r_w/L_p compared with (solid line) the predictions of Eq. (69). Adapted from Fig. 4 of Fine and Driscoll (1998), courtesy of C. F. Driscoll.

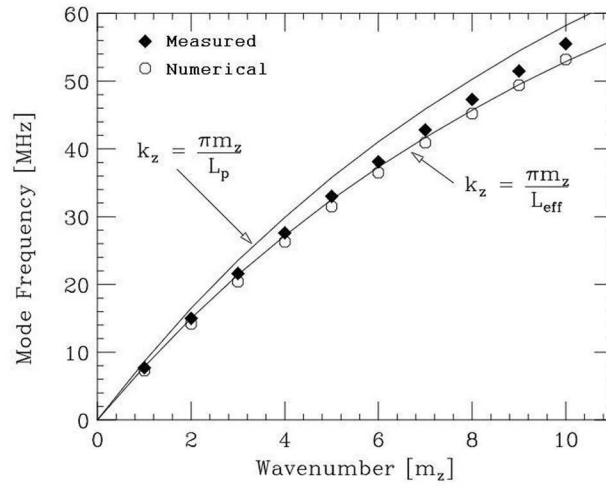


FIG. 17 Measured dispersion relation of Trivelpiece-Gould modes in a pure electron plasma. Adapted from Danielson and Driscoll (1999).

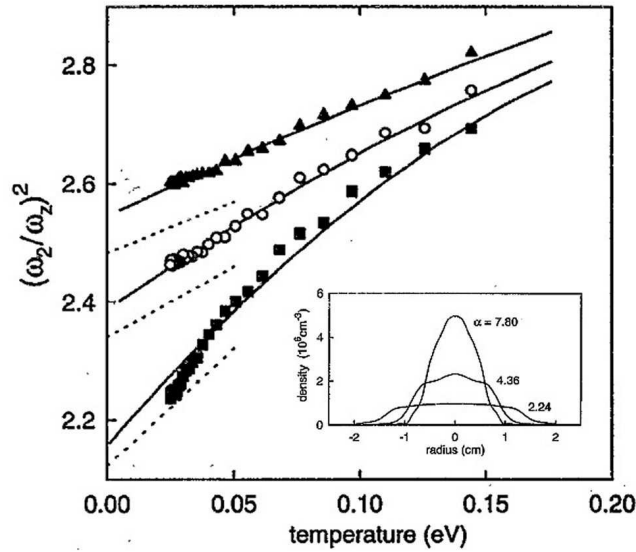


FIG. 18 Measured quadrupole ($l = 2$) mode frequency *vs.* plasma temperature for plasmas with three different aspect ratios (profiles shown in the inset) from Tinkle *et al.* (1994). Solid lines are the results of numerical simulations, and the dashed lines are the predictions of cold fluid theory.

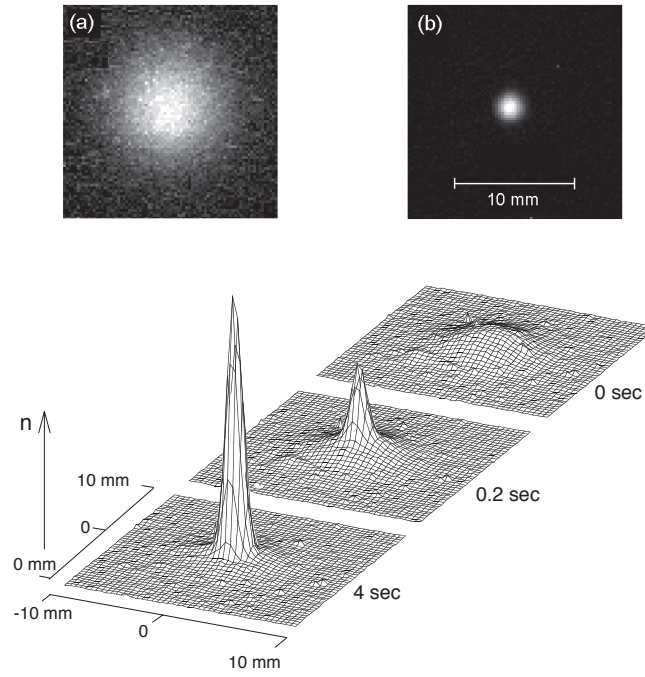


FIG. 19 Digital camera images of positron plasmas at (a) $t = 0$ and (b) $t = 4$ s; and (below) radial profiles of a positron plasma with $N_{\text{tot}} = 5 \times 10^7$ positrons, during rotating wall compression with $f_{\text{RW}} = 2.5$ MHz. From Greaves and Surko (2000).

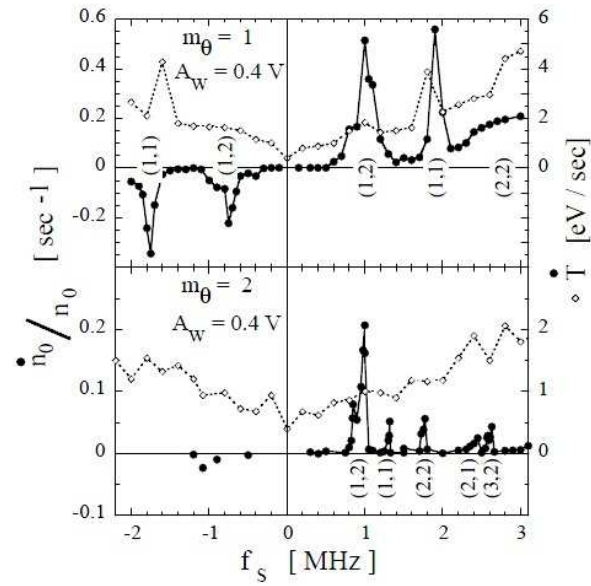


FIG. 20 Electron plasma compression rate (\bullet , n_0/n_0) and heating rate (\circ , \dot{T}), using driven Trivelpiece-Gould modes as a coupling mechanism and cyclotron cooling: (above) $m_\theta = 1$, and (below) $m_\theta = 2$. See Andregg *et al.* (1998) for details.

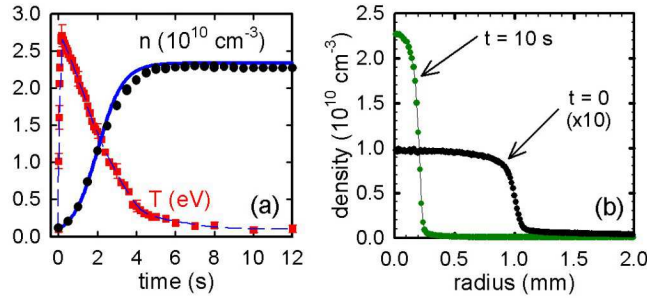


FIG. 21 (color online) (a) Plasma density and temperature *vs.* time during strong-drive excitation of an electron plasma cooled by cyclotron radiation. (b) Radial profile before compression ($t = 0$) and after reaching steady-state ($t = 10$ s). Adapted from Danielson and Surko (2006b).

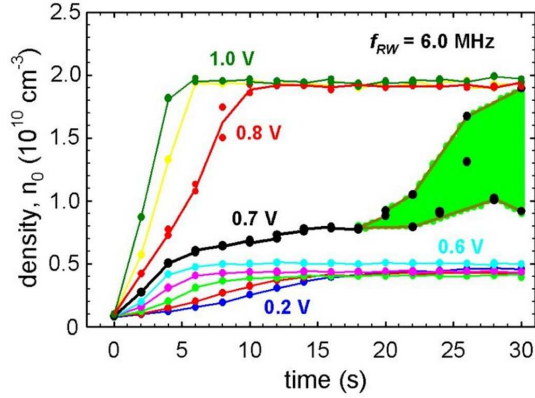


FIG. 22 (color online) Strong-drive compression: plasma density *vs.* time at fixed ω_{RW} . As the drive amplitude is increased, there is a transition from a low-density state to a high density steady state that is approximately independent of the drive amplitude. The shaded area indicates the transition region between the two states. Adapted from Danielson and Surko (2005).

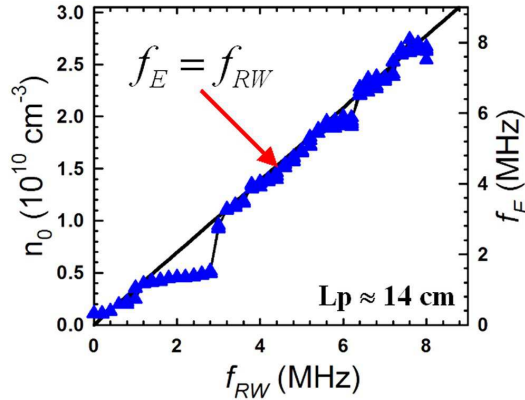


FIG. 23 (color online) Steady-state density after strong-drive compression for a broad range of frequencies showing that the steady-state plasma rotation frequency is close to the drive frequency (solid line is $\omega_{RW} = \omega_r$). The gap between 1 and 3 MHz is due to a zero-frequency mode; see the text for details. Adapted from Danielson and Surko (2005) and Danielson and Surko (2006b).

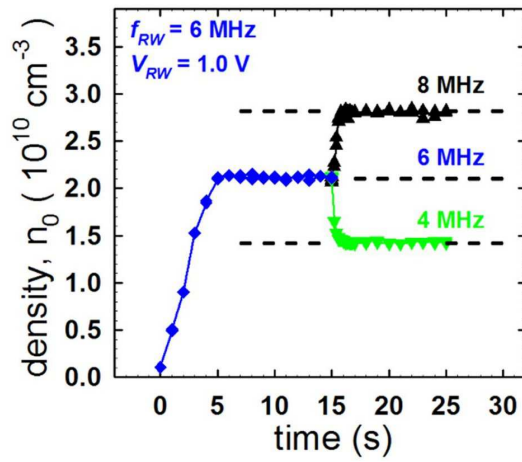


FIG. 24 (color online) Plasma density *vs.* time for strong-drive compression showing rapid adjustment to new steady-state density when the drive frequency is changed abruptly. Adapted from Danielson and Surko (2006b).

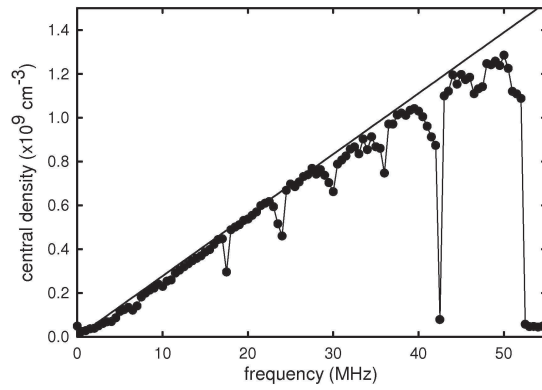


FIG. 25 Positron density *vs.* drive frequency in the First Point Scientific, Inc. RW experiment ($B = 0.04$ T) using buffer gas cooling (CF_4 , $p \sim 3 \times 10^{-7}$ torr). The solid line is the no-slip condition ($\omega_{RW} = \omega_r$). The maximum positron density reached was a record for leptons, $\sim 17\%$ of the Brillouin limit. The sharp dips at specific frequencies are due to ZFM's. (R. G. Greaves, unpublished.)

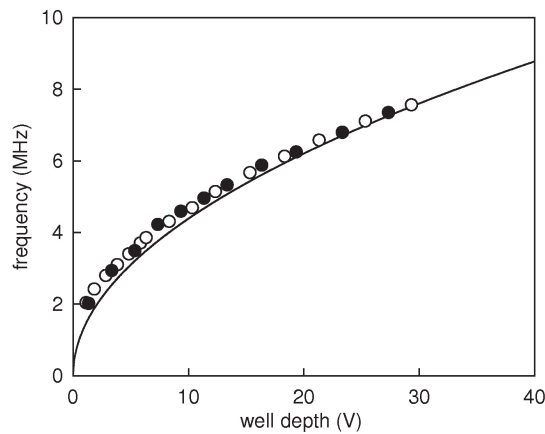


FIG. 26 Rotating wall frequency for maximum compression (or expansion) as a function of the parabolic well voltage for radial compression in the single particle regime. The solid line indicates the single-particle bounce frequency. From Greaves and Moxom (2008).

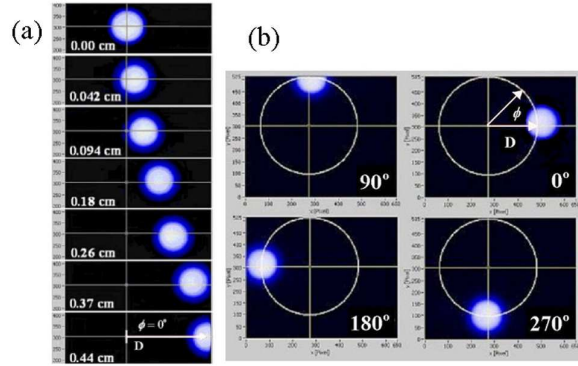


FIG. 27 (Color online) (a) Plasma images for different values of the diocotron-mode drive frequency thus producing different radial displacements d for the phase $\theta = 0^\circ$. Note that the plasma extent and shape remains approximately the same, independent of d . (b) Plasma images for different angles θ , for $d = 0.26$ cm. From Danielson *et al.* (2006).

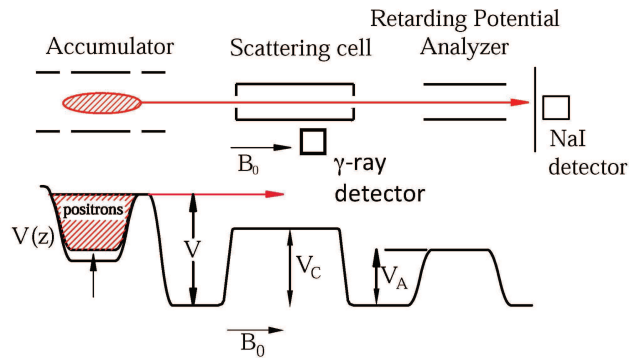


FIG. 28 (color online) Schematic diagram of a trap-based positron beam used in atomic and molecular physics experiments: (above) experimental arrangement; and (below) the electrical potential profile along the magnetic axis. After trapping and cooling, the bottom of the potential well is raised to force particles over the end gate at potential V and through the scattering cell at potential V_c , which sets the beam energy $\epsilon = e(V - V_c)$ in the scattering cell.

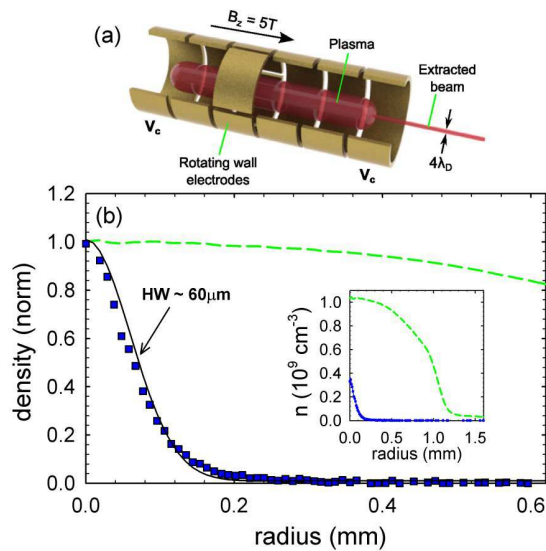


FIG. 29 (color online) (a) Cartoon of the experimental arrangement used to extract beams of small spatial extent from an SCP in a PM trap; (b) Normalized profiles for the (■) beam and plasma (dashed green line). The inset in (b) shows the density for both on an absolute density scale (i.e., in the trap). From Danielson *et al.* (2007b).

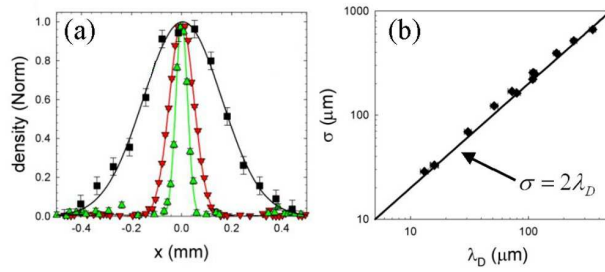


FIG. 30 (color online) (a) transverse profiles of beams extracted from plasmas with different densities (■) $1.9 \times 10^{15} \text{m}^{-3}$, (▼) $6.5 \times 10^{15} \text{m}^{-3}$ and (▲) $1.2 \times 10^{16} \text{m}^{-3}$; and (b) the transverse width of the extracted beam *vs.* the Debye length of the parent plasma. From Danielson *et al.* (2007b); Weber *et al.* (2008).

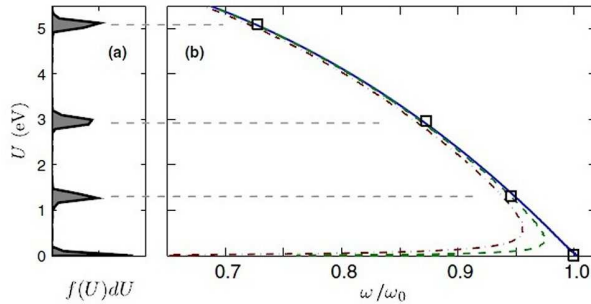


FIG. 31 Energy of antiprotons after an autoresonant chirped drive is applied with different final frequencies: (a) energy distributions of 15,000 antiprotons after reaching the frequencies shown; and (b) mean calculated energy *vs.* chirp frequency, normalized to linear bounce frequency for the trap potential well. Figure from Andresen *et al.* (2011a).

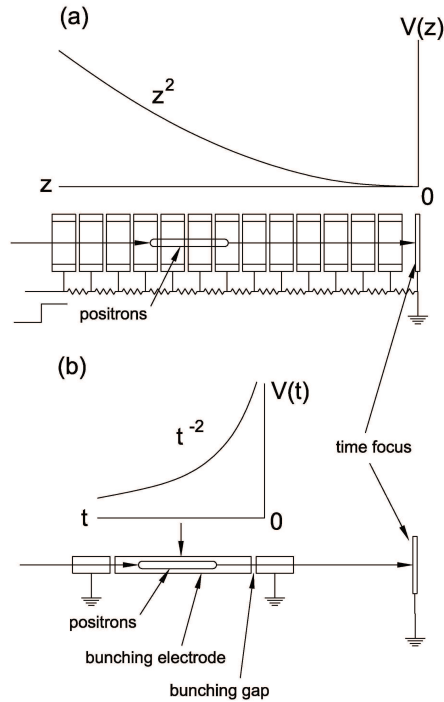


FIG. 32 Arrangement for: (a) Harmonic potential bunching; the resistor divider chain is configured to produce a harmonic potential within the buncher electrode structure when a high voltage pulse is applied to the left end of the chain. (b) Timed potential bunching: the potential on the buncher is raised according to a $1/t^2$ ($t < 0$), as the positron pass through the buncher gap. In both cases the spatial extent of the positron pulse must be shorter than the respective electrode structure.

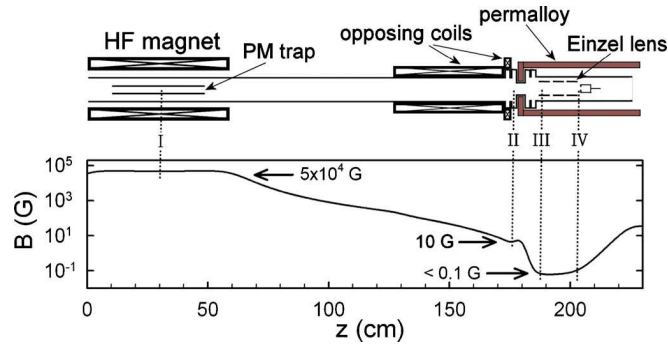


FIG. 33 (color online) (upper panel) Schematic diagram of an experiment to (non-adiabatically) extract an electron beam from a plasma in a PM trap in a 5 T field, then electrostatically focus the particles into a Faraday cup. (lower panel) The magnetic field profile along the direction of the extracted beam. Saddle coils (not shown) used to align the field at $z \approx 140$ cm. From Weber *et al.* (2010).

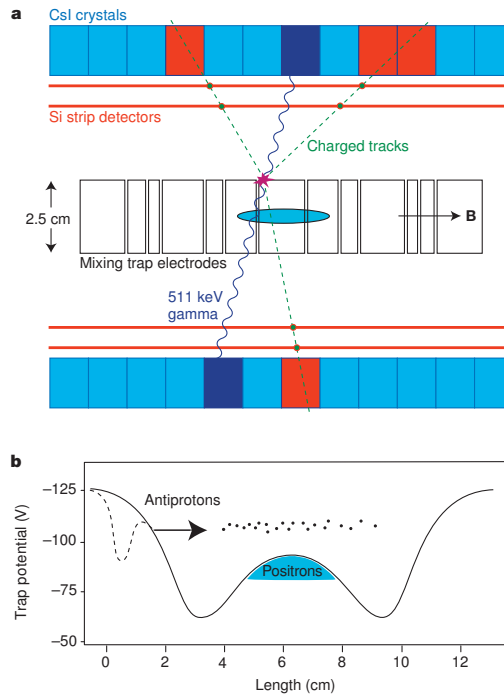


FIG. 34 (color online) (a) ATHENA mixing trap and antihydrogen detector, with the positron cloud (blue ellipse); also shown is a typical \bar{H} annihilation into three charged pions and back-to-back 511-keV photons; (b) (solid line) the electrical potential during mixing, and (dashed line) immediately before antiproton transfer. From Amoretti *et al.* (2002).

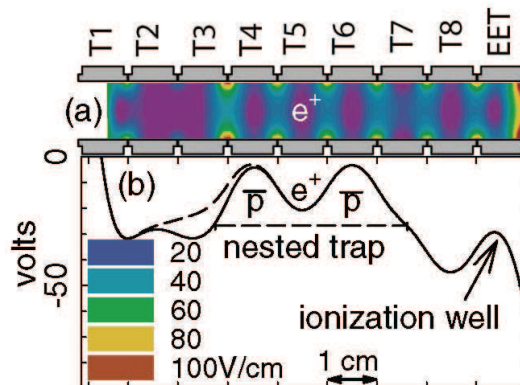


FIG. 35 (color online) (a) ATRAP electrode arrangement for nested Penning traps. Shaded regions indicate the magnitude of the electric field (i.e., used to ionize the \bar{H}); (b) potential on axis for positron cooling of antiprotons (solid line) during which \bar{H} formation takes place; (dashed line) modified potential used to launch \bar{p} into the well. (Gabrielse *et al.*, 2002).

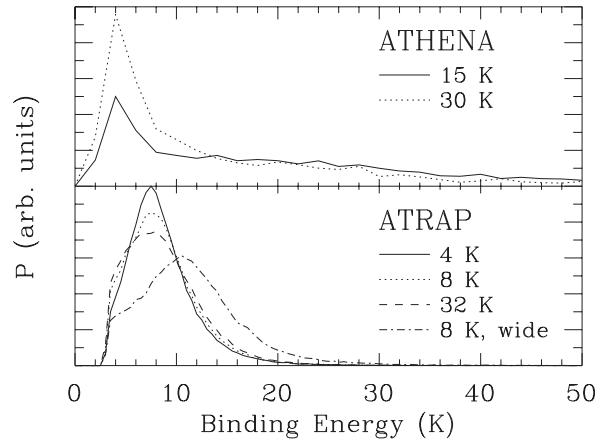


FIG. 36 Simulation of the probability P for an \bar{H} atom to have a given binding energy for the assumed positron plasma temperatures indicated. To survive a 25 V/cm field, an atom needs a binding energy greater than ~ 40 K. From Robicheaux (2004).

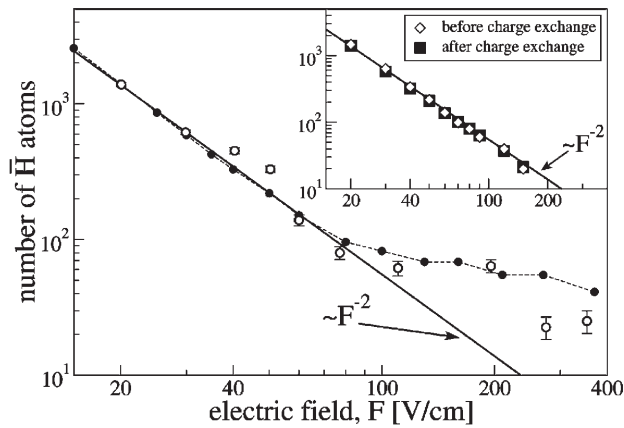


FIG. 37 Analysis of ATRAP data for the field-ionization spectrum of \bar{H} atoms that survive an electric field F compared to Monte Carlo calculations assuming an \bar{H} temperature of 2 meV; (inset) analysis to verify that charge exchange effects do not alter the spectrum. See Pohl *et al.* (2006) for details.

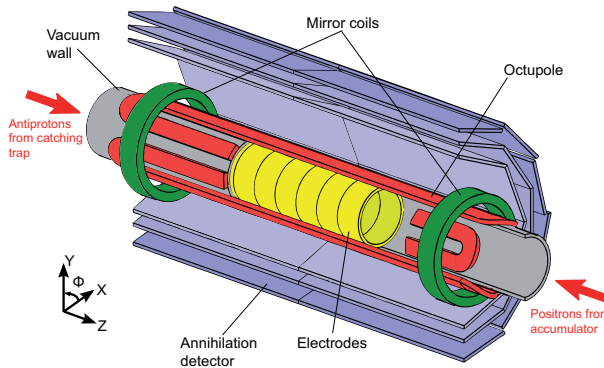


FIG. 38 (color online) Illustration of the inner section of the ALPHA experiment showing the PM trap electrodes and the minimum- B neutral trap, with octupole and mirror coils, and the silicon-based annihilation detector. From Amole *et al.* (2014).

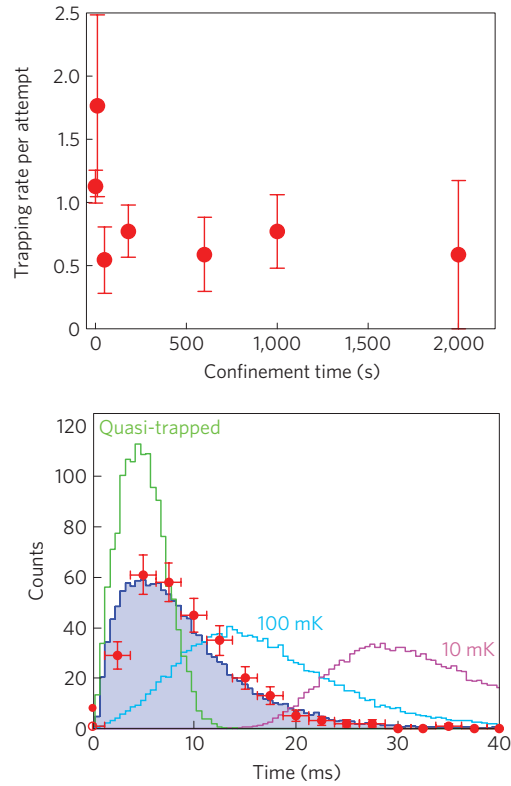


FIG. 39 (color online) (above) ALPHA data for the number of trapped \bar{H} per attempt as a function of confinement time; and (below) comparison of the time distributions between the data (red circles) with simulations for various initial energy distributions (histograms). The shaded histogram represents the best fit. See Andresen *et al.* (2011b) for details.

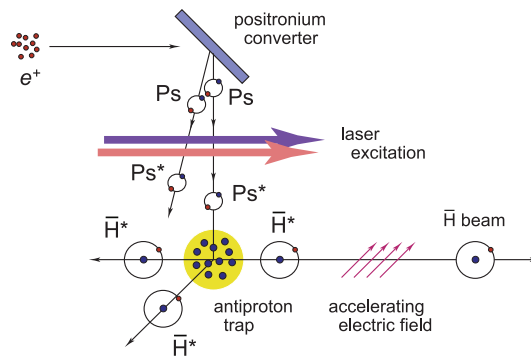


FIG. 40 (color online) Overview of the AEGIS proposed experiment to measure the deflection of an \bar{H} beam due to Earth's gravity (Doser *et al.*, 2012).

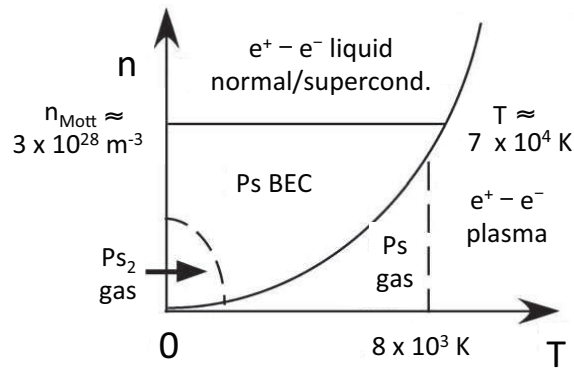


FIG. 41 Schematic phase diagram of the electron-positron many-body system as a function of density n and temperature T [adapted from Yabu (2004)]. While the quantum e^+e^- liquid is beyond current technology, besides the studies (in progress) of Ps_2 , it is possible to contemplate near-term studies of a Ps BEC and a classical pair plasma.

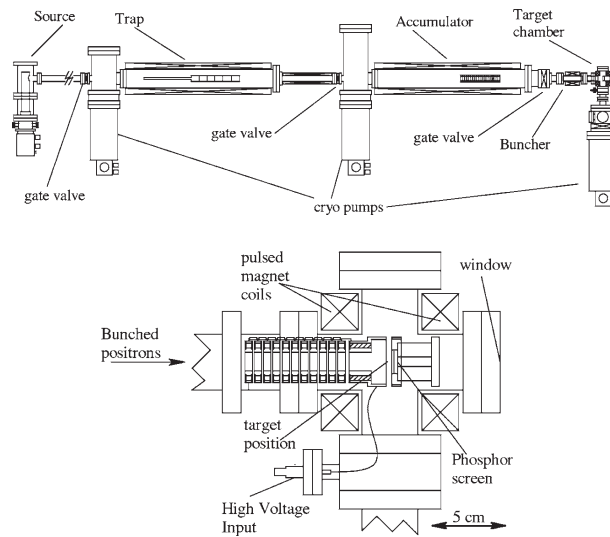


FIG. 42 Apparatus for creating a dense Ps gas and the Ps_2 molecule; (above) BGT and accumulator; and (below) pulsed magnet and sample location. From Cassidy *et al.* (2006a).

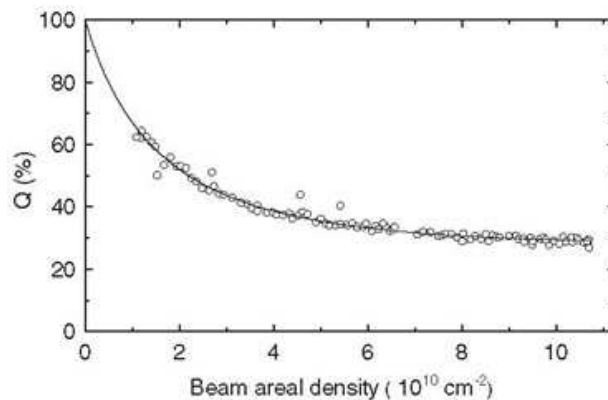


FIG. 43 (\circ) normalized quenching parameter Q plotted as a function of the beam areal density n_{2D} impinging on porous silica; and (—) fit to a density-dependent decay function (Cassidy *et al.*, 2010c). At large n_{2D} , all but spin aligned Ps atoms quench. Assuming spin alignment from the ^{22}Na is preserved, the asymptotic high-density value of Q will be the initial degree of spin polarization p_0 . The expected value in those experiments was $p_0 = 0.35$ as compared with the measured value of $p_0 = 0.28$. See Cassidy *et al.* (2010a) for details.

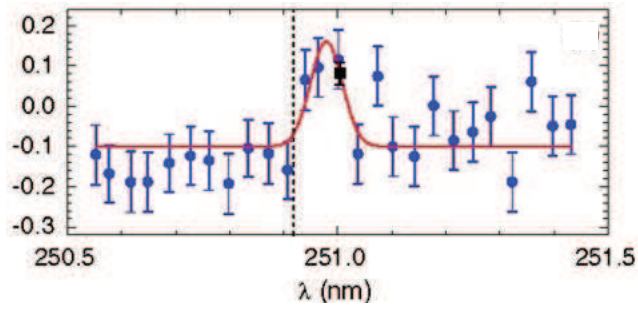


FIG. 44 (color online) Normalized, delayed fraction of annihilations *vs.* the probe laser wavelength for Ps_2 in porous silica. A second laser ionizes the Ps_2 , once excited. Vertical dashed line is the expected position of the Ps_2 resonance in vacuum. See Cassidy *et al.* (2012b) for details.

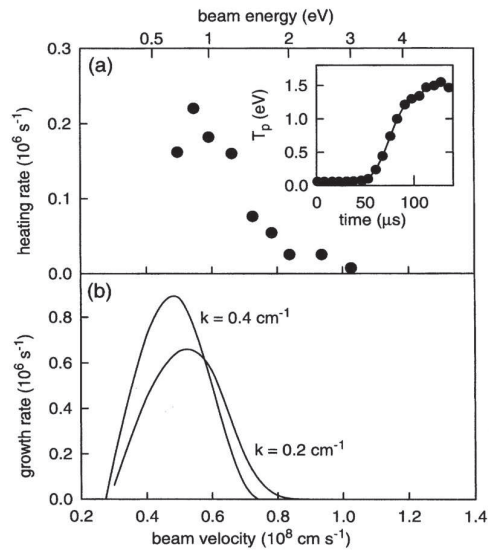


FIG. 45 Beam-plasma interaction in the cylindrical trap: (a) positron heating rate (inset: time-resolved positron heating); and (b) the calculated growth rates for waves with wavenumbers of 0.4 and 0.2 cm^{-1} . See Greaves and Surko (1995) for details.

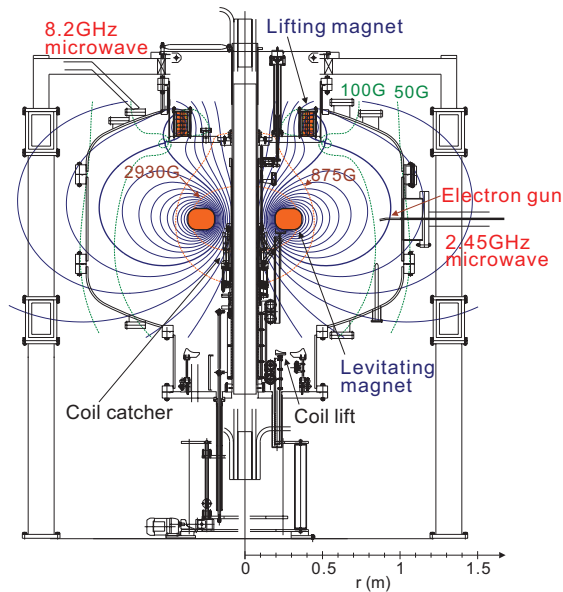


FIG. 46 (color online) Schematic diagram of the RT-1 ring trap which is a superconducting levitated dipole. (Yoshida *et al.*, 2013).

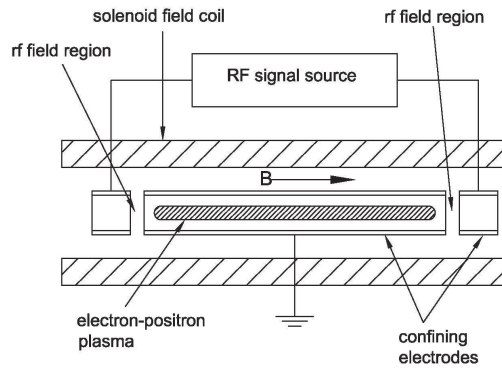


FIG. 47 A Penning-Paul trap for pair plasma confinement (Greaves and Surko, 2002b).

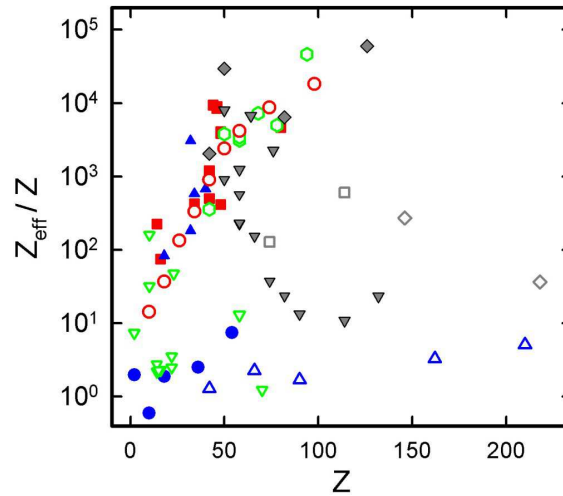


FIG. 48 (color online) Experimental values of the normalized annihilation rate Z_{eff}/Z plotted against the total electronic charge Z on the molecule, demonstrating the importance of chemical composition on annihilation rates: (●) noble gases, (▽) simple molecules, (○) alkanes, (△) perfluorinated alkanes, (□) perchlorinated alkanes, (◊) perbrominated and periodated alkanes, (■) ring alkanes, alkenes, and alkynes, (▲) oxygen containing compounds, (○) ring hydrocarbons, (▼) substituted benzenes, and (◆) large organic molecules. From Iwata *et al.* (1995).

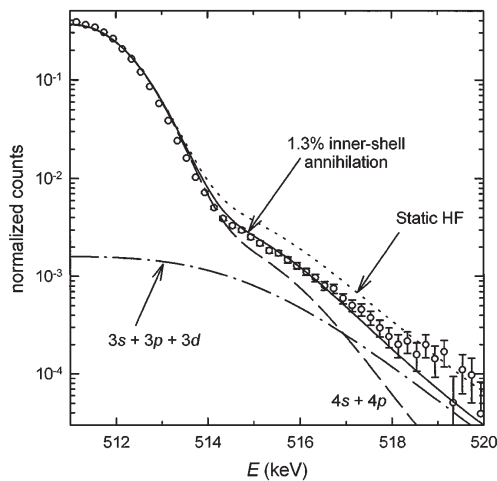


FIG. 49 The Doppler-broadened γ -ray spectrum resulting from positrons annihilating on Kr atoms. Shown are (○) experimental data, (⋯) a static Hartree-Fock calculation, and (—) the best fit to the data which includes a 1.3% contribution from inner-shell electrons. See Iwata *et al.* (1997a) for details.

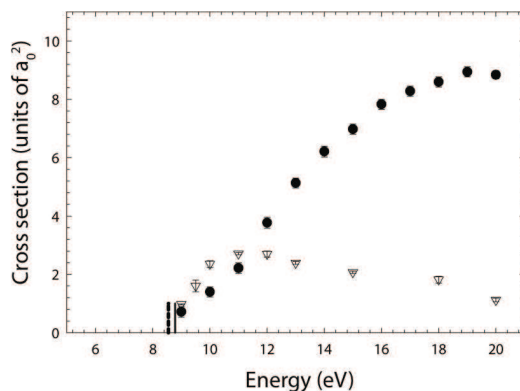


FIG. 50 Electronic excitation, (∇), (Sullivan *et al.*, 2001) and positronium formation, (\bullet), (Marler and Surko, 2005a) cross sections for molecular nitrogen as a function of incident positron energy. The region of energies around 10 eV, where electronic excitation dominates, is optimum for the operation of the BGT.

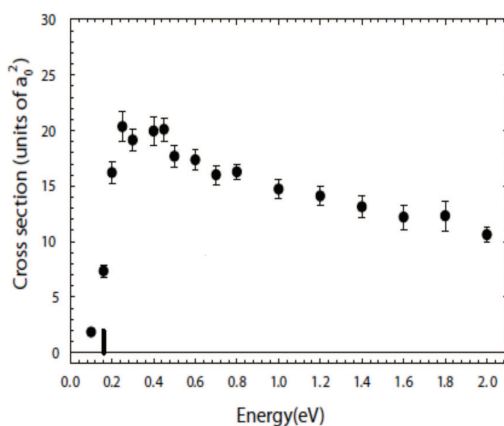


FIG. 51 Positron-impact cross section for excitation of the ν_3 vibrational mode of CF_4 as a function of incident positron energy in atomic units $a_0^2 = 2.8 \times 10^{-21} \text{ m}^2$. This relatively large cross section above the threshold energy, $\epsilon_i = 0.16 \text{ eV}$, provides a very efficient positron cooling mechanism. Reprinted from Marler and Surko (2005b).

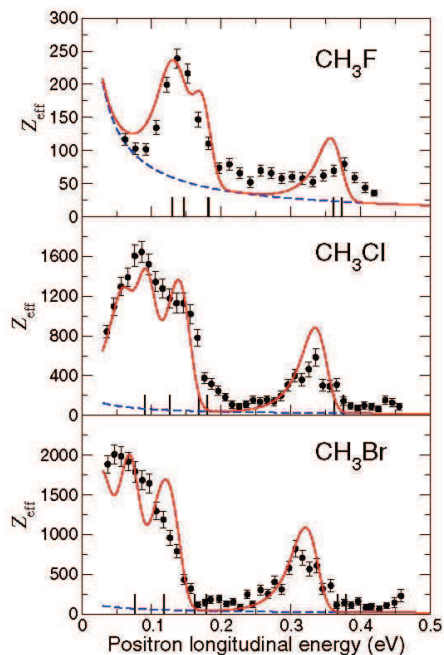


FIG. 52 (color online) Comparison between measured Z_{eff} (\bullet , Ref. (Barnes *et al.*, 2006)) and theoretical Z_{eff} (solid curves) for $\epsilon_b = 0.3$ meV (CH_3F), 25 meV (CH_3Cl), and 40 meV (CH_3Br). Dashed curves show the non-resonant contribution $Z_{\text{eff}}^{\text{dir}}$. Vertical bars show the energies of molecular fundamentals. The only fitted parameter in each spectrum is ϵ_b . From Gribakin and Lee (2006b).

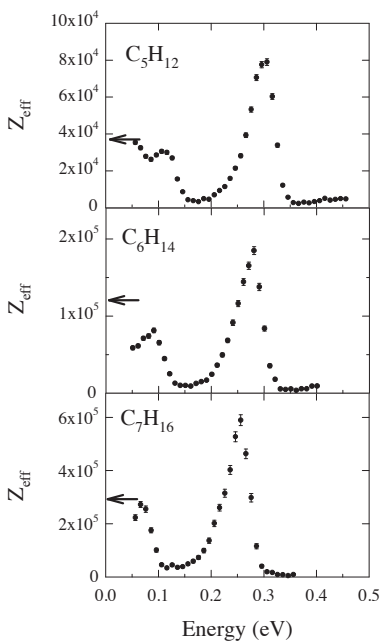


FIG. 53 Z_{eff} as a function of incident positron energy for the alkanes ($\text{C}_n\text{H}_{2n+2}$). Arrows on the vertical axis indicate Z_{eff} for a room temperature thermal distribution of positrons. As molecular size increases, so does ϵ_b ; the Z_{eff} value increases and the spectrum shifts to lower energy. From Barnes *et al.* (2003).

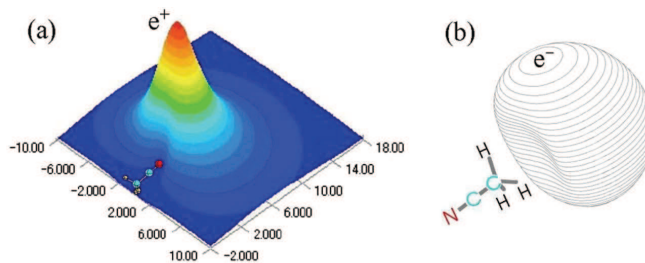


FIG. 54 (color online). Contour plots of calculated bound (a) positron (Tachikawa *et al.*, 2011) and (b) electron (Simons, 2008) wave functions for the positive and negative acetonitrile (CH_3CN) molecular ions. The positron does not penetrate the valence shell due to repulsion from the nuclei, and the electron is kept outside due to Pauli exclusion. From Danielson *et al.* (2012).

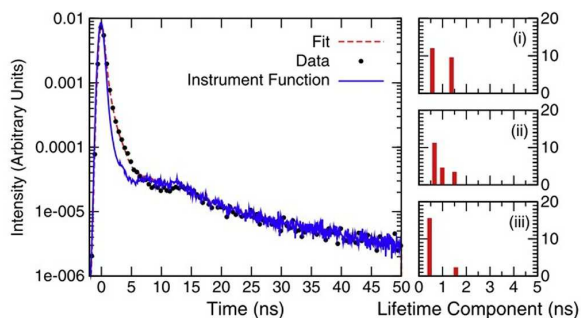


FIG. 55 Left: instrument function and lifetime spectrum for a chitosan biopolymer from a trap-based lifetime system. Right: extracted lifetime components for three different samples (Chaudhary *et al.*, 2010).

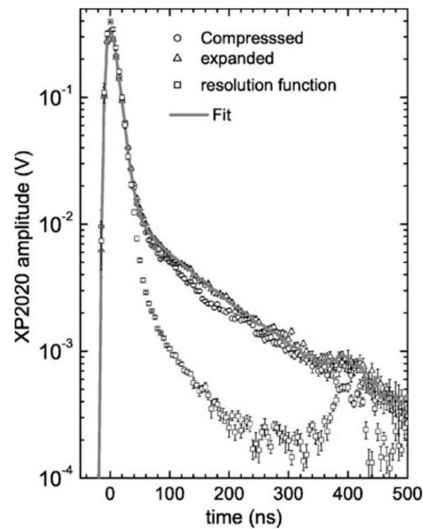


FIG. 56 Single shot lifetimes for porous silica samples with higher and lower densities of positrons in each bunch (labeled “compressed” and “expanded”, respectively). The resolution function is also shown. From Cassidy *et al.* (2006c).

TABLES

TABLE I A selection of positron emitting nuclides showing the half life, positron end point energy, and the branching ratio for positron emission *vs.* electron capture.

Nuclide	Half life	E_{\max} (keV)	% e^+
^{11}C	20.4 min	960	100
^{13}N	10.0 min	1198	100
^{18}F	110 min	633	97
^{19}Ne	17.3 s	2235	100
^{22}Na	2.60 y	545	90
^{27}Si	4.16 s	3789	99
^{58}Co	71 d	475	15
^{64}Cu	12.7 h	652	18
$^{68}\text{Ge}/^{68}\text{Ga}$	271 d	1899	88
		822	11
^{79}Kr	35h	600	7
^{126}I	13 d	1130	0.8
		460	0.2

TABLE II Typical parameters for different types of positron sources.

Source	Moderator	Flux (s^{-1})	Diameter (mm)
Na-22	tungsten foil	10^5	3 mm
Na-22	neon	10^7	8 mm
LINAC	tungsten	5×10^7	20 mm
Reactor	platinum	10^9	7 mm

TABLE III Positron cooling in a PM trap using molecular gases at 2.6×10^{-8} mbar: time τ , for direct annihilation; measured cooling time, τ_c ; and the energies of the vibrational quanta, ϵ_i . Data from Refs.(Greaves and Surko, 2000, 2001).

Gas	$\tau_a(s)$	$\tau_c(s)$	$E_\nu(eV)$
SF ₆	2200	0.36	0.076, 0.19
CF ₄	3500	1.2	0.16
CO ₂	3500	1.3	0.29, 0.083
CO	2400	2.1	0.27
N ₂	6300	115	0.29

TABLE IV Design parameters of a 21 cell multicell trap for 10^{12} positrons. Adapted from Danielson *et al.* (2013).

Parameter	Value
Number of cells ($m \times p = 7 \times 3$)	21
Total positron number, N (10^{12})	1.0
Magnetic field (T)	5
Total electrode length, L (m)	1.0
Electrode package diameter, $2R$ (m)	< 0.08
Plasma radius, R_p (m)	0.002
Plasma length, L_p (m)	0.2
Confinement voltage, V_c (kV)	2
Cell spacing (cm), D	2.0
Space charge potential (kV)	1.5
Rotating wall frequency (MHz)	4

TABLE V Parameters of a proposed Penning-Paul trap pair-plasma experiment (Greaves and Surko, 2002b).

Parameter	Value
density (m^{-3})	10^{13}
plasma length (m)	0.3
plasma radius (m)	0.005
wall radius (m)	0.01
particle number N	5×10^8
rf frequency (MHz)	200
rms rf voltage (V)	100
rf potential well (V)	5
buffer gas pressure (torr)	10^{-6}
plasma temperature (eV)	0.5

TABLE VI (Color online) Positron- and electron-molecule binding energies ϵ_b (meV), permanent dipole moments μ (D), and dipole polarizabilities α ($10^{-30}m^3$) for selected molecules. Positron data for ϵ_b from Danielson *et al.* (2010, 2012), electron data from Hammer *et al.* (2003), and values for μ and α are from the CRC (2008).

Molecule	μ	α	$\epsilon_b(e^+)$	$\epsilon_b(e^-)$
Aldehydes				
 acetaldehyde, C ₂ H ₄ O	2.8	4.6	90	0.6
 propanal, C ₃ H ₆ O	2.5	6.5	120	1.0
 butanal, C ₄ H ₈ O	2.7	8.2	142	1.2
Ketones				
 acetone, C ₃ H ₆ O	2.9	6.4	173	2.6
 2-butanone, C ₄ H ₈ O	2.8	8.1	195	1.8
 cyclopentanone, C ₅ H ₈ O	3.3	9.3	230	2.8
Nitriles				
 acetonitrile, C ₂ H ₃ N	3.9	4.4	180	19
 propionitrile, C ₃ H ₅ N	4.1	6.5	245	15
 isobutyronitrile, C ₄ H ₇ N	4.3	8.1	275	12